University of Bath

UNIVERSITY OF BATH

PHD

Improvements in quality through weld thermal cycle modelling

Kirk, Christopher Selby

Award date:
1997

Awarding institution:
University of Bath

Link to publication

IMPROVEMENTS IN QUALITY

THROUGH

WELD THERMAL CYCLE MODELLING

Submitted by

Christopher Selby Kirk

for the degree of PhD

of the University of Bath

1997

COPYRIGHT

C S Kirk

UMI Number: U114497

UMI

Dissertation Publishing

UMI U114497

ProQuest

Dedicated to

Tessa,

Sam and Tom

Abstract

This thesis considers semi-automatic welding processes and shows, that through a detailed assessment of electrode extension and its effect on heat transfer, that improvements in quality may be achieved through consideration of heat flow in welded joints, and that by effective modelling of all thicknesses of material that these processes could be capable of achieving industrial requirements on a consistent basis and moreover, that quality levels can be increased.

A new single equation has been derived, partially differentiated, and transposed into a series of new equations to model the cooling rates in the weld heat affected zone, and associated influencing factors such as preheat and speed of travel. The equations derived have been further developed to include coefficients and assumptions to enable the modelling of fillet welds across a range of thicknesses, including taking into account the effect of thermal contact resistance between the two plates. Such work is considered to be the first published work presenting analytical equations to enable rapid indications of the weld thermal cycle in such joints and the equations may, when used in conjunction with hardness prediction theory, be used to predict the microstructure and hardness in the heat affected zone. The model has been validated successfully with a practical experiment using micro-alloyed steel across a range of thicknesses and the final equations have been simplified to enable rapid calculations, which it is believed will contribute to improving quality through weld thermal cycle modelling.

Contents

Table of Figures

Table of Tables

Acknowledgements

Nomenclature

dT/dt	=	cooling rate of the weld and HAZ, °C/s
k	=	thermal conductivity of the metal, J/s.mm.°C
v	=	heat source velocity, mm/s
Q	=	heat source power, J/s
To	=	original uniform plate temperature before welding, °C
Tc	=	temperature at which the cooling rate is to be determined, °C
T_p	=	peak temperature, °C
T_a	=	austenetization temperature, K
ρ	=	density of the material, g/mm^3
C	=	specific heat of the solid material, J/g.°C
g	=	thickness, (gauge), of the plate, mm
r	=	radial distance, mm
e	=	exponent
2λ	=	ρC/k, s/mm^2
x,y,z	=	Cartesian co-ordinate of a point in the plate frame, mm
t	=	time, s
n	=	naperian logarithm
R	=	universal gas constant
H	=	activation energy of the process, J/mole

Note: The term, (g), is used to represent thickness, having previously used by Rosenthal, since time uses the term, (t).

- Nomenclature for Chapter 7 and 10 :

In order to maintain compliance with existing theory, some symbols relating to heat flow in welding have been replaced in Chapters 7 and 10, with the following.

a	=	mean radius of the contact spots, mm
b	=	mean radius of the surface asperities, mm
Rtc	=	value of the thermal contact resistance, $mm^2.K.W^{-1}$
ξ	=	b/a
x,y,z	=	Cartesian co-ordinates
\<parameter\>*	=	non-dimensional value of the parameter \<parameter\>
C	=	curvature at a point of the surface, mm/mm
erf	=	error function
ki	=	thermal conductivity of the plate i, $J/mm.s.°C$
m_{0i}	=	mean peaks square height of the surface i (Si), mm^2
m_{2i}	=	mean square curvature of the surface i (Si), mm/mm
Ei, vi	=	Young's modulus, N/mm^2, and Poisson coefficient of the plate i
m_0	=	mean peaks square height of the equivalent surface, mm^2
m_2	=	mean square curvature of the equivalent surface, mm/mm
Ac	=	real contact area, mm^2
An	=	apparent, (nominal), area of contact, mm^2
Rn	=	Thermal contact resistance, machined plate
Rp	=	Thermal contact resistance, shaped plate
Ψ	=	Contact ratio, %
W	=	load applied on the interface, N
E	=	Young's modulus of the equivalent surface,

$$\frac{1}{\dfrac{(1-v_1^2)}{E_1} + \dfrac{(1-v_2^2)}{E_2}}$$

1. Introduction

The worldwide desire to raise quality standards, promoted by the ISO 9000 series, has led to an increase in the use of full quality systems. As these are principally organisational, they place greater reliance on procedures and instruction sets, and in welding these are evident in the form of procedures, such as those approved in accordance with the AWS D11, ASME IX and EN 288, (ISO 9956:1995), standards. Further, EN 729:1994, (ISO 3834:1995), 'Quality requirements for welding-Fusion welding of metallic materials', insists that welding procedures are mandatory if a full ISO 9000 quality scheme is in operation.

Within the global requirement for higher quality output, a need therefore exists to examine welding process variables and characteristics more closely in order to achieve greater consistency of output. The semi-automatic welding processes assist in meeting demands for increases in productivity, matched with the potential for lower costs, but, unfortunately, the processes suffer from inherent defects such as lack of fusion and penetration, which may result in weldments being unreliable in service. Further, the increasing use of thinner, stronger sections due to advances in micro-alloying, create a potential for problems regarding estimation of the effect of heat transfer in weldments using such material.

This thesis considers a number of these aspects and examines the hypothesis, (*Chapter 2*), that weld thermal cycle modelling may be used as a means by which quality may be improved. Welding engineering is pan-disciplinary and is undertaken in operations in many major industrialised sectors. The scope of welding processes is examined in a review in *Chapter 3* which discusses the principal processes with a brief review of the physics and metallurgy of welding. The chapter concludes with a review of heat transfer as far as it

affects welding, and this notably highlights that much current theory is based on equations developed in 1935. In this respect, whilst it is acknowledged that recent work has been undertaken to directly consider the heat transferred in different joint set-ups, the equations derived are complicated and cumbersome.

In considering semi-automatic welding in particular, it is necessary to assess the development of the process and consider how improvements have affected quality. *Chapter 4* considers this matter, and observes that changes to wire resistivity can markedly affect quality. Following a review of welding practices the chapter examines the results of two feasibility studies which illustrate the impact of variations to electrode extension, concluding that the weld heat affected zone integrity may be compromised as a result.

Having regard to the impact of changes to arc energy, and consequently the heat affected zone, *Chapter 5* examines modelling of the weld thermal cycle by considering the deficiencies of the major equations in current use and, through the development of a series of new equations, (the Continuous Heat Flow Equations), prepares the foundation for future developmental work. Validation of the new equations thus derived, presented an opportunity to consider the possibility of direct application to typical joint configurations used in industry. Examination of the effect on T-fillets which encompassed a number of different problems simultaneously was considered and *Chapter 6* introduces work in this respect and discusses the potential effect on fillet joints where the upper plate may be at any angle to the lower plate.

During the course of the investigation into fillet welds, a key hypothesis that a thermal discontinuity exists in the majority of fillet welded joints was considered. *Chapter 7* discusses the examination of this theory, and the validation of computer modelling in respect of the thermal contact resistance, whilst *Chapter 8* considers the effect of thermal contact resistance on the Continuous Heat Flow Equations previously derived.

Development of the series of new equations and the complicated mathematical treatment of the effect of the thermal discontinuity prompted the work reported in *Chapter 9* to simplify the findings and to develop a means by which welding engineers would have reasonably simplified equations to assist rapid prediction of the weld thermal cycle without recourse to extensive computer facilities.

The theoretical work was successfully validated with practical experiments which are detailed in *Chapters 10 and 11*, and these chapters report on the evidence gathered to support, (with some limitations), the accuracy of the mathematical modelling discussed earlier.

In concluding in *Chapter 12* that new equations have been developed which can assist in prediction of the weld thermal cycle it is noted that traditional models for predicting heat flow in T-fillet welds may not be complete as they appear not to take thermal contact resistance into account.

The thesis provides clear documentary evidence of original work, and is cross referenced to existing theories, full details of which are recorded in *Chapter 13*. The work contains some mathematical treatments and experimental results which are disclosed in the *Appendices* to improve the structure of the final document.

It is considered that the reported research complements the existing welding theory of heat flow due to a transient heat source, and significantly extends it by declaring a series of new equations to enable modelling across a range of material thicknesses, and by providing what is believed to be the first analytical solutions to the phenomena of thermal discontinuities in fillet welded joints.

2. Hypothesis, aims and objectives

2.1 Hypothesis

2.1.1 Welding processes

Improvements to the qualitative output of metal-arc inert or active gas welding and flux-cored wire metal-arc welding are necessary to enable them to maintain their place as leading processes.

These processes suffer from a number of inherent defects which may be minimised by correction to operator training and improvements to process control through the dissemination of knowledge on the importance of welding parameters.

Through the use of alloying elements within the core of a tubular electrode, defects may be minimised through absorption across the arc and interaction in the weld pool. However, these advantages cannot be maintained if electrode extension is not controlled to a precise degree. The profound influence which changes in electrical characteristics exert in transfer modes warrants further examination and quantitative analysis.

2.1.2 Heat Transfer

Heat transfer in welding is relative to the energy input, the mass effect of the material, and the environment. As outlined above, electrode extension plays a significant role in determining the final current drawn and consequential energy available across the arc. Further, many products utilise micro-alloyed steels for high performance, and these are now available in thinner section thicknesses than their earlier counterparts.

Given that existing equations are available pertaining to the calculation of heat transfer in thick or thin steels, it is considered important to develop an equation which is both relatively easy to use but which permits approximation of heat transfer in intermediate plate thicknesses. This will enable better approximation of heat transfer in those intermediate thickness steels used in many structures and pressure vessel applications, with a consequent improvement in quality.

Application of models for predicting weld thermal cycles to many industrial operations is exacerbated by the inability of equations to model complex joint configurations. A feasibility study and review of the literature suggests modelling fillet welded joints is particularly troublesome since it is observed that a thermal discontinuity is present in most circumstances. The derivation of analytical solutions to model this phenomena will further improve the predictive capability of welding engineers.

2.2 Research Aims and Objectives

2.2.1 Aims

To improve design and fabrication capability through consideration of process parameters and by creating or developing mathematical equations for the prediction of heat transfer activity in various thicknesses of material, and in fillet welded joints, with particular attention to the semi-automatic welding processes.

2.2.2 Objectives

To establish the effect of electrical, thermodynamic, and physical process changes on welding output.

To conduct research into the effect of changes to electrode extension in semi-automatic arc welding.

To prove a definitive link between current drawn, penetration, joint design and electrode extension in a constant potential constant wire feed system.

To improve design and fabrication capability by considering, developing, and validating mathematical equations for the prediction of heat transfer activity in intermediate thicknesses and complex joint configurations displaying thermal discontinuities during the semi-automatic welding processes.

2.2.3 Restrictions

Research is limited to hypo-eutectoid steels, having a thickness range between 10 mm and 30 mm, in the semi-automatic arc welding processes, below 500 amps, in the bead on plate and T-fillet joint configurations.

3. Review of welding processes and heat transfer

3.1 Introduction

The process of welding appears to be defined in three distinct areas of expertise, namely, the physics of welding, the metallurgy of welding, and the mechanics of welding.

In the first two domains, as the subject has become more quantitative, the requirement for a good knowledge of mathematics has increased. Mass flow in welding is not readily comprehensible without a good knowledge of fluid dynamics, which in turn requires expertise in vectors and vector analysis through applied mathematics, (Lancaster, 1984, p. vi). Certain knowledge of gas interactions is necessary, coupled with magnetic and electrical phenomena, and a good understanding of the laws of physics including elementary quantum physics and thermodynamics, need to be combined to attain reasonable levels of metallurgical knowledge and heat flow. The phase changes involved in interaction across the arc, typically through all states of solids, liquids, gases, and finally, high speed plasmas, are important base concepts, and these must be thoroughly understood.

The third domain of welding consists of the application of the mechanics of applying the various processes, namely the design of weldments and edge preparations, methods of applying pre-heat and post weld heat treatment, run sequencing, process selection and techniques, and these are principally the function of the welding engineer, (Lancaster, 1987, p. 4).

3.2 Process Quality, Physics of Welding and Welding Metallurgy

3.2.1 Process quality and assessment

The worldwide desire to raise quality standards promoted by the ISO 9000 series (formerly in Britain and Europe, BS 5750, and EN 29000), has led to an increase in the use of full quality systems. As these are principally organisational, they place greater reliance on procedures and instruction sets, and in welding these are now evident mainly in the form of the ASME IX and BS EN 288 standards. The European Standard BS EN 288 substantially replaces BS 4870 and has had full effect since 1992. Whilst it is possible, by reference to BS EN 288 Part 1 (5.2), and BS EN 288 Part 6, 'Approval related to previous experience', to approve a current Welding Procedure Specification by reference to satisfactory authenticated welding experience (such as procedures approved under BS 4870, BS 2633, BS 2971, or BS 5135), this could well lead to the use of procedures which do not comply with the stringent requirements of BS EN 288 Part 3, and BS EN 25817. This is particularly likely if the test piece is of thin walled section. In the main therefore, and in any event all new procedures, will need to be re-assessed and re-tested before approval may be certificated.

Guidance on quality levels for imperfections is expounded in BS EN 25817:1992, and is used to establish the acceptability of welds when seeking compliance with BS EN 287 or BS EN 288.

Generally, procedure and welder approval tests follow the accepted global restrictions on fusion, penetration, micro-fissures/cracks, and porosity, but tightened restrictions on cap and root bead height exacerbates the problems encountered with inherent defects common to the MIG/MAG processes, (Welding Handbook, 1991, p.146-149), (see Table 3-1 below).

	BS 4870/4871	ASME IX	BS EN 287/288/25817
Volumetric NDT	100%	Optional	100%
Individual Solid Inclusions	l=0.5g 6mm max w=1.5 mm max	3 mm max	0.3g 3 mm max
Linear Solid Inclusions	8% of 12g by length	1g of 12g by length	N/A
Indiv. Porosity	0.25g 3 mm max	0.2g 3 mm max	0.3g 3 mm max
Group Porosity	2% by area	7% by area approx.	4% by area
Elongated Indications	l=6 mm max w=1.5 mm max	0.2g 3 mm max	0.3g 2 mm max per 100 mm
Cap Height(#)	Smooth, no max	N/A	1 mm + 0.1 cap dim. max 5 mm
Excess Penetration(*)	3 mm max, some excesses perm.	N/A	1 mm + 0.3bead dim. max 3 mm

Cap height #

Root penetration
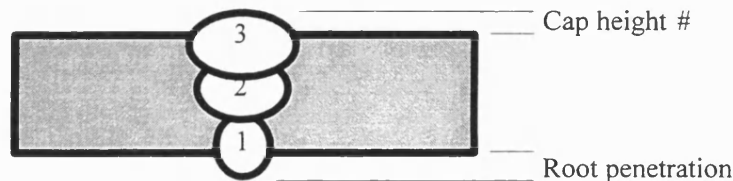
Table 3-1 : Comparison of Quality Guidelines in Welding - Guide for Butt Welds 3mm to 10mm in thickness

The use of flux cored electrodes markedly assists in the reduction of porosity, as the chemical composition of the gas in solute which would give rise to the cavity, has been reduced by the interaction of flux agents, which have deoxidised or denitrified both the liquid metal from the electrode, and also in the weld pool prior to solidification, (Welding Handbook, 1991, p. 169). This is also a particularly efficient reaction, assisting the plasma column equilibrium by causing multiple ionisation, since the first, and sometimes the second stage ionisation potential of the most common core elements within the electrode are all below that of the first stage ionisation potential of the argon shielding gas, (The Physics of Welding, 1984, p. 15), (Welding Handbook, 1991, p. 170).

3.2.2 Physics of welding - Gas shielding in semi-automatic welding

The delivery of the shielding gas to the area surrounding the arc and the weld pool has remained substantially unaltered since the process was introduced in the 1950's. The supply of gas at reasonable flow rates through a tubular shroud is effective in reducing defects, but is extremely susceptible to side draughts. Additionally, chemical composition of the gas is extremely important in the effective maintenance of the arc column and internal plasma jet stream.

The action of the arc is extremely complex even in relatively stable working conditions such as those experienced in tungsten inert gas arc welding, and more so as the electrode composition is constantly changing from solid through liquid to vapour and undergoing severe magnetohydrodynamic forces. The result of this violence is that the surrounding gas shield is subject to turbulence precisely at the time when it should be at its most stable if it is to contribute effectively to the maintenance of virtually total thermal equilibrium by ensuring optimisation of electron collision through the ionisation of the gas.

This whole problem is compounded by the fact that the shielding gas shroud and contact tip is being moved in relation to the work piece as welding progresses. It has been reported by (Okada, Yamamoto, and Harada, 1979), using a He-Ne laser as a light source with a band pass filter, that eddy turbulence occurs behind the shielding gas shroud, particularly at low flow rates. This reporting further confirms that it is reasonable to assume that oxygen and nitrogen from the atmosphere **can** combine with the molten electrode moments before it strikes the weld pool, and furthermore in sufficient quantities to induce both porosity and cavity creation, notwithstanding the fact that the introduction of diatomic gases to argon may alter the rate of absorption, (Lancaster, 1987, pp. 53-69).

Porosity will occur, when nuclei for the heterogenous nucleation of bubbles are present in the supersaturated weld metal, (Lancaster, 1987, p. 72), and the rate of

escape of the bubbles is less than the rate of solidification. Under marginal conditions, this will form at the weld boundary, whereas elongated indications will form at the solidus/liquidus boundary, and progress as solidification occurs. Since the material transferred across the arc may be supersaturated with atmospheric gases if the shield has been disturbed, the efficiency of the chemical reaction provided by the flux core is reliant upon the slag-metal interaction in the weld pool. Should the supply of reagent be insufficient, porosity will occur to some degree. Progress has been made in the development of flux compositions, but it is important to give further attention to ensuring the adequacy of shielding gas as welding takes place.

It has been reported, (Lancaster, 1987, p. 151), and (Raja, Rohira, Srinivasmurthy, and Ramura, 1989), that the outer metal sheath of the cored electrode, melts at a faster rate than the flux core, thereby acting in a manner which is the reverse of a manual metal-arc electrode. Further, by photography, it has been shown that the central flux tapers, and is surrounded by the plasma column, as the arc root is at the metal sheath, not the flux core. This suggests that any deterioration in the cover provided by the shielding gas, would permit instantaneous reaction of the liquid portion of the electrode with the atmosphere. It is therefore reasonable to assume that the gas, (oxygen and nitrogen), in solution, are transferred into the weld pool directly, not by poor reaction with the flux agents in the plasma column, but by inconsistent protective gas shielding. Even with adequate shielding, (as exists most of the time), care must be exercised, since excesses of an oxidised metallic element will affect the mechanical properties of the weld, notwithstanding that this assists compliance with the standards by minimisation of porosity.

3.2.3 Metallurgical Discontinuities - Lack of Fusion

Lack of fusion at the root, side wall, or inter-run, causes inconsistencies in the quality of the process as a whole. Despite recent advances in the creation of synergic pulsed MIG/MAG and semi-robotic machinery, one must make a basic observation that the size of the arc emanating from say a 4mm manual metal arc electrode to that of say a 1.2mm solid or cored wire is very different, despite their similarity in deposition rate. This leads to the supposition that fusion problems are being encountered through the inconsistencies in overall size and the directionability of the arc, and this markedly affects the ability to maintain optimum temperatures at the faster travel speeds in MIG/MAG welding. The advancements in a number of cored electrodes enhance deposition, but these are generally unsuitable for thin walled sections.

A welding power source has individual volt-ampere output characteristics, and in MIG/MAG this is principally linear. Subject to the arc length being self adjusting, variations in voltage affect the spread of the arc, and the area of penetration appears to be determined by the heat of the molten metal transferred as droplets or vapour, and the depth of penetration by their impact in the molten weld pool, (Essers and Walter, 1979). The mode of metal transfer changes with current output, (see Section 3.5.3 below), but any increases in electrode extensions, reduce the current level at which modes change, since the ohmic heating effect weakens the boundary between the liquid drop and the solid tip, resulting in an increase in the drop frequency, (Rhee and Kannatey-Asibu Jr, 1991).

3.3 Process Descriptors

In order to correctly confirm opinions for drawing specific research objectives it is necessary to review all major welding processes, their development, and their

current state. The number of processes in this diverse field is extensive and hierarchical listings have been drawn up for use principally in the European Union and EFTA countries on the one hand, and the Unites States of America and the rest of the world on the other.

These are grouped into six main classifications as detailed in Table 3-2.

1	Arc welding	
2	Resistance welding	
3	Gas welding	
4	Pressure welding	
7	Other welding	
9	Brazing, soldering and braze welding	
Reference numbers 5, 6 and 8 are not used		

Table 3-2 : Main welding groups

Due to space restrictions it is not possible in this thesis to summarise any other than the six leading, (general engineering and fabrication), fusion welding processes where heat input is provided by an electric arc.

These are:-

111	Metal-arc welding with covered electrode
114, 136 and 137	Flux-cored wire metal-arc welding with or without an inert or active gas shield
121	Submerged arc welding with wire electrode
131 and 135	Metal-arc inert or active gas welding
141	Tungsten inert gas arc welding
15	Plasma arc welding

Processes and process variations, their descriptors and codes as detailed above may be found in BS EN 24063:1992, (ISO 4063:1990).

3.4 Metal-arc welding with covered electrode

3.4.1 Overview

Metal-arc welding with a covered electrode, is an arc welding process in which coalescence of metal is achieved by heat from an electric arc between the tip of a solid or cored metal electrode and the parent metal being welded.

This process is one of the most widely used welding processes, (Lancaster, 1992, p. 26, and Welding Handbook, 1991, p. 44). Its major disadvantage is that it is manual, and welding is discontinuous. As such it has limited potential in main stream production environments though its qualitative output and flexibility makes it widely used for short run work, and ease of use and portability of equipment enables it to be used in traditional site work. The process is capable of good quality output, with reliance on technique by the welding operative.

The process uses electrodes which are coated with a flux capable of generating a gaseous protective shield, with slag forming properties, and elements which assist ionisation in the arc, and are manufactured with or without a core which may contain additional elements. The utilisation of cored electrodes permits an increase in deposition rates and the creation of an alloy weld metal. The electrode content is closely matched to the material to be welded and improvements to the process are unlikely outside the development of flux formulations. The heat generated at the tip of the electrode enables temperatures of approximately 5000°C to be achieved, thereby enabling almost instantaneous melting of the parent metal and the tip of the electrode.

3.4.2 Power sources

The power source used for this process may be either alternating current, (AC), or direct current, (DC). Each source has its own limits and correct operation of electrodes depends on matching to the application with the power source and electrode polarity and operating range.

Recent improvements in transformer/rectifier design now include a range of inverter type power sources achieving reduction in their size and weight thus enhancing portability and ease of operation, particularly in site work.

The equipment must be capable of delivering a constant-current output rather than a constant-voltage, as the 'flat' characteristic produced by the latter, produces a relatively large change in current for a given voltage change, (arc length). Constant-current sources permit variation in arc length with little effect on the current due to the 'drooping' characteristic.

3.4.3 Electrodes

Electrodes are classified according to application and are manufactured, tested and designated mainly in accordance with BS EN 499:1995, 'Welding Consumables - Covered electrodes for manual metal arc welding of non-alloy and fine grain steels'.

Designation of electrodes through a numbering/lettering code system enables selection of electrode and close matching to specific application requirements. The code indicates such items as, strength and elongation, impact properties, chemical composition and type of covering.

Electrodes as mentioned are covered with a bonded flux which may be acid, cellulosic, rutile, or basic, or a combination.

Acidity of fluxes are indexed, and one widely accepted formula recognised by the International Institute of Welding (IIW), is the Basicity Index, (BI), as detailed in Equation 3.1, below.

$$BI = \frac{CaO + CaF_2 + MgO + K_2O + Na_2O + 0.5\,(MnO + FeO)}{SiO_2 + 0.5\,(Al_2O_3 + TiO_2 + ZrO_2)}$$

Equation 3.1

where oxide or flouride contents are in weight %.

The welding characteristics and mechanical properties of a covered electrode are influenced by the homogeneous mixture of substances in the covering, (BS EN 499). The Standard most adequately describes the different coverings in Annex A to the Standard. By reducing the organic content of the flux coating, notch characteristics may be improved through the decrease in hydrogen content of the weld metal, as detailed below.

Description	Index
acid	less than 1
neutral	1 to 1.5
semi-basic	1.5 to 2.5
basic	over 2.5

Table 3-3 : Basicity of a flux according to the IIW Basicity Index (BI)

3.4.4 Applications

The process is quite flexible and may be used to join a wide range of materials including carbon steels, low alloy steels, stainless steels, cast iron, copper, nickel, aluminium and aluminium alloys.

The process is dependent upon short electrodes and these cannot be used satisfactorily below approximately 1.6 mm material thickness, but contrarily there is no real upper limit save for the time taken to deposit, and where deposition rates need to be maximised it may be more appropriate to select submerged arc welding or flux cored arc welding.

Applications are diverse, as the process requires relatively simple equipment, and is used confidently in workshop or on site in ships, bridges, cross country pipe-lining, or general fabrication and construction.

3.5 Metal-arc inert or active gas welding

3.5.1 Overview

This semi-automatic welding process produces coalescence of metal by heat from an electric arc between a consumable wire electrode and the work-piece with shielding gas providing a zone of exclusion around the arc to inhibit the ingress of the surrounding atmosphere which would be deleterious to the weld.

It was introduced in the 1920's, (Welding Handbook, 1991, p. 110), and was commercially available in 1948. Originally using only an inert gas to shield the arc, principally in the welding of aluminium, it became known by its acronym MIG, (metal inert gas), but as the process has developed to use low current

densities and reactive gases such as carbon dioxide, it should now be more correctly referred to as **either** metal-arc inert gas welding, (MIG), **or** metal-arc active gas welding, (MAG).

The principal use of solid wires in this process is supplemented with cored wires which is discussed extensively elsewhere in this review.

The description as a semi-automatic process refers to the self regulation of the electrical characteristics of the arc and consistent feeding of consumable electrode. It is normally operated with a hand held gun but lends itself to mechanisation and the use of robotic welding cells enjoying substantial increases in productivity over metal-arc welding with a covered electrode and increases in consistency of quality in all positions where it has advantage over submerged arc welding.

The equipment consists of a power source and motorised wire feed unit with gun assembly, cabling and liners to transmit electricity, shielding gas and wire electrode. The gun normally houses a trigger micro-switch to activate the wire feed motor and gas solenoid.

3.5.2 Power Source

The power source is a constant-voltage power supply transformer/rectifier or inverter. The process operates using direct current normally with the electrode positive utilising medium currents with low voltage.

Recent advances in computerisation enable the use of micro-processor control to adjust the waveform and this permits pulsing.

3.5.3 Metal transfer

The International Institute of Welding, (IIW), classifies metal transfer, (The Physics of Welding, 1984, p. 210), into three basic groups as detailed in Table 3-4.

Transfer Type		Welding Process (example)
1	**Free flight transfer**	
1.1	Globular	
1.1.1	Drop	Low current MIG/MAG
1.1.2	Repelled	CO_2 MAG
1.2	Spray	
1.2.1	Projected	Intermediate current MIG/MAG
1.2.2	Streaming	Medium current MIG/MAG
1.2.3	Rotating	High current MIG/MAG
1.3	Explosive	Covered electrodes
2	**Bridging transfer**	
2.1	Short-circuiting	Short arc MIG/MAG
2.2	Bridging without interruption	Welding with filler wire addition
3	**Slag protected transfer**	
3.1	Flux-wall guided	Submerged arc welding
3.2	Other modes	Covered electrode, Cored wire, Electroslag

Table 3-4 : IIW Classification of transfer types

There are three basic transfer modes in MIG/MAG welding. These are

1   Short circuiting transfer

2   Globular transfer

3   Spray transfer

These transfer modes depend on a number of factors, (Welding Handbook, 1991, p. 112, 113), of which the most important are,

1   Magnitude and type of current

2   Electrode diameter

3   Electrode composition

4   Electrode extension

5   Shielding gas

Briefly, the short circuiting transfer type occurs only at low currents and depends on the consumable electrode short circuiting the arc, whereupon metal is transferred into the weld pool. When the short circuit occurs, the wire electrode melts as a combined result of Joule heating, with conduction, radiation and convection from the weld pool and arc. As the electrode melts the arc is re-initiated. At certain stages, spatter may develop due to the liquid metal bridge between wire electrode and oscillating weld pool superheating and exploding through almost instantaneous vaporisation. To control this tendency toward explosive separation, the rate of current increase is controlled by inductance of the power source to permit heating of the electrode, but avoid violence in the arc, and therefore spatter. Whilst metal is only transferred during short circuiting the choice of shielding gas may affect the final weld deposit. Additions of Oxygen (O_2) reduce surface tension in the weld pool and Carbon Dioxide (CO_2) promotes deep finger like penetration, though with higher spatter levels due to a tendency toward volatility and explosion in the arc.

Globular transfer occurs at most current ranges in two primary types, (drop and repelled). As discussed by Lancaster in (The Physics of Welding, 1984, p. 209), the use of carbon dioxide shielding gas promotes random globular transfer, the drops formed being repelled away from the weld pool prior to final necking and mass/gravitational attraction into the weld pool. The Lorentz pinch effect is primarily responsible for droplet detachment and is a consequence of the electromagnetic forces at the end of the electrode. In circumstances where globule detachment causes short-circuiting the resulting liquid bridge is commonly vaporised which is why pure carbon dioxide welding is less favourable in manufacturing, (spatter), notwithstanding its low cost.

If the shielding gas used is essentially argon rich, it is possible to move to the next group of transfer modes, that of spray transfer.

Spray transfer is highly dependent on the factors mentioned above, and for each diameter wire, there is an optimum range above which spray transfer occurs. In recent work, (Kirk, Mileham and Yeo, 1995b) suggest that this transition current occurs as a result of a sinusoidal wave pattern at low currents decreasing in intensity, becoming flat in aspect as the transition current is approached, at which stage the mechanism of transfer appears to change. This phenomena, suggests therefore that the change to spray transfer may not be instantaneous, but may well be a function of the gradually increasing current density.

Regardless of the transition current at which spray transfer occurs, the function is dependent on the type of shielding gas. When shielding gases contain more than approximately 10% carbon dioxide, transition to spray transfer is inhibited due to the size of the globule and its repelling nature. Thus when welding using high currents with an essentially CO_2 shielding gas, (or argon with high % of CO_2), the transfer is globular, and at low currents the most effective transfer is short circuiting.

Spray type transfer is advantageous in terms of both deposition and penetration, but is a little more difficult to control due to the heat and fluidity of the weld pool, and thus its use in all positions, whilst quite possible, is limited to certain conditions. Additionally, it is not readily effective for welding thinner materials and therefore the availablitiy of micro-processor, imbalanced, controlled waveforms, is exploited through pulsing of the arc. During the early stages of development, pulses were only available at mains frequency or multiples thereof, (Lancaster,1992, p. 36). As electronic programming improved, the resulting pulse variables, have, in Great Britain, been called 'synergic algorithms', with power sources having 'synergic control', (Lancaster, 1992, p. 37). The effect is to produce background control of current for melting of the electrode and higher pulses of current to project the melt in spray transfer mode.

3.5.4 Shielding Gases

This is discussed in detail in the section on flux-cored wire metal-arc welding with or without an inert or active gas shield. The coding and content of shielding gases is detailed in BS EN 439:1995, 'Welding consumables - Shielding gases for arc welding and cutting'.

3.5.5 Consumable Electrodes

Specifications for wire electrodes are determined by application standards and generally by BS EN 440:1995, 'Welding consumables - Wire electrodes and deposits for gas shielded metal-arc welding of non alloy and fine grain steels'. This standard provides a coding system detailing strength and elongation, impact properties, and chemical composition. The standard relates to the shielding gas used as detailed by BS EN 439:1995 mentioned above. The standard refers to the

chemical composition of the wire consumable in its manufactured state, and not to its deposited matrix, which is reserved for cored wires.

Wires in this class are solid or contain powdered metallic mixtures within a core. This permits addition of elements which would detract from manufacture in a wire form. They are frequently coated with copper to assist reduction of friction in the wire liner, and to promote electrical conductivity and corrosion resistance in storage.

3.5.6 Applications

The process may be used for a wide variety of applications depending on application approvals. Such approvals, (Lloyds Shipping, etc.), are only granted for specific combinations of shielding gas and electrode composition. Whilst the process exhibits good productivity, particularly when compared with welding using a covered electrode, it has a number of inherent defects such as porosity, incomplete fusion and incomplete joint penetration, and special considerations to provide adequate inspection are necessary in critical joints. In a number of application, welder approval, and weld procedure approval standards, the process is subject to additional destructive tests, success in which is mandatory before approval is granted.

3.6 Flux-cored wire metal-arc welding with or without an inert or active gas shield

3.6.1 Introduction

In the application of welding engineering it is vital to select filler metals which will produce deposits which closely match the mechanical and metallurgical

properties of the parent metal, or, in the case of surfacing, enhance its qualities; and in all cases to a quality level established to negate any incidence of failure due to defect.

As the weld metal solidifies it will possess its own unique metallurgical properties, and these will be affected by critical cooling rates, which themselves are relative to the process and thickness and grade of material being welded. Observance of critical cooling rates is paramount to achieving reduction of metallurgical disturbances in the heat affected zone (HAZ) and correct welding procedures are necessary to maintain optimum values in all welding and service conditions.

In process selection, designers, fabricators and manufacturers need to be aware of the selection constraints which may affect outcome of the final structure or product, and the costs which accompany their decision.

Welding by means of metal-arc welding with a covered electrode, is long established and is the traditional choice of designers due to its proven effectiveness in a variety of circumstances. However, in many cases, flux-cored wire metal arc welding with or without an inert or active gas shield (FCAW), may be utilised to provide equivalent metallurgical and mechanical properties but with a significant increase in productivity, and with a potential for lowering of costs.

In the specific case of welding with such a cored (tubular) wire, many objections are raised on the basis of cost of consumable alone, (compared with solid wires as an example), without full observance of the fact that cored wire technology is not primarily intended to provide an alternative to gas-shielded solid wire welding in the general fabrication of thin sections, but provides a complementary or alternative process to metal-arc welding with a covered electrode. That is to say, cored tubular wires are continuous electrodes which provide substantially the

same (or better) deposition characteristics as the covered electrode with the convenience and versatility of solid wire welding.

3.6.2 The Process

The cored (tubular) wire welding process uses a power source which is substantially the same as that used for metal-arc welding with inert or active gas shield, in that it utilises a direct current output which displays flat characteristics with at least a DC positive electrode. (Some cored wires effectively use DC negative electrode polarity, and in most cases can utilise higher currents than that for solid wire, similar to submerged arc welding, (SAW).

The consumable wire used, is of tubular construction and operates with or without a shielding gas of carbon dioxide (CO_2) or carbon dioxide with argon mix (CO_2,Ar). In the Americas, helium is widely used in place of argon due to the cost effectiveness of utilising substantial underground reserves. Gas flow rates, where used, are at the rate of 10-20 litres per minute.

The gun used with the process is essentially the same as that used for solid wire (MIG/MAG) welding, though water cooled units are required at higher currents.

Capital cost for such equipment is approximately 3 times that of AC manual metal arc welding equipment, and approximately 2 times that of DC manual metal arc welding equipment.

3.6.3 Consumables - Shielding Gases

Unlike solid wires, cored wires are analysed on the actual weld metal deposited rather than on just the chemical analysis of the original wire. This is because the

final alloys depend much on the chemical reactions in the arc column and weld pool, since the tubular wire is filled with dry powder constituents. For this reason it essential to use all cored wires in accordance with manufacturers guidelines for selection and use of appropriate shielding gas if correct chemistry of deposit is to be achieved as some reactions are deleterious to the mechanical properties in service.

The core of the wire contains a number of elements and these include deoxidisers and denitrifiers. Carbon dioxide shielding gas, used to advantage in FCAW because of its low cost and ability to increase temperature and penetrative aspects, whilst relatively inactive at room temperature becomes metastable at high temperatures and dissociates in the arc to carbon monoxide (CO) and oxygen (O), (Welding Handbook, 1991, p. 159), as shown below.

$$2CO_2 \rightarrow 2CO + O_2$$
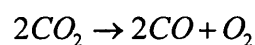
The result is that the shielding gas becomes extremely reactive and this must be counteracted by deoxidisers contained in the core of the electrode (principally aluminium [Al]). However, in addition to dissociation in the arc, carbon dioxide can react in a reversible reaction with iron at elevated temperatures as in the following chemical equation.

$$Fe + CO_2 \leftrightarrow FeC + CO$$

the carbon monoxide liberated, dissociates to carbon and oxygen, thus;

$$2CO \leftrightarrow 2C + O_2$$
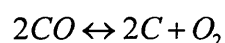
Such reversible reactions can affect the balance of carbon within the weld metal due to the carburising effect in metals with less than approximately 0.05% carbon and the decarburising effect in metals with more than approximately 1.0% carbon,

(Welding Handbook, 1991, p. 169). In the arc column, any gases formed may be dispersed, but when transmitted to the weld pool as a supersaturated solution, carbon monoxide gas evolves to form bubbles of gas which may not escape as the weld pool solidifies and will thus contribute to porosity. (Kirk and Mileham, 1994).

As noted above, deoxidisers are added to negate any potential for the carbon to oxidise by addition of elements which have greater affinity for oxygen than that of carbon. These elements are principally aluminium, silicon and manganese. The chemical reactions are;

$$Si + 2O \rightarrow SiO_2$$
$$2Al + 3O \rightarrow Al_2O_3$$
$$Mn + O \rightarrow MnO$$
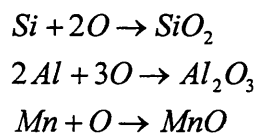
Thus, the quantity and type of non-metallic deoxidation products generated, are directly related to the specific shielding gas and deoxidants used. In an ideal reaction, these will float to the surface of the weld pool and become incorporated in the slag cover, leaving less than 0.05% metallic aluminium in the weld metal with a consequent reduction in the effect on the mechanical properties of the weld, (Welding Handbook, 1991, p. 170).

Consequently, use of wires which are formulated for use with 100% carbon dioxide shielding gas should only be used with that gas, as, if for example, Ar 80%, CO_2 20% were used, it is likely that surplus aluminium or other deoxidants would exist in the weld pool in their elemental form and, (in this example), would increase propensity to brittleness of the weld metal.

Conversely, a wire formulated to be used with an argon mix gas shield (say Ar 80%, CO_2 20%) would give a very porous weld with a shielding of 100% CO_2, as insufficient deoxidisers are present in the wire to absorb the dissociated oxygen.

3.6.4 Consumables - Electrodes

The consumable cored tubular electrode is a hollow, low carbon or stainless steel sheath, filled with dry powdered elements and compounds.

Cored wires are classified as gas-shielded or self-shielded (those which do not require additional external gas shielding). Core contents vary from manufacturer to manufacturer but consist mainly of elements and compounds which act as deoxidisers, denitrifiers, slag formers, arc stabilisers, shielding agents, and alloying elements depending on desired properties of deposit, which enhance strength, hardness, toughness, creep resistance and corrosion resistance. Chemical formulations are closely guarded commercial secrets and some are protected by patent.

The advantage of cored wires is that because the additives are held in a protective sheath they do not require the addition of binding agents (necessary with arc welding electrodes to bond the flux and additives to the outside of the electrode), and thus they are less sensitive to moisture pickup with consequential reduction in diffusible hydrogen. Thus, even rutile (cost effective flux composition) electrodes give a relatively low hydrogen deposit. This being the case, tubular electrodes require only moderate storage conditions as solid wires, and do not require baking prior to use. Significantly, the diffusible hydrogen from some electrodes can be as low as 3ml/100g improving reduction in propensity to hydrogen cracking.

Most cored wires operate with a DC positive polarity, but by controlling the ionisable materials in the core, some wires can operate using a negative electrode polarity, (Welding Handbook, 1991, pp. 170, 171), enhancing the penetrative and deposition rate of this welding process. Such polarity change was previously difficult to use with the MIG/MAG process without the addition of a 5% O_2 shield requiring the use of deoxidisers or by treatment of the wire with coatings to make it thermionic, and consequently increasing cost.

Flux compositions, as with their covered welding counterpart, contain titanium dioxide, [rutile], (TiO_2); or basic, containing calcium carbonate, [limestone], ($CaCO_3$); or calcium fluoride, [fluorspar], (CaF_2).

3.6.5 Applications

As previously mentioned, designers may insist on the application of processes at the design stage, and the use of a covered electrode may erroneously be demanded without consideration of alternatives. In particular more attention may be made of the approvals given to electrodes than to the process, and as solid wire welding electrodes may not attract adequate approvals, use of covered electrodes may be determined from ignorance rather than through preference.

In establishing process selection either at the design stage or later at the manufacturing or fabrication stage, automation is considered, and for large scale operations use of SAW may well be desirable with its continuity of high integrity deposit and accuracy of joint. However, in smaller developments particularly where joint access is limited, manual or semi-automatic welding processes are used. In general fabrication, the solid wire process (MIG/MAG), displays advantages with its relatively low consumable cost, though an absolute assurance of quality is diminished with inherent defects, (Kirk and Mileham, 1994), and care needs to be exercised depending how critical the joint is. In a number of cases where a critical application is under review, use of covered electrodes is the first consideration with its exceptional track record and approval of electrodes. However, with further evaluation of economic considerations, such a process demonstrates significantly poor deposition rates, and whilst not a major problem in countries where labour pay rates are low, is of particular concern to all where cost of downtime of a plant is considered. Each consideration is therefore based mainly on requirements for weld integrity and criticality, cost of labour, cost of

downtime, and cost of maintenance scheduling with preservation of optimum output.

Use of cored wire technology is commonplace in the United States of America and Japan, and now accounts for a substantial proportion of weld metal deposited. In the United Kingdom however, the technology is generally used only in offshore work and specialist applications, for, as in the majority of countries, concern over consumable cost appears to dictate process selection, seemingly without regard for considering management techniques which could demonstrate that alternatives may provide better profitability and productivity.

3.7 Tungsten inert gas arc welding

3.7.1 Overview

The tungsten inert gas arc welding process produces coalescence of metal through heat produced by an electric arc between a non-consumable electrode and the work-piece within a gas shield, inhibiting ingress of the atmosphere.

It is capable of producing high quality welds and is used extensively in a wide range of industries.

The possibility of using helium to shield the arc and weld pool was first investigated by Hobart in 1920, (Welding Handbook, 1991, p. 74), but it was not until the 1940's that the process was developed more extensivly, initially to weld aluminium and magnesium.

In Europe the terminology suggests a restriction to inert gas alone, but it should be noted that under certain conditions, non inert shielding gases may be used, and the

general section description in BS EN 24063:1992, at **14,** of 'Gas-shielded welding with non-consumable electrode', permits process variations to be added.

3.7.2 Power Sources

Advances in transformer/rectifier technology with the introduction of inverter equipment greatly extends the process through the availability of smaller, lighter power sources.

The process utilises an alternating current, (AC), or direct current, (DC), constant current power source, depending on the material to be welded, and these supplies are available generally in AC sine wave, AC square wave, DC and pulsed DC.

By using AC, the process is most effective in welding aluminium and aluminium alloys, as the reverse cycle assists in breaking down tenacious surface oxides.

As the AC supply undergoes a cyclical reversal of polarity, the arc will be extinguished as the current decays to zero and the thermionic tungsten electrode becomes positive, as it is not able to transmit electrons until the voltage is raised sufficiently to initiate cold-cathode emission, (Welding Handbook, 1991, p. 86). To negate this, the process utilises high frequency, high voltage sparks in parallel with the arc, and combined with an inert shielding gas such as argon which has a low ionisation potential, extinction of the arc may be avoided.

Utilisation of micro-processor controlled power sources permits variation of the balance of the sine waves or square waves and this may be used to good effect in promoting oxide clearance and balancing of the current and voltage flow to reduce the need for reduction in power rating, (overheating), caused by the core magnetisation due to the DC component.

3.7.3 Non-consumable electrodes

Electrodes are manufactured in a number of sizes and are for use with different applications. Those manufactured for use with DC usually require that the electrode be set to DC electrode negative, (DCEN), as with the electrode set positive, (DCEP), the electrode will not have the cooling effect due to electron evaporation, but conversely heated by electron bombardment. Thus, a given DCEN electrode would only handle approximately 10% of the current if set up as DCEP.

Electrodes for DC welding are pure tungsten with additional elements to promote current carrying capacity and greater stability of the arc.

Thorium oxide, (ThO_2), (thoria), is a low-level radioactive material which is added to the pure tungsten in small amounts, (1% to 2%). The effect is to increase current carrying capicity by approximately 20% and promote arc striking. The thoriated electrode is designed for DCEN application and although it may be used for AC it is not desirable as it is difficult to maintain the balled end and tends to overheat with electron bombardment on the half cycle.

Cerium oxide, (CeO_2), (ceria), is not radioactive and was developed and used from 1980 as a potential replacement for thoriated electrodes. It is normally added (2%) to the pure tungsten to reduce vaporisation and therefore may be used with either AC or DC. It is, of course, safer!

Lanthanum oxide, (La_2O_3), (lanthana), is not radioactive, was introduced around the same time as ceriated electrodes and exhibits similar benefits. It is added as a 1% alloy.

Zirconium oxide, (ZrO_2), (zirconia), is the preferred choice for AC welding, being able to withstand erosion and overheating. It is an excellent choice for radiographic quality welding where tungsten contamination must be minimised.

Other additional classifications include additions of developmental oxides such as yttrium oxide or magnesium oxide and/or where specific arc characteristcs are required.

All the above referenced to Welding Handbook, (1991, pp. 80, 81).

3.7.4 Filler Material

Filler wire for this process is classified under a number of codes and standards. The standard, BS EN 440:1995 discussed previously, details most chemical combinations for steels, but BS 2901, (due for revision) is also used.

Filler wire for the process is usually administered manually, but the process to some degree, lends itself to mechanisation and the addition of hot or cold wire through wire drive systems similar to MIG/MAG applications is becoming acceptable and leads to increased productivity, particularly in orbital welds.

3.7.5 Shielding Gases

The shielding gases detailed in BS EN 439:1995 cover most applications though it is noted that the argon produced for welding has 99.997% purity not 100% as suggested in the standard. Manufacture and containment of 100% argon is extremely expensive.

It is common in the USA to specify helium as the inert shielding gas as this is cheaper than argon as it can be extracted from vast underground reserves of natural gas in that country.

As helium is much lighter than argon a gas flow rate of two to three times that of argon is required in the flat, horizontal-vertical, and vertical positions.

3.8 Submerged Arc Welding with wire electrode

3.8.1 Overview

Submerged arc welding produces coalescence of metals by heating them with a bare metal electrode and the work-piece, submerged under a blanket of granular fusible flux. It appears first to have been developed in the USA in the 1930's, and was developed into Electroslag welding by the E O Paton Welding Institute in Russia.

The flux assists stability of the arc and determines the chemical and mechanical properties of the final weld, and is deposited via a hopper, running in front of the weld head.

The process enjoys substantial automation, (though some semi-automatic welding with hand-held guns is used), and is a popular choice for structural workshop fabrication capable of operating at up to 2000 amps in the flat position.

3.8.2 Power Supply

Several power source types may be used effectively, for example, DC constant current, DC constant voltage, AC or combination. Modern AC supplies make effective use of technology to produce a square waveform which reduces the problems of polarity reversal on the half cycle.

3.8.3 Consumables

Weld head travel is usually accomplished through tractor driven carriages, and this enables the use of thicker wires than would be available for semi-automatic welding, whilst enabling full automation. The electrodes are bare wire, or cored, (similar to flux cored arc welding electrodes), and these duplicate the complex alloys in the parent material thus enabling desired weld characteristics.

As with many wire electrodes, the solid wires are normally copper coated to provide maximum electrical conductivity whilst reducing friction in the wire liners and assisting corrosion control in storage. Wire diameters vary but are generally available in diameters between 1.6 mm and 6.4 mm, permitting a wide current application range between 150 amps to 1600 amps.

Wire electrodes are closely matched with flux combinations as the final weld analysis depends on the interaction across the arc and in the weld pool. In order to qualify for certain codes, (shipbuilding etc.), only certain combinations are approved.

Whilst the normal mode of operation is with a single wire, some process variants use double, triple, single wire with a hot wire, or metal powder additions to assist deposition and productivity. At current densities above 125 A/mm^2, electrode

extension is an important variable, (Welding Handbook, 1991, p. 214). Electrode extension, (contact tip to work-piece distance, see Table 3-5 below), may be increased to assist the burn-off rate. This occurs as a consequence of the increased heating of the wire electrode, and the increased wire feed speed, but at long extensions, problems occur with arc wander, and these are therefore reserved for surfacing applications, where both high deposition and low penetration are desirable, and the poor arc control is within acceptable limits.

Electrode diameter		Max. Electrode Extension
2.0 mm	}	
2.4 mm	}}	75 mm
3.2 mm	}	
4.0 mm	}	
4.8 mm	}}	125 mm
5.6 mm	}	

Table 3-5 : Suggested maximum electrode extensions in submerged arc welding,
(after Welding Handbook, 1991, p. 215)

3.8.4 Fluxes

Fluxes as before mentioned provide natural shielding of the arc and assist in determining the chemical and mechanical properties of the final weld.

Fluxes are available in a fused or bonded form and may be mechanically mixed for highly critical welding operations. Fused fluxes are made from dried mixed

materials which are then melted in a furnace. Such fluxes are chemically homogenous and normally not hygroscopic, but as a result of the manufacturing process their ability to retain deoxidants is limited. Bonded fluxes are similarly made from dried materials but the mixture is bonded with potassium silicate or sodium silicate, pelletised and baked at low temperature, with consequent improvement in retention of deoxidants and alloying elements. Bonded fluxes are hygroscopic and commonly contain chemically bonded H_2O, and storage requirements are therefore similar to manual electrodes.

3.8.5 Applications

Submerged arc welding is widely used for pressure vessel, ship, bridge and structural welding, as it is highly adaptable to automation. It is capable of high deposition and penetration rates, whilst also enabling effective monitoring of weld quality.

3.9 Plasma arc welding

3.9.1 Overview

Plasma arc welding is an arc welding process which produces coalescence of metals by transfer of energy through a constricted arc, either in the form of a transferred arc (between the electrode and the workpiece), or a non transferred arc, (between the electrode and the constricting nozzle.

The process is essentially an extension of the tungsten inert gas (TIG) welding process, though with a substantially higher arc density, (up to approximately 3 x

10^{10} W/m^2). By this definition of arc density the process falls within the grouping of High Power Density Welding, (Physics of Welding, 1984, p. 269).

The process appears first to have been developed as a gas vortex stabilised device by Schonherr in 1909, (Welding Handbook, 1991, p. 330), when arcs up to several metres long assisted arc research. Through work by Gerdien and Lotz, (1922), and Gage, (1953), the first cutting torches were developed in 1955, and plasma arc welding developed commercially in 1963.

3.9.2 Principles

As before mentioned, the process develops a high arc density and the arc plasma has a higher velocity due to the constriction in the nozzle.

Additional shielding gas is provided to ensure that atmospheric pickup does not occur, essentially through the medium of a gas cup similar to that in gas shielded welding. The arc constricting nozzle through which the gas passes determines the rate of flow by dimensioning the tapered electrode (similar to TIG) and an outer surround, usually of copper. The electrode is recessed into a plenum chamber and maintenance to ensure correct dimensions is necessary for correct functioning.

Due to the constriction, the arc which develops is collimated, and is stiffer than that radiating from TIG torches, and is less susceptible to changes in electrode to work piece distance, as shown in Figure 3-1.

Cathode (-)

Arc Plasma

Anode (+)
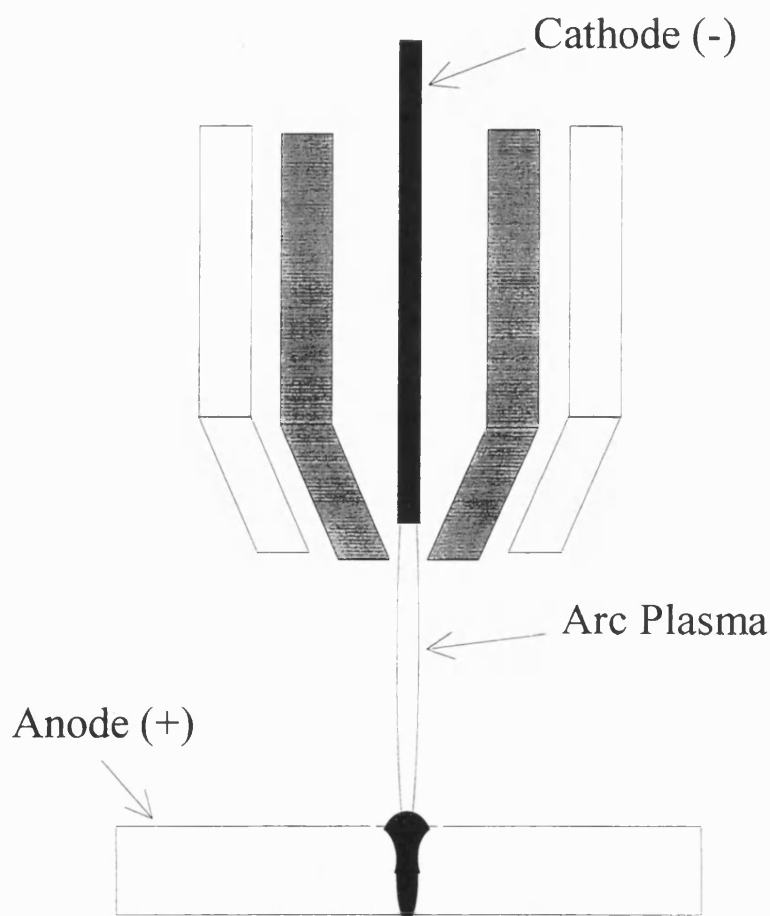
Figure 3-1 : Plasma Arc collimated plasma flow

As the gas is superheated by the arc as it passes through the plenum chamber surrounding the cathode, it expands and exits through the constricting orifice at high velocity.

Overall the relative insensitivity to changes in electrode extension and the stiffness of the resulting arc enable this process to be used in sensitive applications and it may be used for welding all materials currently welded by the TIG process.

The high current densities approach that of laser welding and, as with that process, substantial thicknesses may be welded with apparently little metallurgical disturbance and narrow heat affected zone. The non transferred arc, (not illustrated), is used for cutting and for welding non-conductive materials, (as the

plasma jet alone transfers the heat), but the transferred arc, which makes use of the work-piece to complete the circuit, generates heat at the anode through electron bombardment in addition to the heat transferred by the plasma column, (Figure 3-2, refers).
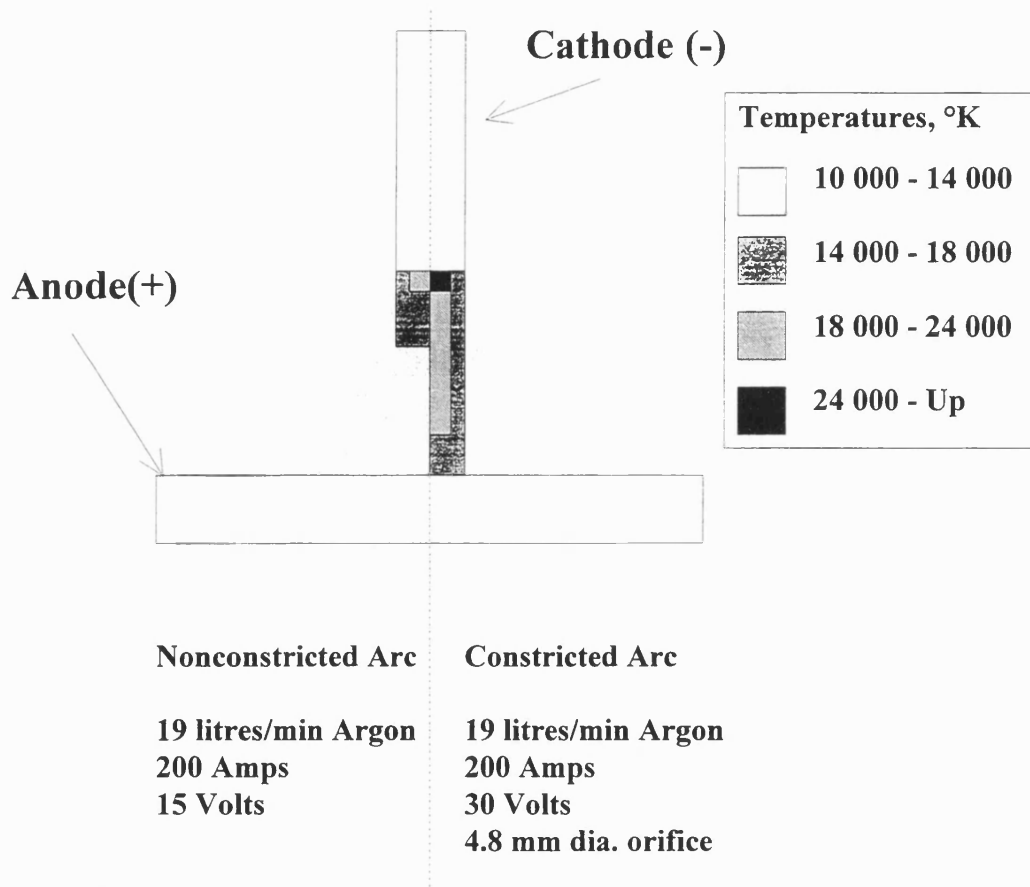
Figure 3-2 : Comparison of Nonconstricted, (TIG), and Constricted, (Plasma Arc), temperature ranges

3.9.3 Shielding Gases

Shielding gases used with the process consist essentially of argon (inert with a good ionisation potential), mixed with hydrogen (up to 15%) or helium. The choice of shielding gas depends primarily on the material to be welded, with helium and hydrogen creating a hotter arc though with a tendency to porosity if the hydrogen is excessive.

3.9.4 Applications

As a result of the controllability of the arc, the process appeals to the aerospace and nuclear industries. It is capable of delivering from 0.1 amps to 50 amps, (micro-plasma) and in medium to higher currents, (50 to 500 amps), enables single pass welding with little distortion in a range of material thicknesses from 0.25 mm to 6 mm., (penetration may be greater but single pass welding is usually limited to 6 mm.)

The process may be used on most materials with a negative electrode DC power supply with drooping characteristic and thus TIG power sources may be used adding to flexibility and efficiency in capital acquisition.

The lack of high frequency overlays, (used in TIG welding to start or maintain the arc), provides opportunity to use this process where interference may, as in the case of robots, be unacceptable.

3.10 Heat Transfer

3.10.1 Weld cooling rate theory - Survey of the literature

One of the first analytical equations addressing heat transfer in welding and cutting appears to be by Rosenthal, (1935), expanded later by Rosenthal, (1941). This is described later in Chapter 5.

Rosenthal derived equations to describe heat flow in thin plate, which he called 'two-dimensional', and thick plate, which he called 'three-dimensional', situations.

The simplified equations postulated are strictly only valid for calculation of the weld centreline, cooling rate, (the x-axis), at a point immediately behind a heat source, travelling at constant velocity. They do not account for the effect of heat transfer through convection or radiation, though this was considered briefly by Jhaveri, Moffatt, and Adams, (1962).

The restriction mentioned presents a problem which is somewhat complex, in that the point heat source creates a phase change in the metal from solid to liquid, and this absorbs some heat during transition. This is then released as "secondary" or "delayed" heat on solidification shortly behind the heat source by nature of it moving at a constant velocity. The effect of this on the cooling rate may be approximated by integrating a general factor as discussed in the literature, (Rosenthal, 1941), (Hess, Merrill, Nippes, and Bunk, 1943), and (Nippes, Merrill and Savage, 1949), but for more accurate prediction this may now be better accomplished by numerical methods.

In (Hess, et. al., 1943), complementary work to consider the effect of material thickness on cooling rates, particularly those falling between the 'perfect' thin or thick plate, introduced a 'Beta' factor which was tabulated for specific materials. These tabulations were used to effect in the creation of a system which would permit estimation of the cooling rate for a material of intermediate thickness, but many assumptions were required and the resulting method was cumbersome.

Hess, et. al., (1943), and Christenson, Davies, and Gjermundsen, (1965), showed that the equations satisfactorily predict the distance between temperature isotherms, in addition to cooling rates, for a wide range of materials, and this is also discussed in a substantial study by Rykalin, (1957), according to Christenson, et. al.. Further, Jhaveri, Moffatt and Adams, (1962), illustrated, through investigation into peak temperatures, that an estimation of the cooling rates in 'intermediate' material thicknesses could be approximated using interpolation of graphs of the thin and thick plate equation outputs.

As mentioned, the equations are strictly valid for the centreline, and in order to study the effect of heat transfer on the metallurgical implications in the heat affected zone, it is therefore necessary to move the locus of the equation from the centreline of the weld to a point in the heat affected zone. Thus, equations were postulated, (Adams, 1958), which could predict the cooling rate outside the centreline with an estimated inaccuracy of only 5% and these are referred to widely for approximate solutions. For more rigorous work, the fact remains that whilst complex, Rosenthal's equations in their full form offer good close approximation of the heat transfer in welding, given the constraints of the inaccuracies due to estimation of thermal constants. The work of Grosh, Trabant and Hawkins, (1955), attempted to mathematically equate the effect of changing thermal properties given that thermal diffusivity remained constant for various temperatures. Integration of the final equations and approximations for linear change into the Rosenthal equation are not possible, without resorting to high degree algebraic or trigonometric equations, though this has been attempted recently with the work reported by Boo and Cho, (1990), and Jeong and Cho, (1997).

3.10.2 Weld cooling rate theory and weldability - Survey of the literature

In examination of the weldability of steels, and in particular the potential to negate hydrogen induced cracking, which occurs through rapid cooling of the material below the 200°C threshold for hydrogen diffusion, Cottrell and Bradstreet, (1954), and Cottrell and Bradstreet, (1955), considered the Rosenthal equations, but pursued the use of experimental output of CTS, (Controlled Thermal Severity), tests to propose early nomographs for use in Britain.

In a study by Baker, Haddrill and Roberts, (1971), a number of practical weld tests were discussed and compared in relation to the standards imposed in Britain and those in Japan. It was suggested that in Britain, the critical hardness levels were more appropriate to the CTS tests, rather than the Y-slotted groove restraint cracking tests (a very severe cracking test used principally in Japan), and they suggested that use of a Y-groove test would lead to lower critical hardness levels being defined and thus increase the margin of safety provided by current procedural recommendations. Further, CTS tests are extremely difficult to replicate with any accuracy despite their continued use in Britain, and are therefore relegated, in their opinion, to supplementary test status. In terms of definitive tests, dilatometric, thermal analysis, fracture mechanics and implant tests are to be preferred, with chemical composition being used as a check test. In this respect, continued examination of theory is considered valid.

Later, Bailey, (1970a), and Bailey, (1970b), illustrated a substantial nomograph, which appears to have been adopted for use in the then BS 2642, and which appears later to have been developed into the range of nomographs in BS 5135.

Use of CTS tests and the experimentally determined 300°C cooling rates used by Bailey and others, creates a situation which clearly diverges away from the

theoretical equations developed in the rest of the world, and replaces them with graphical images which are used extensively in Britain.

The lack of technical training in calculating cooling rates and welding heat affected zone peak temperatures in Britain appears to fall significantly behind other parts of the world, primarily in the USA and Japan, and thus welding engineers and designers in Britain, have less experience in applying basic theorems, which, it is considered, would increase innovation, given the new ranges of steels now available.

4. The significance of wire resistivity in semi-automatic welding quality

4.1 Introduction

The use of the semi-automatic welding processes, provides increases in productivity, but inherent defects in the process (Welding Handbook, 1991, pp. 146-149), inhibit its acceptance in meeting requirements for consistent quality at a standard high enough to match the requirements of BS EN 288, or in meeting a number of the fitness for purpose requirements for many applications, notwithstanding that imperfections may be individually assessed using Engineering Critical Analysis (ECA), as expounded in Published Document PD 6493.

Flux cored arc welding, (FCAW), goes some way to reducing the inherent defects principally elongated cavities and irregular porosity through the interaction of elements from within the core of the tubular electrode. As consistent quality of the content of tubular electrodes has increased, this has enabled it to compete in qualitative output with traditional processes, and yet provides increased productivity through continuous electrode supply. Use of the process will undoubtedly increase, particularly in Europe, where its use falls far behind that of the United States of America and Japan, (Yeo, 1989).

The use of cored wires can result in higher consistent quality, but care needs to be exercised in the control of welding parameters, and of these, electrode extension is particularly important, Yeo, (1993).

4.2 Welding Practices

Involuntary movements by the welder during torch manipulation cause disturbances in circuit resistance as a result of changes to electrode extension, which, though controlled quickly by the constant potential power source (displaying flat characteristics), lead to variations in arc voltage, current flow and consequently arc length, (Yeo, 1993), and these changes affect weld bead width and penetration, thus affecting quality of output.

The adjustment to electrode extension by the welder, can be used to control weld pool/penetration behaviour with some grades of wire, and welder skill determines the extent to which this is used. However involuntary movements do occur, particularly when long runs are required, as a result of operator fatigue or positional inflexibility. These must be minimised if high quality output is to be maintained on a consistent basis.

4.3 Electrical Characteristics

The equipment commonly used, is of the constant potential type which is used in combination with constant wire feed rates. Changes in circuit resistance resulting from variations in electrode extension, cause rapid changes in current, and consequently burn-off rate. The rapid restoration and regulation of the desired arc length in constant potential systems is what made semi-automatic welding a viable process. Joule heating of the wire projecting from the contact tip accelerates the

ability of consumption in the arc, as when the temperature is increased, less energy is required to initiate phase changes to liquid and vapour states, (Kirk and Mileham, 1994).

Having observed that correct electrode extension is desirable to assist transfer characteristics and effectiveness, any work which promotes enhancement to welder skill in maintaining constant electrode extension will elevate the process, (Kirk and Mileham, 1994), and this is vital to secure consistently high welding output.

4.4 Practical tests

Previous sections have indicated that changes to electrode extension can change deposition characteristics. A review of the literature has already revealed that changes to electrode extension are important but the reported results tend toward qualitative assessment. In considering this aspect and in order to address the deficiency, two feasibility tests were conducted to assess this matter on a quantitative basis.

4.5 Preparatory work - Test 1

4.5.1 Test Overview

In a practical experiment, a 1.2mm diameter self shielded cored electrode was examined to determine in broad detail, the extent to which changes in electrode extension actually caused variation to current flow, penetration, and weld contour. The experiment was aimed at providing raw data as a base for further research, in what is otherwise a neglected area of study. The experiment was conducted with minimal setting up constraints, to emulate as far as possible what actually happens

in normal shop or site fabrication. The experiment does not purport to define precise measurements, but illustrates in practical terms the variances which may be expected under reasonably normal conditions, and provides a base from which to launch further exploratory work.

The electrode used, was a cored wire with a lime-fluorspar flux fill, to specification AWS A5.20-79 E 70T-4 E 70T-G.

Manufacturer's recommendations were for the electrode to be operated using a DC positive constant potential power source with contact tip to work piece distance of 40mm for general fabrication, and 50mm for build up prior to hard-facing. The test equipment and the material used are detailed in Table 4-1.

Material: BS EN 10025:1993 S275.	Dimension:150mmx40mmx6mm
Storage: As delivered condition at 20°C.	Travel Speed: 5mm/sec.
Travel Method: Motorised, Flat Bed.	Position: Flat, (PA).
Torch: Binzel, 70° drag to workpiece.	Contact Tip: Copper 1.2mm
Wire Liner: Coiled Wire.	Wire Speed: 9,12,& 15m/min.
Power Source: Kemppi Kempomig 3500S.	Meter: MU20D.

Table 4-1 : Test equipment and material - Test 1

4.6 Results and Discussion - Test 1

Penetration into the parent metal was measured with a vernier microscope at the deepest part of the fusion zone. Some samples showed evidence of variation in penetration caused by lateral and transverse fluctuation of the electrode which was observed during welding, and this was presumed to be due to the release of internal stresses inherent in the wire due to manufacture. Depth of penetration changed by as much as 20% for 5mm adjustments to electrode extension,

confirming that changes to electrode extension can affect consistent quality of output.

Current flow decreased with increases in electrode extension, with consequent decrease in weld width and penetration, but, with constant deposition rates (due to controlled wire feed speeds), reinforcement, overall, remained the same. Arc voltage, as a function of electrode extension, clearly influences weld width. An analysis of results reveal that current varied by up to 15% for a 5mm decrease in electrode extension, and 2% for a 5mm increase in electrode extension.

These results, are believed to be the first quantitative results of their kind to address this area of study, namely, that with constant wire feed speed in a constant potential system, current is dependant on electrode extension. Electrode extension, weld width and penetration, relative to test piece are illustrated in Figure 4-1.

4.7 Methodology - Test 2

4.7.1 Test Overview

In a practical experiment, a 1.2mm diameter solid wire electrode was examined to determine in broad detail, the extent to which changes in electrode extension caused variation to current flow, penetration, and weld contour. The experiment was aimed at providing raw data as a base for further research, and to provide comparative data for experiments concerning flux cored wires, in what is otherwise a neglected area of study. The experiment was conducted with minimal setting up constraints, to emulate as far as possible what actually happens in normal shop or site fabrication. The test equipment and the material used are detailed in Table 4-2.

Electrode
Extension

Weld width
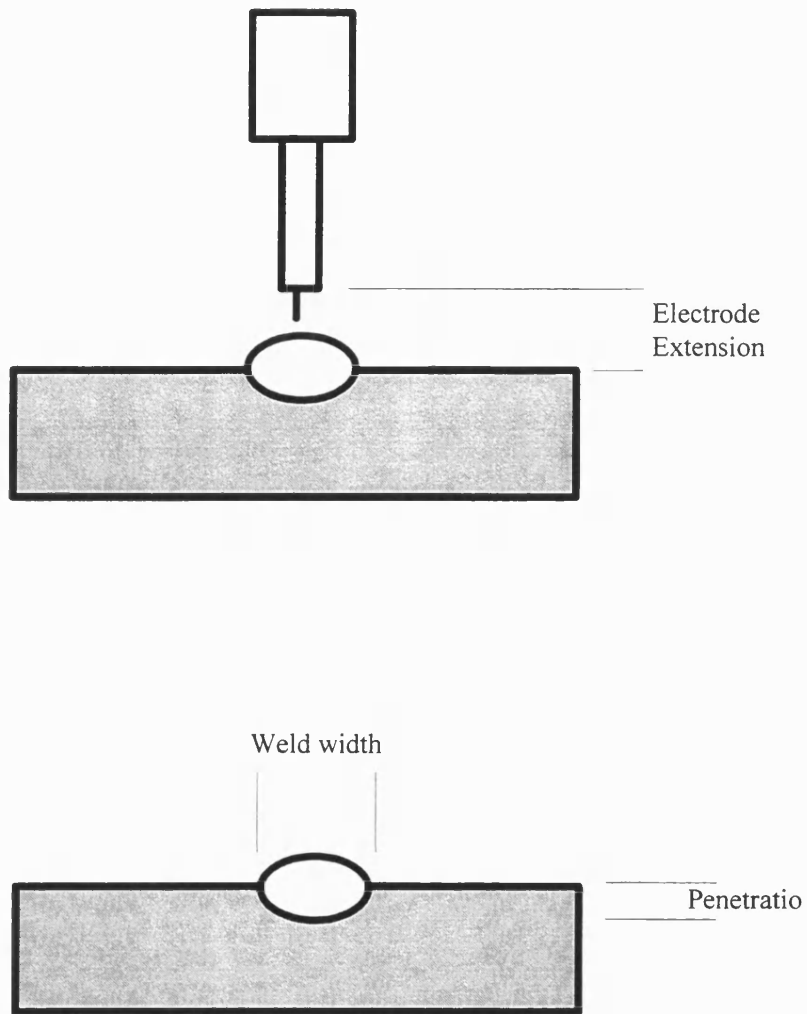
Penetratio

Figure 4-1 : Electrode extension, weld width and penetration, relative to test piece

The electrode used, in this, the second of three tests, was a 1.2mm solid, copper coated, MIG/MAG wire electrode, of standard chemical composition in accordance with BS 2901.

Material: BS EN 10025:1993 S275.	Dimension:150mmx40mmx6mm
Storage: As delivered condition at 20°C.	Travel Speed: 5mm/sec.
Travel Method: Motorised, Flat Bed.	Position: Flat, (PA).
Torch: Binzel MB36, 70° to workpiece.	ContactTip: Copper, 1.2mm
Wire Liner: Coiled Wire.	Wire Speed: 2.2, 3.8, & 5.4m/min.
Power Source: Kemppi Kempomig 3500S.	Meter: MU20D and as text
Shielding Gas: 12% CO_2, 2% O_2, 86% Ar.	Gas Flow Rate: 15 litres/min

Table 4-2 : Test equipment and material - Test 2

4.7.2 Computerised Data Capture

For this test, a computer based data capture system was used. Two electrical circuits were used which enabled smoothing of the data, (voltage and current), captured, prior to recording by a computer, and for each test piece, a sample of 10,000 data points for voltage and 10,000 data points for current was recorded through a fast analogue to digital converter, connected to a 486DX2 66MHz PC, operating with appropriate software control and data management. 27 test welds were made using various welding parameters as detailed in Table 4-3.

4.7.3 Voltage Circuit

The voltage was measured by attaching a connector to the main power cable adjacent to the contact tip at the welding gun, thus eliminating resistance loss in cabling, and yet permitting uninterrupted gas shield through the gas nozzle.

The circuit was differential with each input going through a 20:1 attenuator. This was followed by a passive low pass filter with an f_0 of 30kHz. The signal then passed to a unity gain differential amplifier which was followed by an active 2 pole Butterworth filter with an f_0 of 5 Hz.

4.7.4 Current Circuit

The current was measured in the return cable.

A Hall effect device was used to provide a voltage signal proportional to the welding current, with a sensor output of 200A » 200mV. This signal passed through a passive low pass filter with an f_0 of 20kHz, to a differential amplifier with a voltage gain of 10. The amplifier was then followed by an active 2 pole Butterworth filter with an f_0 of 5Hz.

4.8 Results and Discussion - Test 2

4.8.1 Context

Much work has already been done in connection with the evaluation of the transfer, electrical and operational characteristics of semi-automatic arc welding, (Welding Handbook, 1991, pp. 110-155), and it was not the original intention to attempt to find new, or develop existing characteristics of the process, but to provide comparative data for experiments concerning FCAW, particularly concerning the effect of changes to electrode extension.

The results of this experiment confirmed that small changes in electrode extension in the order of 2mm to 5mm with this particular solid wire electrode, using the parameters recorded, do not materially affect the current drawn, and therefore, reasonably stable output may be expected from the process under typical operating conditions.

However, an analysis of the recorded data provided provisional evidence which suggests that when welding at low wire feed rates, the current drawn varies significantly, in regular sinusoidal cycles, independent of minor changes to electrode extension, but dependant on current flow and as a consequence of variations to wire feed rate.

Further, it may be inferred from this provisional evidence, that such changes in current create opportunities for imperfections to emanate from sites coinciding with decreases in current flow.

The work, (Adam and Siewert, 1990), to evaluate the use of computers to enhance the Statistical Process Control, (SPC), of the welding process goes some way to independently confirm the findings of this experiment as they also recorded definitive sinusoidal changes in the electrical characteristics of this process.

As electrode extension is increased, both the current drawn and the upper transition ranges decrease, consequently adjusting the frequency of droplet transfer and thus increasing the likelihood of imperfection arising.

Porosity will occur, (Kirk and Mileham, 1994), when nuclei for the heterogenous nucleation of bubbles are present in the supersaturated weld metal, and the rate of escape of the bubbles is less than the rate of solidification. Under marginal conditions, this will form at the weld boundary, whereas elongated indications will form at the solidus/liquidus boundary, and progress as solidification occurs. It follows that reduction in heat transfer however this is generated, will alter the

position of the solidus/liquidus boundary, and this may give rise to the possibility of imperfections.

Lack of fusion at the root, side wall, or inter-run, causes inconsistencies in the quality of the process as a whole, and lack of side wall fusion is particularly serious as it is so difficult to detect by radiography. Despite recent advances in the creation of synergic pulsed MIG and semi-robotic machinery, fusion problems are still encountered, (Kirk and Mileham, 1994), principally through the inconsistencies in overall size and the directionability of the arc. This markedly affects the ability of operators to maintain optimum temperatures at the faster travel speeds used in semi-automatic arc welding. The advancements in a number of cored electrodes enhance deposition and reduce incidence of imperfections, but these are generally unsuitable for thin sections.

4.8.2 Arc Energy

It is very important to be aware of arc efficiency for the calculation of heat input rates with regard to metallurgical stability, and is particularly useful for instance, in weld procedure preparation.

Arc energy is a method by which one may consider the heat introduced into a joint, and it is employed here to illustrate the consequences of the cyclical changes in the current flow under consideration.

BS 499, defines arc energy at 32048 as:

'the amount of heat introduced by the welding process per unit length of weld, and may be defined by the formula'

$$\frac{EI}{v}$$

where, (BS 499 nomenclature):

E is the arc voltage (in Volts)

I is the welding current (in Amperes)

v is the welding speed (in mm/sec)

The original formula is derived for use in manual metal-arc welding with adjustments for each process. The MIG/MAG and FCAW processes use the same formula.

From the data recorded, an example was taken of the highest and next lowest transient. The results in terms of arc energy are detailed in Table 4-3 below.

It will be observed that arc energy varied in extreme cases, by up to 42% of the maximum reported energy level. The actual variance in such a case, (see Table 4-3 below), is caused by a recorded current drop of 65 amps. In the data captured during one second of time, similar cyclical (sinusoidal) variances occurred up to seven times. As wire feed rates were increased, the frequency of cycles increased, but the variance between upper and lower current values diminished. Whilst the currents flowing during this experiment did not exceed 220 amps, and therefore did not pass through the reported transition current level, (at which dip transfer switches to spray transfer), it is expected that this gradual change in sinusoidal wave pattern due to changes in current would continue linearly to the transition

value whereupon it will become flat in aspect. Note that transition current values are dependent upon electrode extension.

This being the case, it is reasonable to suggest that change to spray transfer may well **appear** to be instantaneous, but is in fact a function of current.

Electrode Extension	WFS m/min	Volts V	Amps A	welding speed mm/sec	(Arc Energy) kJ/mm	% Arc Energy Reduction
20	2.2	19.2	121.7	6	0.389	
20	2.2	19.6	88.5	6	0.289	25.7%
20	2.2	19.2	120.0	6	0.384	
20	2.2	19.6	78.9	6	0.258	32.8%
30	2.2	19.2	105.5	6	0.338	
30	2.2	19.6	59.9	6	0.196	42.0%
30	2.2	19.1	114.7	6	0.365	
30	2.2	19.6	73.5	6	0.240	34.2%
20	5.4	18.75	213.6	6	0.668	
20	5.4	19.07	197.1	6	0.626	6.3%
20	5.4	18.8	207.2	6	0.649	
20	5.4	19.1	195.9	6	0.623	4.0%
30	5.4	19.2	156.7	6	0.501	
30	5.4	19.3	140.6	6	0.452	9.8%
30	5.4	19.1	148.7	6	0.473	
30	5.4	19.2	144.0	6	0.461	2.5%

Table 4-3 : Comparison of maximum and minimum arc energy liberated at different wire feed rates and electrode extensions

4.9 The significance of electrode extension on cooling rates and the HAZ

4.9.1 Cooling Rates

In the examination of arc energy, the formula expounded above is adequate for a first approximation but in evaluating precise heat effects on the material to be welded, it is also necessary to account for heat transfer efficiency (being in the range 0.8 to 1.0), (Welding Handbook, 1987, pp. 68 and 78), and this revises the equation for net energy to:

$$H_{net} = \frac{f_1 EI}{v}$$

where f_1 is heat transfer efficiency.

In the tests discussed at Section 4.6 above, it was determined that current increased by 15% for a 5mm reduction in electrode extension.

This will therefore affect the net energy input and consequently the cooling rates, dimensional extent of the heat affected zone, and the propensity to metallurgical defect, typically the hardness in hardenable steels.

Simplified equations for calculation of the effect on cooling rates may be determined using the following equations, (after Welding Handbook, 1987, pp. 76, 77):

For thick plates (6 or more passes)

$$R = \frac{2\pi k (T_c - T_o)^2}{H_{net}}$$

and for thin sections

$$R = 2\pi k \rho C \left(\frac{t}{H_{net}}\right)^2 (T_c - T_o)^3$$

Where, for example, according to the Welding Handbook, 1976:

R =   the cooling rate, at a point on the weld centre line when that point is

cooling past the temperature Tc, (°C/s)

k =   0.028 (thermal conductivity of the metal), J/mm . s °C

Tc =   550°C (satisfactory for most steels, Welding Handbook, 1987, pp. 75)

To =   20°C (initial plate temperature)

ρC =   0.0044 (volumetric specific heat), J/mm^3 . °C

t =   thickness of material, mm

According to the Welding Handbook, (1987, p. 79) in considering calculations for a fillet weld, the effective energy input (H_{net}), may be reduced by one third to account for the three dimensional thermal conduction effect caused by such a joint set-up. However later discussions in this thesis will show that this may well not be valid.

Through examination of these equations, it will be appreciated that the critical cooling rate is essentially a property of the material. Also, the rate of cooling from peak temperatures can have significant effects on the metallurgical and mechanical properties, (Lancaster 1992, pp. 83-97). Thorough appreciation of

such factors lead to calculation of preheat temperatures to reduce the effect of undesirably fast cooling rates, and the avoidance of hardness in the heat affected zone.

Significantly, not all wire manufacturers declare optimum electrode extensions. In cases where preheat has been calculated in accordance with established principles (such as the formula above, or BS 5135), and if longer than optimum electrode extensions are incorrectly used, cooling rates will be increased to a potentially dangerous level, such that propensity to brittle fracture may well be likely.

In summary, the significance of maintaining the optimum electrode extension to control energy input cannot be over-emphasised, and limitations on energy input must be included in process specifications, especially in handling sensitive alloys.

4.10 Influence on Metallurgy

4.10.1 Overview

The maintenance of adequate strength and notch-toughness in the heat affected zone of welds, depends on the dissipation of welding heat in order to form the correct microstructures essential for achieving desired mechanical properties. (Welding Handbook, 1987, p. 108).

The subject has been widely studied and the principle method for control of unacceptable metallurgical disturbances is the combined control of heat input and preheat of the parent metal. A lowering of the cooling rates is beneficial as this permits appropriately timed phase changes in the structure of the weld. A valid welding procedure is therefore crucial to obtaining consistency in this respect, and

is particularly important in the welding of hardenable metals or large sectional thickness.

Minor changes to electrode extension in the semi-automatic welding processes, markedly alters total energy input, and as a consequence, affects the penetration, fusion, and dilution of the parent metal, (Kirk and Mileham, 1994), and (Kirk et al, 1995b). The effect on cooling rates may be calculated mathematically using the equations in Section 4.9, but the actual effect on the microstructure of the steels, particularly hardenable steels, must be examined by micro-examination supplemented by micro-hardness and fracture toughness tests, before further definitive generic conclusions may be drawn.

In welding heat treatable steels, the effects of the higher carbon and alloy content on the maximum hardness in the fusion and heat affected zones of the weld must be considered. Deposits of flux-cored wire metal-arc welding consist mainly of pro-eutectoid ferrite with side plates, with smaller areas of acicular bainite and lath martensite, (Lancaster, 1992, pp. 41, 42). The presence of pro-eutectoid ferrite and martensite in the structure reduces notch ductility and such metallic structures are changeable with heat input and longevity (critical cooling rates). These deposits are affected by the addition of alloying elements of varying amounts. Aluminium has the effect of closing the gamma loop in the iron-iron carbide equilibrium diagram up to a maximum content of 1.2%, at which point no transformation takes place. However, the resulting structure needs refining through the addition of austenitic stabilisers such as carbon and manganese, and further, nickel may be added to improve toughness, (Lancaster, 1992, p. 41-43). As a result of increasing the carbon content, the as-quenched martensite in these steels is hard and brittle, and thus is responsible for the formation of hard cracks even before the fabrication is placed into service. These are principally caused by internal stresses on cooling, the brittleness of martensite, and thus this combination makes such welds more susceptible to hydrogen embrittlement.

Specifically the influence on welding metallurgy may be considered in two main areas:

1   Weld Metal Fusion Zone - Influence on solidification cracking

2   Heat Affected Zone - Changes to micro-structure through prolongation or curtailment of cooling rates within the boundaries of critical levels.

The primary influence on the heat affected zone depends on a number of factors, of which the most significant are correctness and applicability of the welding procedure. Further, the chemical content of the parent metal in its original form, the process used, and the total energy input during the welding operation, which gives rise to changes in weld thermal cycles and ultimate width of the heat affected zone are notable. Higher heat inputs will also affect grain size to a degree, and this may result in a reduction of the toughness of the final weldment. As plate sectional thickness increases, so the effect of changes to electrode extension increase the changes to weld and parent metal thermal cycles and risk of defects increases. Notwithstanding that multiple runs in a weldment may increase toughness through re-crystallisation, the possibility exists for cracks or weaknesses to remain through incorrect operation. This is important in fabrications which are subject to dynamic loading and/or operation at reduced temperatures where the brittle/ductile transition temperature is approached.

4.10.2 Dilution and solidification cracking

Dilution of the parent metal is affected to some degree by total energy input and problems may arise (particularly propensity for solidification cracking) if undesirable elements (sulphur exacerbated by carbon) which are present in the parent metal become concentrated in the weld metal fusion zone causing the development of the intergranular liquid films at certain temperature ranges which initiate hot cracking. Traditionally, manganese is added to counteract this

problem by inhibiting the formation of sulphides, but the effectiveness of this element will be reduced in the presence of aluminium, and research into this area is necessary as aluminium is a common element within the core of self shielded cored wires. This also gives rise to the presence of low melting point films.

4.10.3 High temperature region of the heat affected zone

Low carbon, low alloy steels have a BCC structure at room temperature, and therefore changes to, or prolongation of, high temperatures approaching the metal boiling point, will affect grain growth in both the heat affected zone and the fusion zone, as, on cooling, new grains will nucleate at existing grain boundaries which have been enlarged. Whilst saturated sulphur from the parent metal composition (giving rise to intergranular precipitation of liquid films with low melting points), is unlikely to be a problem in this region of the heat affected zone, adverse changes to energy will ultimately affect the toughness.

4.10.4 Medium temperature region of the heat affected zone

The risk of hardening in this region is most likely to occur due to rapid cooling through the austenitic and ferritic phases, and because cooling rates are a function of, *inter alia*, total energy input, the medium temperature region of the HAZ may be profoundly affected by electrode extension.

The finer size of grains in this grain refined region improves notch ductility, but nevertheless, the cooling rate can be high enough for hardening to occur. The principle method for reducing the incidence of undesirable metallic structures is through preheating, and the carbon equivalent formula postulated by the International Institute of Welding is commonly used to assess the chemical composition of alloyed steels and their propensity to cause defect. A high carbon

equivalent value suggests higher hardenability and the parent metal therefore requires preheat.

4.10.5 Low temperature range in the heat affected zone.

Strain-age embrittlement occurs at temperatures approximating 200 °C when strain is present and when nitrides or carbonitrides begin to precipitate. This has the effect of moving the impact transition temperature upward by approximately 50°C, (Lancaster, 1992, p. 92). The problem is less apparent in deposits made by self-shielded wires because of the potential for denitrification activity within the arc and the weld pool, but this only remains within acceptable boundary limits if the electrode extension is effectively controlled.

4.10.6 Conclusions and Review

In broad theory, the circuit resistance, (Joule heating (I^2R)), and its effect on ultimate arc voltage, considerably alter transmission across the arc. The test output confirms theory, but it is especially noted that current flow varies considerably when using cored wires if electrode extension is reduced, and this will alter penetrative aspects. It is desirable to increase penetration in all but a number of cases, though care has to be exercised where metallurgical stability of the parent metal needs to be maintained, and where the process is used in making root, (first pass), runs where welding is conducted from one side only.

The requirement to control the welding operation consistently, is vital if quality is to be maintained, and, more importantly, to comply with European Standards, both weld width, contour and penetration bead height (dimensioned against parent metal thickness) require vigorous control, (Kirk and Mileham, 1994). The feasibility tests show, that whilst modern equipment can give adequate

supply/rectifier output control, the actual weld deposited can vary significantly as a result of changes to electrode extension.

Quality of penetration, linked with incomplete fusion, either in the root or side wall, is of paramount importance in appraisal and use of applications.

In the case of test two, it is concluded that there is no significant effect to current by minor changes in electrode extension, (±2 mm), when using a 1.2mm solid steel wire electrode designed for MIG/MAG welding.

It is suggested that, based on provisional results there is a good case to research further the sinusoidal type cyclical current change, (Adam and Siewert, 1990), which occurs at low wire feed rates in a constant potential MIG/MAG system. It is suggested that the likelihood of defects occurring increases when current is minimised, especially when using low wire feed rates, and that quality improvements to the process may be achieved by directing attention to this matter.

Further, if electrode extension is increased, corresponding changes in cooling rates may be so significant that they increase the likelihood of hardening in the heat affected zone of many steels.

5. Modelling the weld thermal cycle and microstructure

5.1 Introduction

In studying the transformation kinetics of austenite to assess hardenability, consideration must be given to accurate prediction of the microstructure on the basis of chemical composition and welding parameters and the relation between microstructure and mechanical properties.

A number of welding codes give indications of the maximum hardness acceptable in the final weld metal and heat affected zone, (HAZ), (principally to avoid the susceptibility to hydrogen cracking), (for example, EN 288), whilst others, (for example, BS 5135), offer nomographs to assist in the selection of preheat values for ranges of steels suggesting that observance of carbon equivalent values alone provide adequate knowledge.

5.2 Development of the equations

The first analytical equations assessing the temperature distribution in a plate due to a flow of heat were proposed by Rosenthal, and were used to establish the principle of a quasi-stationary state, (Rosenthal, 1935).

These equations are the analytical solutions to the common Laplace's differential equation whose usual expression is :

$$\frac{\partial^2 T}{\partial x^2} + \frac{\partial^2 T}{\partial y^2} + \frac{\partial^2 T}{\partial z^2} = 2\lambda \frac{\partial T}{\partial t}$$

Equation 5.1

where :

$T = T(x,y,z)$ is the temperature field,

λ = the thermal diffusivity.
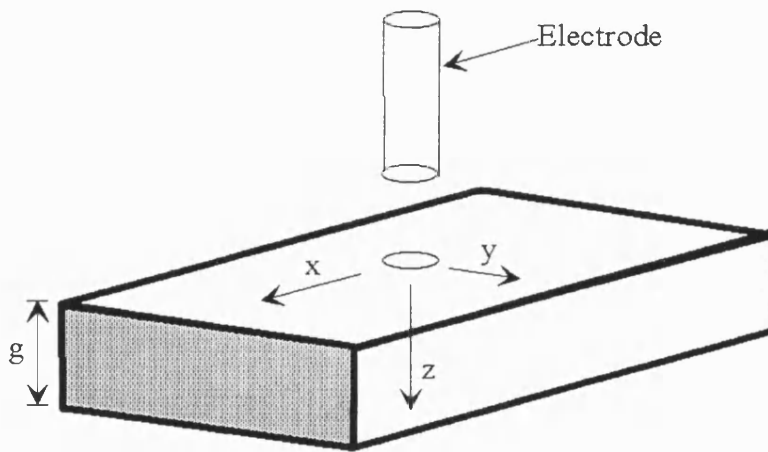
Figure 5-1 Cartesian co-ordinate system used in the equations

Replacing the x term by $\xi = x\text{-}vt$, where ξ is the distance of the point considered from the distance of the point source, (Figure 5-1), differentiating with respect to ξ, and assuming a constant heat source achieving a stable state, namely that it is quasi-stationary, where $\partial T / \partial t = 0$, the equation becomes,

$$\frac{\partial^2 T}{\partial \xi^2} + \frac{\partial^2 T}{\partial y^2} + \frac{\partial^2 T}{\partial z^2} = -2\lambda v \frac{\partial T}{\partial \xi}$$

Equation 5.2

Differentiating and approximating the included modified Bessel function of the second kind, zero order, (Rosenthal, 1941), the equation for temperature change in a thin plate becomes,

$$T - T_0 = \frac{Q}{2\pi \, k \, g} \cdot \left(\frac{\pi}{2\lambda \, v}\right)^{1/2} \cdot \left[\frac{e^{-\lambda \, v[(\xi^2 + y^2)^{1/2} + \xi \,]}}{(\xi^2 + y^2)^{1/4}}\right]$$

<div align="right">Equation 5.3</div>

or, by expanding ξ, and transposing,

$$T - T_0 = \frac{Q}{2\pi \, k \, g(v^2 t^2 + y^2)^{1/4}} \cdot \left(\frac{\pi}{2\lambda \, v}\right)^{1/2} \cdot \left[e^{-\lambda \, v[(v^2 t^2 + y^2)^{1/2} - vt]}\right]$$

<div align="right">Equation 5.4</div>

whilst the equation for temperature change for a thick plate is,

$$T - T_0 = \frac{Q}{2\pi \, k} \cdot \left[\frac{e^{-\lambda \, v[(\xi^2 + y^2 + z^2)^{1/2} + \xi \,]}}{(\xi^2 + y^2 + z^2)^{1/2}}\right]$$

<div align="right">Equation 5.5</div>

which, by expanding ξ, and transposing becomes,

$$T - T_o = \frac{Q}{2\pi k \left(v^2 t^2 + y^2 + z^2\right)^{\frac{1}{2}}} \bullet e^{\left[-\lambda v\left[\left(v^2 t^2 + y^2 + z^2\right)^{\frac{1}{2}} - vt\right]\right]}$$

<div align="right">Equation 5.6</div>

If, by assigning y = 0 and z = 0, (representing the weld centre-line), the exponential expression has the value (1), and thus the function is at maximum. Rosenthal used this aspect to derive simplified equations, (Rosenthal 1936 and 1941), which are,

for thin plate,

$$\frac{\partial T}{\partial t} = 2\pi k \rho C \left(\frac{vg}{Q}\right)^2 (T_c - T_o)^3$$

<div align="right">Equation 5.7</div>

and for thick plate,

$$\frac{\partial T}{\partial t} = 2\pi k \frac{v}{Q} (T_c - T_o)^2$$

<div align="right">Equation 5.8</div>

5.3 Hypothesis for an Equation for intermediate material thicknesses

Whilst the short-form equations, (Equations 5.7 and 5.8), are valuable, they are limited in their ability to predict cooling rates or temperatures as specific functions of spacial co-ordinates and time, and this is desirable in metallurgical investigations where examination of particular points of interest in the heat affected zone are required.

The primary equations, (Equations 5.3 and 5.5), can be restrictive in this area as they are not able to accommodate prediction of thermal cycles in intermediate material thicknesses, that is to say, where losses due to conductivity are neither wholly three dimensional nor yet wholly two dimensional. This is particularly important since many modern high strength steels are now produced in product forms whose thickness is much reduced over those previously available, and designers in all sectors must have tools available to predict weld thermal cycles in these cases.

Rosenthal observed that both the thin and the thick plate equations behave similarly at large distances or long times. However at points closer to the source, or at small time values, the thin plate equation is unable to accurately predict temperature change for any occurrence other than for limited low values of thickness. There is therefore, a point at which, relative to the thickness and the energy, calculation of the temperature change is not accurate, (since it is neither thick nor thin), and only capable of assessment by reference to nomographs such as that illustrated by Adams, (1958).

As the thin plate equation includes the thickness term, (g), it is logical to concentrate on fitting a parametric curve to this term. As the precise mathematical modelling is somewhat complicated due to the relativity of energy source to plate thickness, a new equation has been developed which more realistically represents the thermal cycle through a range of thicknesses in the intermediate range, yet which retains simplicity of calculation. This thesis considers the development of a logarithmic curve associated with the plate thickness (g), which broadly achieves this objective and, since it differs little at the extremes of thick and thin from the widely examined original equations attributed to Rosenthal, it has been found to be both easy to implement and acceptable to industry, thus enabling modelling of heat flow in materials of intermediate thickness, not previously achievable with certainty.

It is acknowledged that similar extensive work was undertaken, (Hess, Merrill, Nippes, Jr., and Bunk, 1943). In that work, a Beta factor was used which was a tabulated variable, dependent on a number of interlinking parameters. Whilst this gave satisfactory results, the resulting procedure was somewhat cumbersome, and given that such work was of immense value at the time, the increasing availability of computers suggest that a single equation with curve fitting which provides more flexible operation is now more appropriate.

5.4 Development of a Continuous Heat Flow Equation

The Rosenthal equation, (Equation 5.3), modified to include the logarithmic coefficient to base 10 to permit progressive adjustment of the thickness term, which, subject to the lower limit of the 'thin' plate equation, models the Continuous Heat Flow, (CHF) due to a moving heat source in all intermediate thicknesses, is therefore,

$$T - T_o = \frac{Q}{2\pi k\left[10\left(Log_{10}g\right)\right]} \bullet \frac{\left(\frac{\pi}{2\lambda v}\right)^{\frac{1}{2}} \bullet \left[\frac{e^{\left[-\lambda v\left[\left(v^2 t^2 + y^2 + z^2\right)^{\frac{1}{2}} - vt\right]\right]}}{\left(v^2 t^2 + y^2 + z^2\right)^{\frac{1}{4}}}\right]}{\left(\frac{\pi}{2\lambda v}\right)}$$

Equation 5.9

Simplifying, by assigning a coefficient, (C_A), where,

$$C_A = \frac{Q}{2\pi k\left[10\left(Log_{10}g\right)\right]} \bullet \left(\frac{\pi}{2\lambda v}\right)^{\frac{1}{2}}$$

and differentiating with respect to time (t), gives the cooling rate,

$$\frac{\partial T}{\partial t} = C_A \bullet e^{\left[-\lambda v\left[\left(v^2 t^2 + y^2 + z^2\right)^{\frac{1}{2}} - vt\right]\right]} \bullet \left[\frac{\lambda v^2}{\left(v^2 t^2 + y^2 + z^2\right)^{\frac{1}{4}}} - \frac{\lambda v^3 t}{\left(v^2 t^2 + y^2 + z^2\right)^{\frac{3}{4}}} - \frac{v^2 t}{2\left(v^2 t^2 + y^2 + z^2\right)^{\frac{5}{4}}}\right]$$

Equation 5.10

The partial differentiation of Equation 5.9 to Equation 5.10 is detailed in full in Appendix A.

Alternatively, by replacing (C_A) in Equation 5.10 with Equation 5.9, (transposed), the cooling rate may be expressed through its relationship with the coefficient of temperature change, $(T\text{-}T_o)$, (detailed in Appendix A), thus giving,

$$\frac{\partial T}{\partial t} = (T - T_o) \bullet \left[\frac{-v^2 t}{2(v^2 t^2 + y^2 + z^2)} + \lambda v^2 \left(1 - \frac{vt}{(v^2 t^2 + y^2 + z^2)^{\frac{1}{2}}} \right) \right]$$

Equation 5.11

5.5 Determination of Peak Temperature Equations

It is desirable to determine peak temperatures and holding times at such temperatures at specific radial distances from the heat source in order to examine the impact of metallurgical responses such as grain growth and austenetization times relative to heat flow in welding. As time and spatial co-ordinates are relative, and,

where radial distance, $r = (v^2 t^2 + y^2 + z^2)^{\frac{1}{2}}$

then peak temperature becomes,

$$T_p = C_A \bullet \left[\frac{e^{-\lambda v [\xi + r]}}{r^{\frac{1}{2}}} \right] + T_o$$

Equation 5.12

but this is of limited use for calculations where $y \diamond 0$ or $z \diamond 0$ since the exponential expression in Equation 5.12 cannot be eliminated, and therefore time as a direct function may only be determined by numerical methods in an iterative loop.

The following transpositions may be used to determine peak temperature (T_p), and pre-heat temperature (T_o) where evaluation based on a predetermined cooling rate is given.

$$T_p = \frac{\partial T}{\partial t} \bullet \left[\frac{-v^2 t}{2\left(v^2 t^2 + y^2 + z^2\right)} + \lambda v^2 \left(1 - \frac{vt}{\left(v^2 t^2 + y^2 + z^2\right)^{\frac{1}{2}}} \right) \right]^{-1} + T_o$$

Equation 5.13

$$T_o = T_p - \left[\frac{\partial T}{\partial t} \bullet \left[\frac{-v^2 t}{2\left(v^2 t^2 + y^2 + z^2\right)} + \lambda v^2 \left(1 - \frac{vt}{\left(v^2 t^2 + y^2 + z^2\right)^{\frac{1}{2}}} \right) \right]^{-1} \right]$$

Equation 5.14

5.6 Losses due to radiation and convection

It is necessary to consider losses attributable to both radiation and convection.

Radiation from the arc during welding is significant in the potential for preheating plates and sidewalls of plates depending on joint set-up. However radiation losses from the surface of the plate following welding are not considered material when balanced with the losses due to conduction, in regard to metallurgical influences, though they may well be important in matters concerning health and safety of personnel.

Losses due to natural, forced and jet convection, can in certain circumstances be important.

Overall, consideration of losses due to conduction are the most significant regarding their potential to affect metallurgical stability.

5.7 Comparison with the thin and thick plate equations

Given the complexity of the equations which include both time and space co-ordinates it is difficult to directly compare the new equation with other modified or simplified equations which ignore these terms. When predicting the cooling rate or peak temperature for a specific time and spatial co-ordinate the relative positioning of the thin and thick plate equations is such that either the time or distance which yield comparative cooling rates or peak temperatures are inconsistent with meaningful statistical study or illustration when comparing with each other or the new equation. The inclusion of the logarithmic smoothing in the CHF equation, does however permit gradual transition between the two delimiting equations and adequately tracks all three axes in the Cartesian system with the addition of time as the fourth dimension.

The CHF equation performs extremely well when compared with a number of studies of actual data, (Easterling 1983), and in particular, comparison of temperatures close to the weld and the resultant cooling rate in the intermediate thicknesses mentioned, more realistically represents actual phenomena as recorded, and appears to more correctly map the rapid exponential change from fast cooling rate to slow cooling rate as time and space increase. Figure 5-2, Figure 5-3, and Figure 5-4 illustrate this change.
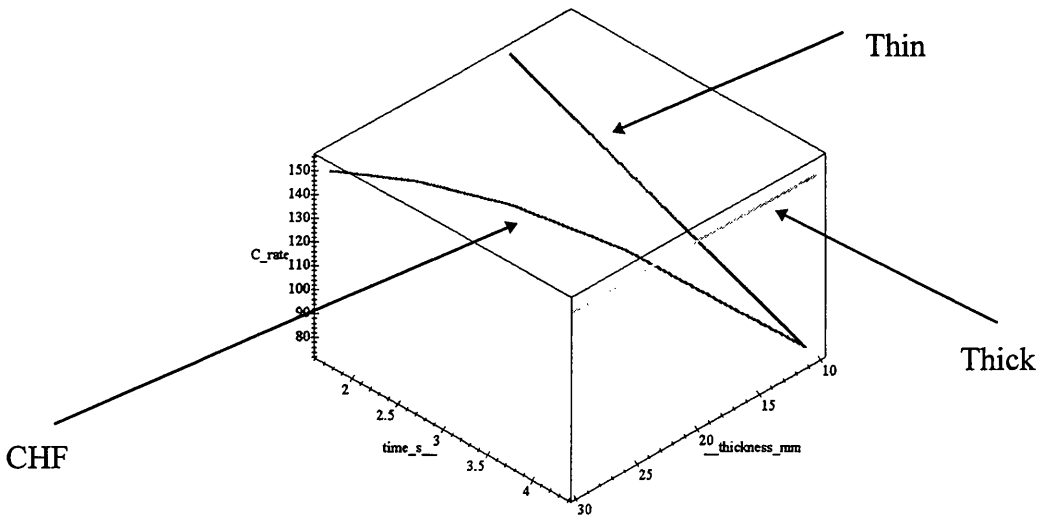
Figure 5-2 Three dimensional image of the comparison between the CHF equation, (Eqn 5.9), the Rosenthal thin plate equation,(Eqn 5.4), and the Rosenthal thick plate equation, (Eqn 5.6).
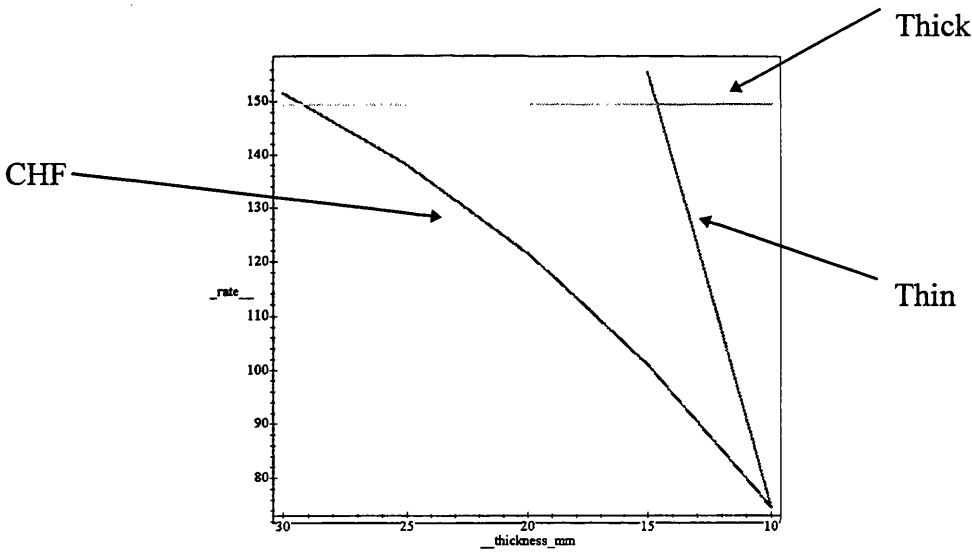
Figure 5-3 Front elevation showing the transition of the CHF equation between the thin and thick plate equations
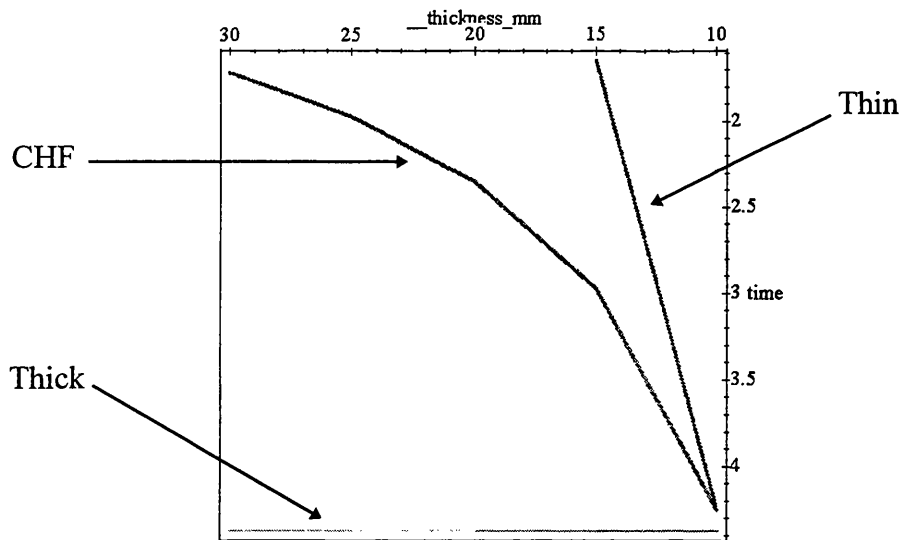
Figure 5-4 Plan view showing the effect of time-space co-ordinates on the transition

The above figures illustrate the predicted cooling rates, (negative cooling rates shown here as positive for clarity in illustration), applicable to materials in the thickness range 10 mm to 30 mm. The welding parameters used were the average energy inputs during the course of experimentation, detailed below in Table 5.1.

Joint type and plate	90° T-fillet - base plate
Thickness range	10 - 30 mm
Current	277 amps
Voltage	23 volts
Speed of travel	4 mm/s
Initial plate temperature	295 K
Distance from weld centreline	2 mm
Electrode extension	15 mm

Table 5-1 Summary of average welding parameters used in the experiment

5.8 Simplification of the CHF equation

One of the advantages of the additional logarithmic coefficient is that it enables modelling of the change in temperature over a range of thicknesses. In the research context, the length and complexity of the equation enables examination of a number of different concepts. However, in practical use the equation can be viewed as somewhat cumbersome. Rosenthal, (1935 and 1941), considered this fact, and assumed that the rate of change of heat adjacent to the weld was similar to that occuring at the weld centreline and deduced that under certain circumstances, the exponential term in the equation could be approximated by the value 1. Thus simplification of the equation would extend its use to more practical daily application, particularly in the calculation of cooling rates. The new CHF equation similarly may be simplified on this basis and the manipulations are presented in Appendix B.

The simplified version of the CHF equation is therefore,

$$\frac{\partial T}{\partial t} = -(T - T_o)^3 \bullet 2\pi k\rho C \bullet \left(\frac{v[10(Log_{10}g)]}{Q} \right)^2$$

Equation 5.15

This is the replacement for Equations 5.7 and 5.8 developed by Rosenthal.

5.9 Thermal bow wave theorem

In considering the responsiveness of the equation to welding conditions, the quasi-stationery state assumes that virtual equilibrium is achieved shortly after welding has commenced, and in ideal situations this is certainly the case for fixed speeds, (Rosenthal, 1935). In considering the rate of conduction of heat however, it is observed that at low welding speeds the speed of travel can be slower than that of the

effective speed of heat transferred by conduction through the mass of the material, (Kirk, Shirvani, Rees, and Mileham, 1996).

In this sense it is conceivable that the temperature change given from Equation 5.9, is, *per se*, a change relative to the temperature of the material at the time of imposition of the energy source and not the original (T_O) temperature assumed in many previous papers. This being the case, it is important to conduct iterative calculations at slow travel speeds to determine the approximate 'pre-heated' temperature of the plate. Certainly this is possible given that x may be expressed in the negative and Equation 5.9 remains valid. In these cases it would be correct to say that in some joint set-ups, root runs and slow travel speeds that welding is never conducted on material at its original temperature.

As a consequence, it is therefore possible with other complementary equations, to mathematically map the increasing plasticity of the plate as welding proceeds to the edge of a joint, and this will undoubtedly be of use to those who program robotic cells and who are able to employ slope out control of current, to avoid burn through or negate the need for step welding. Figure 5-5 illustrates the thermal bow wave theorem in an 11 mm thick plate using a slow travel speed of 2 mm/s and compares the actual temperature profile recorded in a Nb-microalloyed steel, (data transcribed from Easterling, 1983).
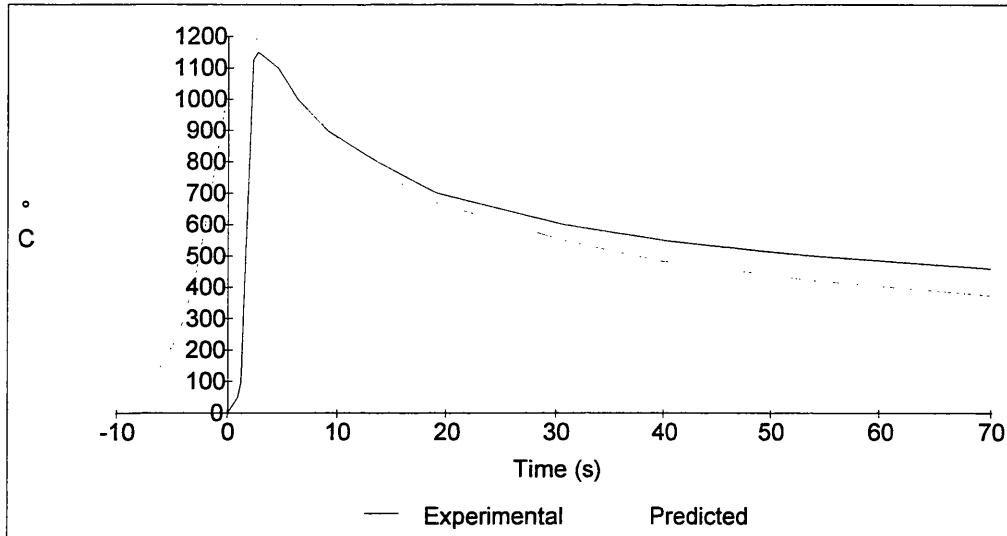
Figure 5-5 Experimental and predicted temperature profile in Nb microalloyed steel showing both the thermal bow wave theorem and accuracy of temperature prediction, after (Easterling 1983)

5.10 Validation of the CHF equation

Preliminary results indicate that the new CHF equation displays close accord with actual weld thermal cycles. The existence of published records (Hess, et. al., 1943) enabled initial comparisons during the research and practical experiments, discussed later in this work, validated the assumptions and methodology used. Table 5-2, Table 5-3 and Table 5-4 below illustrate how the new equation predicts the time temperature and cooling rate data for butt welding of A131-39 Structural Ship Steel, 0.19%C, 0.41%Mn, 0.019%P, 0.045%S, 0.04%Si, 0.08%Cu, 0.04%Ni, 0.02%Cr. The results are tabulated as a comparison with the literature, (Hess, et. al., 1943), notwithstanding reported observations that certain inaccuracies existed with the placement of thermo-couples.   The calculations assume constant speed of travel with an arc efficiency/transfer factor of 0.8, (Welding Handbook, 1987, p. 69).

Temperature of interest		704.44 °C	537.78 °C	371.11 °C	704.44 °C	537.78 °C	371.11 °C
Speed mm/s	Energy J/s	Exp. Time / Calc Time	Exp. Time / Calc Time	Exp. Time / Calc Time	Exp. C rate / Calc C rate	Exp. C rate / Calc C rate	Exp. C rate / Calc C rate
2.98	6400	13.2 / 10.1	33.5 / 20.9	69.1 / 49.8	18.5 / 22.6	6.6 / 10.5	3 / 3.3
5.04	6900	6.8 / 3.4	13 / 8	30.7 / 19.8	58.9 / 46.7	16 / 25.3	6.1 / 8.1
Thickness 12.7 mm, Original plate temperature 22.22 °C							

Table 5-2, Measured and calculated values of times and cooling rates in 12.7 mm steel

Temperature of interest		700 °C	600 °C	500 °C	700 °C	600 °C	500 °C
Speed mm/s	Energy J/s	Exp. Time / Calc Time	Exp. Time / Calc Time	Exp. Time / Calc Time	Exp. C rate / Calc C rate	Exp. C rate / Calc C rate	Exp. C rate / Calc C rate
3.03	8200	10.5 / 10.1	13.2 / 15.5	17.7 / 24.4	48 / 22.6	27 / 14.8	18.7 / 8.6
5.04	7800	5.4 / 3	7 / 4.1	9.3 / 7.2	77.5 / 63.9	55.2 / 39.6	35.4 / 25.3
Thickness 25.4 mm, Original plate temperature 22.22.°C							

Table 5-3, Measured and calculated values of times and cooling rates in 25.4 mm steel

Temperature of interest		704.44 °C	537.78 °C	371.11 °C	704.44 °C	537.78 °C	371.11 °C
Speed mm/s	Energy J/s	Exp. Time / Calc Time	Exp. Time / Calc Time	Exp. Time / Calc Time	Exp C rate / Calc C rate	Exp C rate / Calc C rate	Exp C rate / Calc C rate
2.99	11600	19.4 / 24.8	31.5 / 50.1	52.3 / 134.8	23.2 / 10.7	11.5 / 4.1	5.2 / 1
4.93	9600	10.3 / 5	15.7 / 11.6	24.5 / 33	48.1 / 38.9	24.3 / 16.2	13.6 / 3.9
Thickness 38.1 mm, Original plate temperature 98.89 °C							

Table 5-4, Measured and calculated values of times and cooling rates in 38.1 mm steel

Notes to Table 5.2 to 5.4:

1   Actual times, (s), and cooling rates, (°C/s), for various temepratures of interest as indicated, (after Hess, et. al., 1943).

2   Calculated times and cooling rates predicted using the CHF equations.

5.11 HAZ microstructure and hardness theory

5.11.1 Prediction of critical cooling rates, microstructure and hardness

In examination of hardenability conducted by metallurgists in connection with prediction of hardenability in steel production, tool hardening and tempering, the literature discloses evidence that chemical formulae have been postulated which are statistically satisfactory and which may be applied to welding engineering. These formulae, (Blondeau, Maynier, and Dollet, 1973), (Blondeau, Dollet, and Bastien, 1978), and (Maynier, Jungmann, and Dollet, 1978), suggest that there is high confidence in their ability to predict critical cooling rates from the chemical composition of the base metal of hypoeutectoid steels (<0.8%C), extend the results to prediction of phase transformations, and finally to predict hardness of heat affected zones.

In assessing these formulae it has been of value to find that use of an austenetizing parameter, (discussed below), can adjust the validity of the formulae in connection with the high temperature austenetization encountered in welding situations.

The following formulae are all attributed to the aforementioned authors, and represent critical cooling rates (velocities) at 700°C at which the complete transformation products indicated are present.

Critical velocity for 100% martensite

Log V1(100) = 9.81 - (4.62 C% + 1.05 Mn% + 0.54 Ni% +

0.50 Cr% + 0.66 Mo% + 0.00183 Pa)

Formula 5-1

Critical velocity for 90% martensite and 10% bainite

Log V1(90) = 8.76 - (4.04 C% + 0.96 Mn% + 0.49 Ni% +

0.58 Cr% + 0.97 Mo% + 0.0010 Pa)

Formula 5-2

Critical velocity for 50% martensite and 50% bainite

Log V1(50) = 8.50 - (4.13 C% + 0.86 Mn% + 0.57 Ni% +

0.41 Cr% + 0.94 Mo% + 0.0012 Pa)

Formula 5-3

Critical velocity for 100% bainite

Log V2(100) = 10.17 - (3.80 C% + 1.07 Mn% + 0.70 Ni% +

0.57 Cr% + 1.58 Mo% + 0.0032 Pa)

Formula 5-4

Critical velocity for 90% bainite and 10% ferrite/pearlite

Log V2(90) = 10.55 - (3.65 C% + 1.08 Mn% + 0.77 Ni% +

0.61 Cr% + 1.49 Mo% + 0.0040 Pa)

Formula 5-5

Critical velocity for 50% bainite and 50% ferrite/pearlite

Log V2(50) = 8.74 - (2.23 C% + 0.86 Mn% + 0.56 Ni% +

0.59 Cr% + 1.60 Mo% + 0.0032 Pa)

Formula 5-6

Critical velocity for 90% ferrite/pearlite and 10% bainite

Log V3(90) = 7.51 - (1.38 C% + 0.35 Mn% + 0.93 Ni% +

0.11 Cr% + 2.31 Mo% + 0.0033 Pa)

Formula 5-7

Critical velocity for 100% ferrite/pearlite

Log V3(100) = 6.36 - (0.43 C% + 0.49 Mn% + 0.78 Ni% +

0.27 Cr% + 0.38 Mo% + [2 * (Square root Mo%)] + 0.0019 Pa)

Formula 5-8

where elements are represented by their chemical symbols and in weight per cent, and where Pa is an austenetizing parameter discussed below at Equation 5.16.

5.11.2 Hardness values (HV) before tempering

HV Martensite = 127 + 949 C% + 27 Si% +11 Mn% +8 Ni%

+16 Cr% +21 log Vr

<div align="right">Formula 5-9</div>

HV Bainite = -323 +185 C% + 330 Si% +153 Mn% +65 Ni% + 144 Cr% +

191 Mo%+log Vr (89+53C-55 Si - 22 Mn - 10 Ni - 20 Cr - 33 Mo)

<div align="right">Formula 5-10</div>

HV Ferrite/Pearlite = 42 +223 C% + 53 Si% +30 Mn% +12.6 Ni% +

7 Cr%+19 Mo%+log Vr (10 - 19 Si +4 Ni + 8 Cr + 130 V)

<div align="right">Formula 5-11</div>

Average hardness is weighted volume mean (by summation) of the above micro-structural constituents. Where Vr is actual cooling rate per **hour**.

5.11.3 Austenetizing parameter

In attributing formulae to prediction of microstructure of the heat affected zone which surrounds a weld it is important to acknowledge that the material is heated to values well above the Ac3 temperature, at an extremely rapid rate, held for a relatively short period and then relatively rapidly cooled by the effect of the heat sink due to the surrounding mass of material. This gives rise to a need to consider the solubility of the alloying elements in the melt and therefore all formulae predicting critical cooling rates include an expression to establish equivalence of time and temperature defined as a parametric function to account for variations in austenetizing duration and peak temperature. The austenetizing parameter, (Pa) is calculated as follows:

$$P_a = \left[\frac{1}{T_a} - \frac{(\ln(10))R}{H} \bullet \ln\left(\frac{t}{t_u}\right)\right]^{-1}$$

Equation 5.16

5.11.4 Discussion of micro-structural transformation and hardness prediction

It is thus possible to predict the temperature profile and duration using the new CHF equations, together with the respective cooling rates using Equation 5.10, for any particular point within the material, typically within the weld heat affected zone. It is also possible through application of Equations 5.10 and 5.16, and the Formulae 5.1 to 5.11, to predict the likely outcome in terms of transformation products which in effect creates data relative to a continuous cooling transformation diagram specific to the material composition in question. As any alloying elements affect transformation temperatures, linking common equations for prediction of critical arrest points such as those listed below, permits creation of additional background information similar to that obtained from a metastable Fe-Fe$_3$C, phase diagram, as before, specific to the material in question. Thus by modelling all equations and formulae it is possible now to consider transformation products in the weld heat affected zone as a function of cooling rate and chemical analysis of the base material with reference to a specific metastable phase diagram and CCT curve.

The first critical arrest temperature, (Ac1), may be calculated as follows:

Ac1   =   751-(-16.3 C%)+(34.9 Si%)-(27.5 Mn%)-(5.5 Cu%)

-(15.9 Ni%)+(12.7 Cr)+(3.4 Mo%)

Formula 5-12

(after Kunitake and Ohtani 1967)

The third critical arrest temperature, (Ac3), may be calculated as follows:

Ac3   =   881-(206 C%)+(53.1 Si%)-(15 Mn%)-(26.5 Cu%)

-(20.1 Ni%)-(0.7 Cr%)+(41.1 Mo%)

Formula 5-13

(after Kunitake and Ohtani 1967)

The Bainitic start temperature, (Bs), may be calculated as follows:

Bs   =   830-(270 C%)-(90 Mn%)-(37 Ni%)-(70 Cr%)-(83 Mo%)

Formula 5-14

(after Steven and Haynes 1956)

The Martensitic start (Ms), and finish (Mf) temperature, with 10%, (M_{10}), 50%, (M_{50}), and 90%, (M90), fractions may be calculated as follows:

Ms   =   561-(474 C%)-(33 Mn%)-(17 Ni%)-(17 Cr%)-(21 Mo%)

Formula 5-15

M_{10} =   Ms-10°C M_{90} =   Ms-103°C

M_{50} =   Ms-47°C   Mf   =   Ms-215°C

(after Steven and Haynes 1956)

5.11.5 Discussion and illustration

One of the major developments in steel production is the availability of High Strength Low Alloy Steels (HSLA). Such steels use V, Nb, or Ti as microalloying element additions to C-Mn steel, which exhibit excellent low temperature performance, (high impact resistance at -40°C or less).

HSLA steels are primarily used, *inter alia*, in pipelining, ship and rig construction and pressure vessels, and combine cost reduction with high strength thin section capability providing resistance to brittle cleavage and possessing a low ductile/brittle transition temperature. Essentially, a ferrite-pearlite micro-structure, weldability is apparently good having relatively low carbon equivalent values.

However in any welding scenario, correct welding procedures not only ensure correctness of fabrication and adherence to quality control programmes, but provide

an opportunity to approve procedures through testing, typically to EN 288-3. In order to examine the response of the new CHF equations when linked with the chemical formulae, and to consider the potential benefits for more efficient procedure preparation and accuracy, a model was created and coded into a computer program

Table 5-5 illustrates typical output from the model incorporating the above equations. It was applied to a Nb-microalloyed fine grain HSLA steel (old BS 1501, Part 1:1980, Grade 225 490B, available to specification EN 100028-3:1993, Weldable fine grain steels, normalised, Grade P355), available in a range of thicknesses. As the carbon equivalent maxima can be selected by users, the analysis used in this example was representative of a typical delivery programme as detailed below.

C 0.180 % mass	Si 0.350 % mass	Mn 1.450 % mass	P0.015% mass
S 0.010 % mass	Al 0.040 % mass	Nb 0.030 % mass	Others trace only

Transformation Product	C Rate °C/s
100% Martensite	336.83
90% Martensite, 10% Bainite	216.11
50% Martensite, 50% Bainite	113.11
100% Bainite	95.22
90% Bainite, 10% Ferrite Pearlite	59.07
50% Bainite, 50% Ferrite Pearlite	13.67
90% Ferrite Pearlite, 10% Bainite	5.29
100% Ferrite Pearlite	3.9

Table 5-5 Critical cooling velocities indicated to complete the transformations

EN 288-3 provides acceptance criteria as a guide for hardness values where no external application contract or contractual obligation exists. In this example, the material was a Group 2 steel with a permitted maximum HV of 380 for single run butt and fillet welds where the steel was not heat treated.

Table 5-6 illustrates the output of the model indicating that the cooling rate at

700 °C for 200 amps at 21 volts, (a typical flux cored arc welding output), at a travel speed of 2 mm/s is 32.04 °C/s. If the same parameters were applied to a fillet weld and if energy were to be reduced (Kirk, Mileham and Yeo, 1995), perhaps by increasing the travel speed from 2 mm/s to say 3 mm/s then the cooling rate would increase from 67.4 °C/s to 104.854 °C/s. When applied to hardness calculations, whilst the fillet weld hardness does not quite exceed that maxima stated in EN 288-3, (primarily invoked to avoid hydrogen induced cracking), the predicted fillet hardness values are similar to those actually reported in the failure analysis of the Alexander Kielland oil rig disaster of 1980, (Kielland, 1981), (see Figure 5-6), which with very similar chemical composition, material thickness, and weld parameters, underpins initial confidence in the model.

Distance	y = 3 mm, z = 3 mm		Thickness 25 mm	
Butt	HVM	429.522	Cooling Rate	32.04
2 mm/s	HVB	287.538	Time to cool to 700°C	9.96 s
	HVFP	161.148	Bainite	95.80%
	Average H	282.255	Ferrite Pearlite	4.20%
Fillet	HVM	436.305	Cooling Rate	67.4
2 mm/s	HVB	302.844	Time to cool to 700°C	3.96 s
	HVFP	162.23	Bainite	97.24%
	Average H	306.53	Ferrite Pearlite	2.76%
Butt	HVM	436.7	Cooling Rate	70.38
3 mm/s	HVB	303.735	Time to cool to 700°C	4.12 s
	HVFP	162.293	Bainite	96.33%
	Average H	308.613	Ferrite Pearlite	3.67%
Fillet	HVM	440.335	Cooling Rate	104.85
3 mm/s	HVB	311.938	Time to cool to 700°C	1.19 s
	HVFP	162.873	Martensite	32.39%
	Average H	353.522	Bainite	67.61%

Table 5-6 Analysis of output for a Nb-microalloyed steel
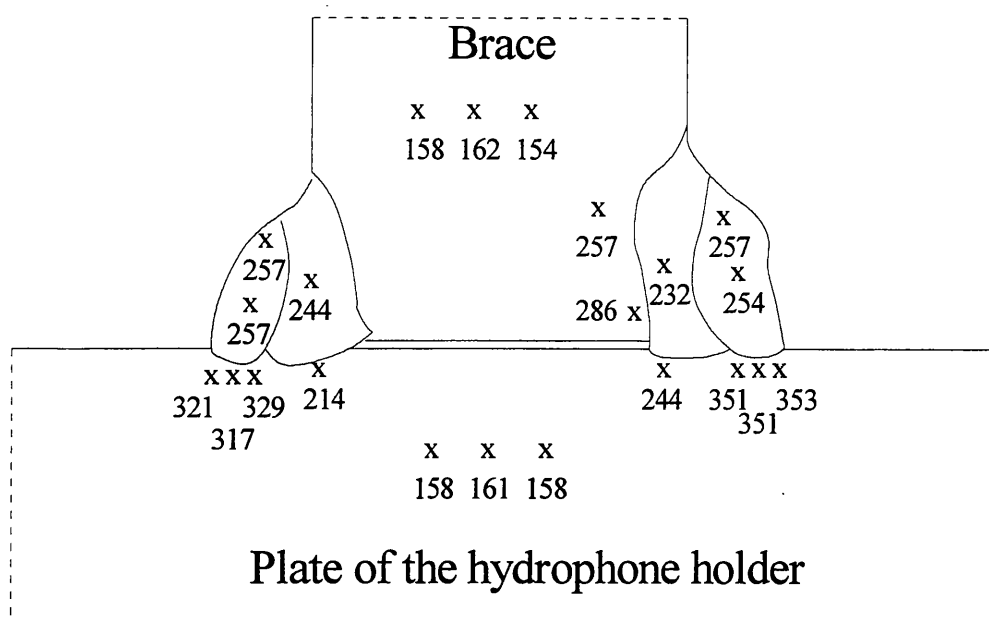
Figure 5-6 Hardness surveys in the weld connections between the hydrophone holder
and the brace, (After Kielland, 1981)

5.12 Comments

A new CHF equation has been developed, which, with related partially differentiated
and transposed equations, predicts the heat flow and cooling rates in plates of
intermediate thickness delimited by the thin and thick plate equations developed by
Rosenthal.

A number of non-destructive tests are utilised, (for example, Ultrasonic Flaw
Detection, Magnetic Particle, Dye Penetrant, Radiography), in performance testing of
either welders or procedures. Despite the success of these tests in revealing defects,
none of the aforementioned tests can reveal anomolies such as unacceptable hardness
in the heat affected zone. The ability to predict defect sites, (unacceptable hardness or
microstructure), in the weld heat affected zone will enable designers, engineers and
fabricators to reduce costs of set-up and procedure development in a range of
hypoeutectoid steels.

6. Modelling the weld thermal cycle in fillet welds

6.1 Temperature distribution im fillet welds

6.1.1 90° T-fillet joints

Development of the CHF equation which models the heat flow due to a moving heat source in any range of thicknesses enables consideration of the effect on complex joint setups such as fillet joints, typically illustrated in Figure 6-1.
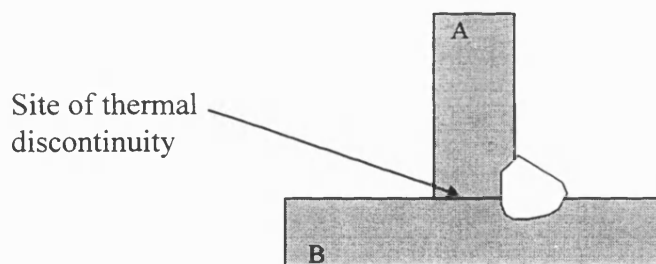
Figure 6-1 : 90° T-fillet joint

From a review of the literature, (for example, Graville, 1968, and Jeong and Cho, 1997)), it is suggested that a thermal disconttinuity could be present between the two plates of a fillet welded joint.

To model this phenomenon, complementary equations have been developed to express the heat flow in, and between, the upper and lower plates. Since the experiment evidences a possible 100% discontinuity, a boundary condition is necessary in order to make each equation independent of each other. This is presumed to be the general case for most welding applications, (Graville, 1968), since the plates

are, in the main, unlikely to be machined prior to fabrication setup, and are therefore
of comparitively coarse surface and contact quality as illustrated in Figure 6-2, below.
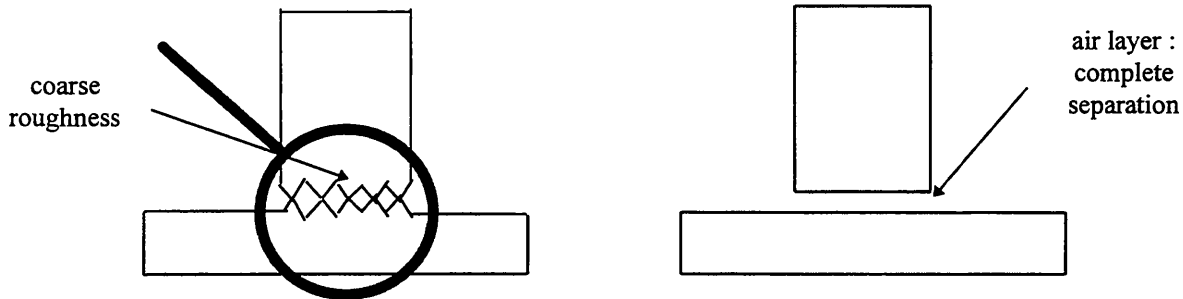
Figure 6-2 : typical causes of thermal discontinuity

Note: Radiation and convection are ignored for the purpose of the equations.

The Rosenthal equations assume that the energy input may be modelled
mathemetically by a point source. However, appreciation of practical welding
applications reveal that each plate receives energy input simultaneously with its
counterpart, and in order to apportion the energy to the two plates, this point source
assumption has been relaxed. Thus, in the case of the symetrical joint, it is assumed
that each plate receives half the energy, (Q/2), see Figure 6-3, (subject to the angle of
the electrode, discussed later).
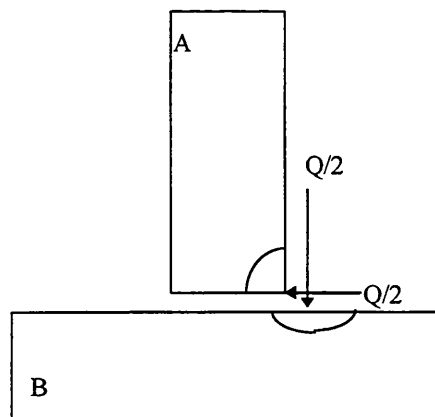
Figure 6-3 : heat input in plates

Thin plates :

In the upper plate, (**plate A**), the temperature gradient produced by the heat source may be solved by adapting the Rosenthal 'thin plate' equation. In the first instance, for a thin and infinitely wide plate, having a theoretically zero thickness, the heat expands radially from the centre point, (see Figure 6-4), which implies the inverse 2π term in the original equation, since the circumference of the circle may be expressed as $2\pi r$, with (r) being ignored on differentiation.
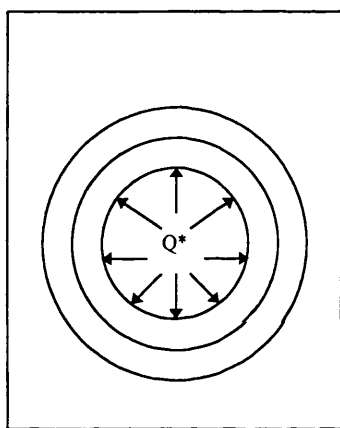
Figure 6-4 : radial expansion of heat in a 'thin' plate

However, at the edge of a plate, the heat flows through half a circle, (see Figure 6-5), (involving a π term only):
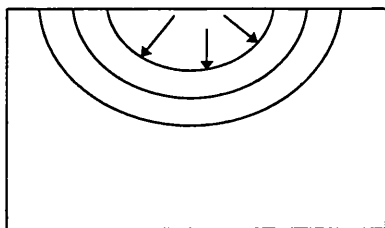
Figure 6-5 : expansion of heat in a semi-infinite plate

Hence, for a 90° T-fillet joint, the Rosenthal 'thin' plate equation required for the upper plate, (where the 2π term is replaced by the π term), is:

$$T - T_0 = \frac{Q/2}{\pi \, k \, g} \cdot \left(\frac{\pi}{2\lambda \, v}\right)^{1/2} \cdot \left[\frac{e^{-\lambda \, v[(\xi^2 + y^2)^{1/2} + \xi]}}{(\xi^2 + y^2)^{1/4}}\right]$$

Equation 6.1

For the lower plate, (**plate B**), the heat input is Q/2, but in this case, the shape is as described for the bead on plate and the equation thus incorporates only the original 2π term, as detailed in Equation 6.2.

$$T - T_0 = \frac{Q/2}{2\pi \, k \, g} \cdot \left(\frac{\pi}{2\lambda \, v}\right)^{1/2} \cdot \left[\frac{e^{-\lambda \, v[(\xi^2 + y^2)^{1/2} + \xi]}}{(\xi^2 + y^2)^{1/4}}\right]$$

Equation 6.2

These two equations explain the relevant shape of the HAZ observed experimentally, and as illustrated earlier in Figure 6.3.

Thick plates :

In the case of the thick plate, it is necessary to consider heat diffusing through a sphere instead of a circle. In this case the principal equation uses shape factors which modify the expression for the area of a sphere $(4\pi r^2)$, noting that (r^2) is ignored on differentiation.

Plate A : Thus, for a corner weld illustrated below, the term in the equation becomes

$\dfrac{Q/2}{4\pi/4} = \dfrac{Q}{2\pi}$, as only a quarter of a sphere needs to be be considered.
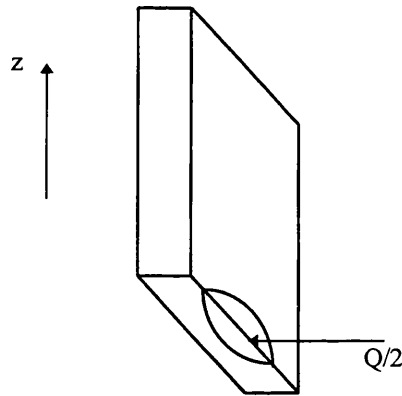
Figure 6-6 : expansion of heat through a quarter of sphere

The amended Rosenthal equation is therefore :

$$T - T_0 = \frac{Q/2}{\pi\,k} \cdot \left[\frac{e^{-\lambda\,v[(\xi^2 + y^2 + z^2)^{1/2} + \xi\,]}}{(\xi^2 + y^2 + z^2)^{1/2}} \right]$$

Equation 6.3

Plate B :

The heat flows through half a sphere in a bead on a plate, since the energy is input on the plate surface and the shape must thus be modified and is inversely proportional to $4\pi/2 = 2\pi$ term. The complete half sphere is illustrated below in Figure 6.7.
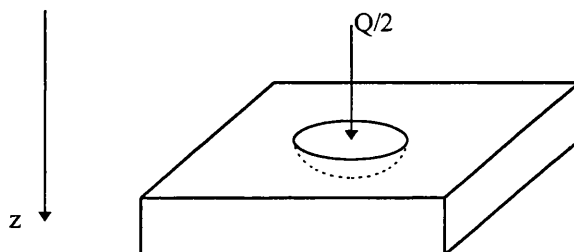
Figure 6-7 : expansion of heat through half a sphere

The solution is as stated by Rosenthal but using Q/2 instead of Q, giving,

$$T - T_0 = \frac{Q/2}{2\pi\ k} \cdot \left[\frac{e^{-\lambda\ v[(\xi^2 + y^2 + z^2)^{1/2} + \xi\ ]}}{(\xi^2 + y^2 + z^2)^{1/2}} \right]$$

<div align="right">Equation 6.4</div>

- **Intermediate plates** :

The equations are deduced with the same method as for the thin plates, but include the logarithmic coefficient adapting the thickness term, (g):

$$\left(T - T_0\right)_A = \frac{Q/2}{\pi\ k(10\log_{10}g)} \cdot \left(\frac{\pi}{2\lambda\ v}\right)^{1/2} \cdot \left[\frac{e^{-\lambda\ v[(\xi^2 + y^2 + z^2)^{1/2} + \xi\ ]}}{(\xi^2 + y^2 + z^2)^{1/4}} \right]$$

<div align="right">Equation 6.5</div>

and

$$\left(T - T_0\right)_B = \frac{Q/2}{2\pi\ k(10\log_{10}g)} \cdot \left(\frac{\pi}{2\lambda\ v}\right)^{1/2} \cdot \left[\frac{e^{-\lambda\ v[(\xi^2 + y^2 + z^2)^{1/2} + \xi\ ]}}{(\xi^2 + y^2 + z^2)^{1/4}} \right]$$

<div align="right">Equation 6.6</div>

6.1.2 T-fillet joint of any angle

It is necessary to consider adaptations of the model to include fillet joints where the angle, (θ), between the two plates is other than 90°, typically as illustrated in Figure 6-8 below, with nomenclature for the distribution of energy illustrated in Figure 6-9.
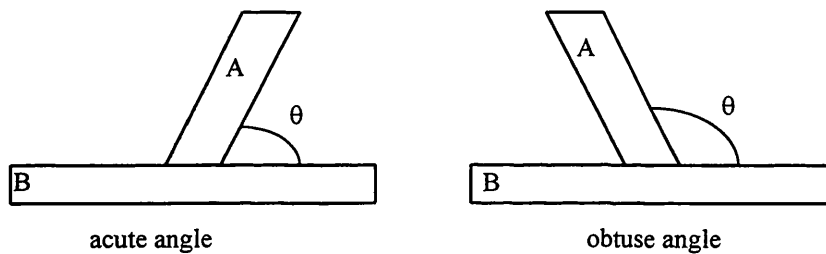
Figure 6-8 : fillet joint at angle θ
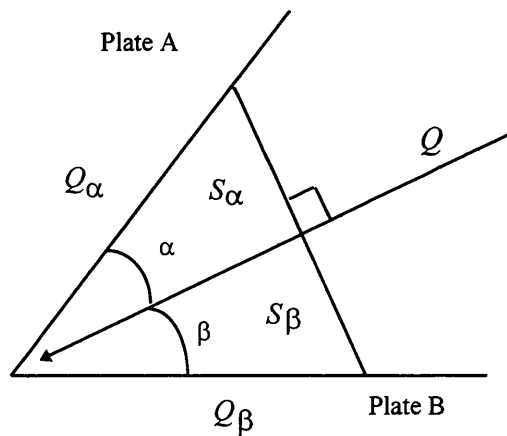
Figure 6-9 : distribution of the input heat between the two plates

The essential difference in calculation of this compared with that for the 90° fillet is the determination of the amount of heat which flows into plate A and B, and consideration of the shape factor for each plate. Considering an electrode bisecting the plate θ angle, at an angle, (α), to the upper plate, and at an angle, (β), to the lower plate, the areas formed between the electrode and the plates may be used to determine the energy which each plate receives. These quantities are Q_α and Q_β, with $Q = Q_\alpha + Q_\beta$, which are proportional to the areas S_α and S_β.

$$\frac{Q_\alpha}{Q} = \frac{S_\alpha}{S} = \frac{\sin\alpha \cdot \cos\beta}{\sin\theta} \text{ and } \frac{Q_\beta}{Q} = \frac{S_\beta}{S} = \frac{\sin\beta \cdot \cos\alpha}{\sin\theta}, \text{ with } S = S_\alpha + S_\beta.$$

In respect of the shape factor for plate A, a corrective term, (φ), is used, which takes into account the θ angle. The first term of the CHF equation, $\dfrac{Q/2}{\pi \ k(10\log_{10}g)}$,

therefore becomes $\dfrac{\phi \ Q_\alpha}{\pi \ k(10\log_{10}g)}$.

φ has been determined by considering three particular values of φ :

When θ→90° and α=β=45° then $Q_\beta = Q_\alpha = 1/2$, so φ→1 .

For the acute angle, i.e. θ<90°, as θ→0 then $\dfrac{\phi \ Q_\alpha}{\pi \ k(10\log_{10}g)} \rightarrow \dfrac{Q/2}{2\pi \ k(10\log_{10}g)}$, so

φ→1/2. In this position, Figure 6-10, the joint can be seen as nearly a bead on a plate.
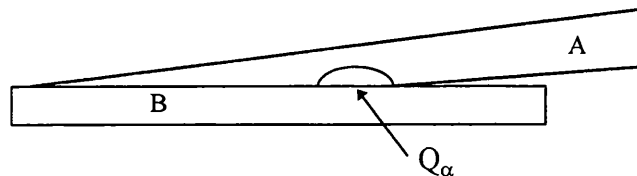
Figure 6-10 : θ→0°

where the equation contains the $\dfrac{Q/2}{2\pi\ k(10\log_{10})}$ term, and thus the equations for plate

A and plate B become the same.

Finally, for obtuse angles $(90 < \theta < 180)$, $\phi\to\infty$, as θ becomes arbitrarily close to $180°$, since the thickness of A tends to zero on the joint: (bead on a plate, zero thickness), illustrated below in Figure 6-11.
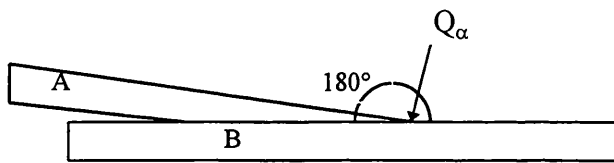
Figure 6-11 : $\theta\to180°$

Therefore , using the cosine of θ, it can be assessed that $\phi=\dfrac{1}{1+\cos\theta}$.

Thus for the upper plate, the final CHF equation becomes

$$\left(T-T_0\right)_A = \frac{Q}{\pi\ k(10\log_{10} g)}\cdot\frac{1}{1+\cos\theta}\cdot\frac{\sin\alpha\cdot\cos\beta}{\sin\theta}\cdot\left(\frac{\pi}{2\lambda\ v}\right)^{1/2}\cdot\left[\frac{e^{-\lambda\ v[(\xi^2+y^2+z^2)^{1/2}+\xi\ ]}}{(\xi^2+y^2+z^2)^{1/4}}\right]$$

Equation 6.7

For plate B, $\phi = 1/2$, since the shape does not change from its original, (2π), state, and

therefore, $Q_\beta = \dfrac{\sin\beta\cdot\cos\alpha}{\sin\theta}\cdot Q$:

$$\left(T - T_0\right)_B = \frac{Q}{2\pi\ k(10\log_{10} g)} \cdot \frac{\sin\beta \cdot \cos\alpha}{\sin\theta} \cdot \left(\frac{\pi}{2\lambda\ v}\right)^{1/2} \cdot \left[\frac{e^{-\lambda\ v[(\xi^2 + y^2 + z^2)^{1/2} + \xi\ ]}}{(\xi^2 + y^2 + z^2)^{1/4}}\right]$$

Equation 6.8

Note: For simplicity the nomenclature of the coefficient ϕ, adjusting π, may be named $C\pi$, and the coefficient adjusting Q may be named, C_Q.

6.2 Industrial application

As has been discussed previously it is suggested that the new CHF equations and their associated formulae predict the weld HAZ properties more accurately than the Rosenthal equations, even when modified with empirical coefficients, (Hess et al). However, they are somewhat complicated since they have been developed primarily for research purposes. It is considered that it would be beneficial if the equations could be simplified, or computer programs developed to enable their use by welding technicians or engineers in practical environments, thus providing rapid indications of the final hardness and microstructure of the heat affected zone.

A computer program has therefore been written to calculate such information, a basic flow diagram of which is illustrated below in Figure 6-12.
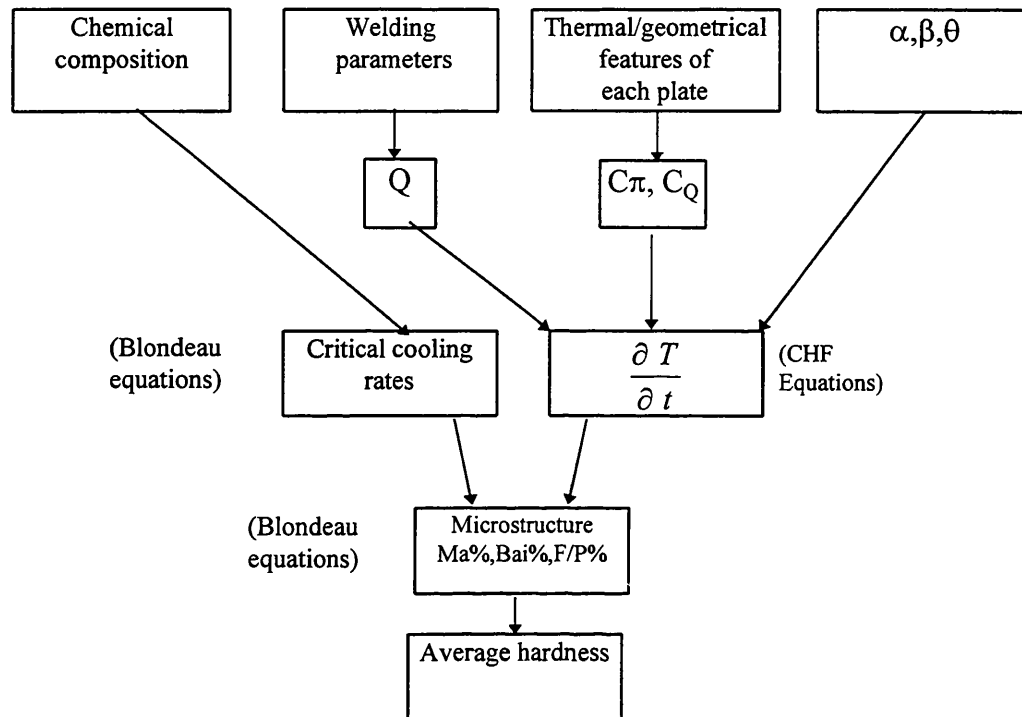
Figure 6-12 : flow diagram of the program

The ability to predict the cooling rates mathematically, combined with empirical hardness and critical velocity formulae, will enable engineers to estimate hardness. Except in specific applications, high hardness is often not beneficial as it may imply brittleness. Thus, the program may provide a tool to reduce both time and costs of set up and procedure development and testing, and may be extended to include robotic sequencing.

In order to validate the equations and the hypothesis of infinite thermal resistance between two plates, physical experimental work has been utilised to analyse the accuracy of the predictive models, examining microstructure, hardness and heat transfer across the interface between the two plates.

7. A mechanical and geometrical approach to thermal contact resistance

7.1 Introduction

In order to validate whether the hypothesis of null thermal contact conductivity used in the equations is correct, the actual contact resistance must be assessed. If thermal conductivity is shown to vary as described in Chapter 6, the computer program may be used to develop data tables for different materials and types of machining.

A number of theories have been proposed, which have led to analytical models of the thermal contact resistance (TCR), between two plates, in contact, under load, but not attributed to welding. According to Salgon JJ, Robbe-Valloire F, Blouet J, and Bransier J, 1997, the thermal contact problem may be decomposed into two relatively independent steps :

1. as TCR is strongly dependent on the interfacial geometrical state, a mechanical model must be used to describe surface deformations under the applied load.
2. The prediction of TCR from the actual state of the interface requires a geometrical model of the contact spot in order to represent the heat transfer across this spot, and find an analytical solution.

The value of the geometrical parameters can be deduced from the initial surface topography of each plate, their mechanical properties, and the contact load. The

TCR is then calculated as a function of both the geometrical parameters and the thermal properties of the materials, as illustrated in Figure 7-1.
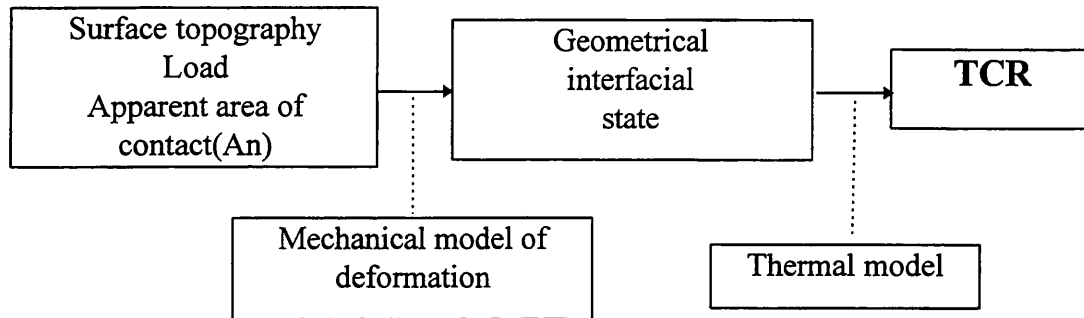
Figure 7-1 : method for assessing the TCR, (after Salgon, et al, 1997).

7.2 Experimental overview - topography

A computer program based on the method proposed by Salgon et al, has been written, and is archived in Department of Mechanical Engineering Internal Report Number 35/97. The key input data are the topographic parameters of the the two surfaces: the mean peaks square height (m_0) and the mean square curvature (m_2). By machining samples so that the range of their thermal resistance value is both wide and measurable, permits an effective study of its influence on the HAZ. A total of 36 plates were machined and examined with each plate subject to two assessments of surface condition.

The topography of the surfaces was measured with a Tallysurf stylus profilemeter, as illustrated in Figure 7-2.
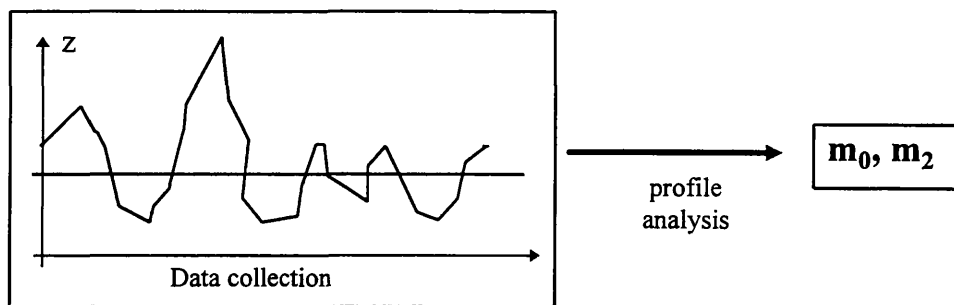
Figure 7-2 : profile analysis - profilemeter

7.2.1 Analytical approach to thermal contact resistance

Thermal contact resistance models using equations pertaining to random gaussian surfaces are usually defined, (Salgon, et al), as the ratio of temperature drop across the interface to the heat flow across the surface : $Rtc = \dfrac{\Delta T}{\Phi}[K\,W^{-1}]$. In this thesis the resistance is reported to the unity of area and expressed in $mm^2.K.W^{-1}$.

- Mechanical and geometrical approach of the TCR:

The first assumption is to consider both the irregularities on a surface, (asperities) and the tips of the peaks thus formed, (contact spots), as similar to a tubular construction. This simplifies the mechanical model of the surface, and is illustrated below, in Figure 7-3.
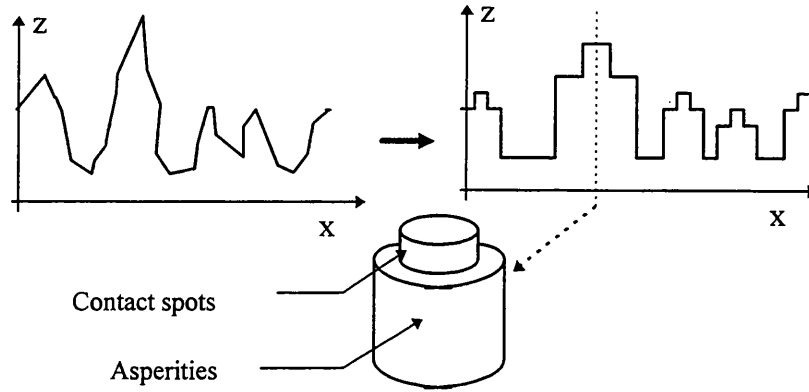
Figure 7-3 : Tube model of a surface

This assumption enables the creation of a representative flux tube called a Holm Tube, which synthesizes the heat transfer across a single medium contact spot, as illustrated in Figure 7-4, below.
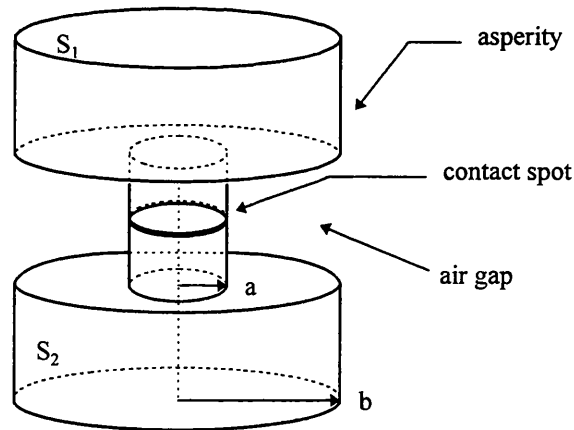
Figure 7-4 : Holm Tube model, (after Salgon et al, 1997).

Further, assuming that the small air gap behaves similar to a vacuum, a reasonable assessment of the TCR, (Salgon, et al, 1997), is given by Equation 7.1,

$$Rtc = \frac{\pi \, b^2}{2ka}(1 - 1.41\xi)$$

Equation 7.1

where (b) is the mean radius of the surface asperities and (a) the mean radius of the contact spots, in the Holm Tube model of contact, where ξ = a/b, and where (k), is the harmonic mean of the thermal conductivities of the two contacting solids, given by,

$$\frac{2}{k} = \frac{1}{k_1} + \frac{1}{k_2}$$

Equation 7.2

Thus, it is necessary to assess (ξ) and (b) as functions of (m_0) and (m_2), the mean values of (m_{0i}) and (m_{2i}).

It is considered that m_0 and m_2 are respectively the mean peak square height and mean square curvature of an equivalent surface, which is the mean surface (Sm) of the two surfaces (S_1) and (S_2). Solving the problem, "(S_1) in contact with (S_2)" is equivalent to solving the problem "(Sm) in contact with a flat surface", typically illustrated in Figure 7-5, below.
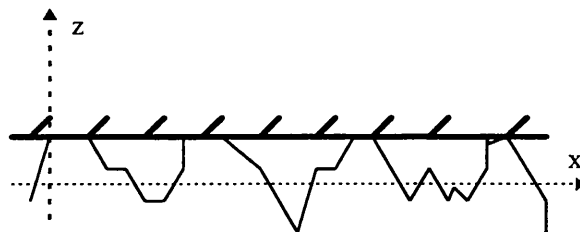
Figure 7-5 : equivalent surface=mean of the two surfaces in contact

In order to perform the intense iterations indicated in solving the problem, the equations developed by Salgon, et al, were coded and run as a computer program, details of which are archived in Department of Mechanical Engineering Internal Report Number 35/97.

7.2.2 Validation

In order to validate the program, a comparison was made between the predictions from the program, the theoretical predictions of Salgon, and the literature experimental data of MacWaid, 1992. Two materials, (aluminium and stainless steel), bead blasted or ground, were evaluated.

Aluminium
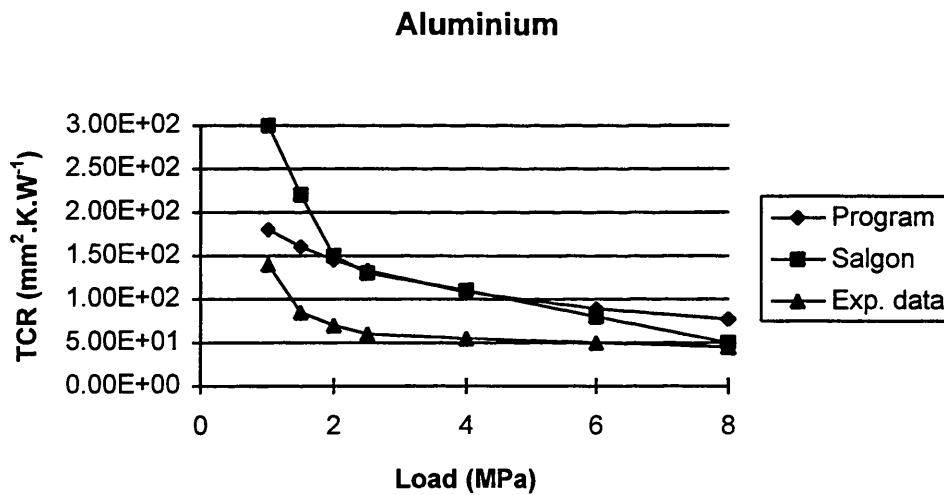
Figure 7-6 : comparison between the program, Salgon and MacWaid data, (Al).
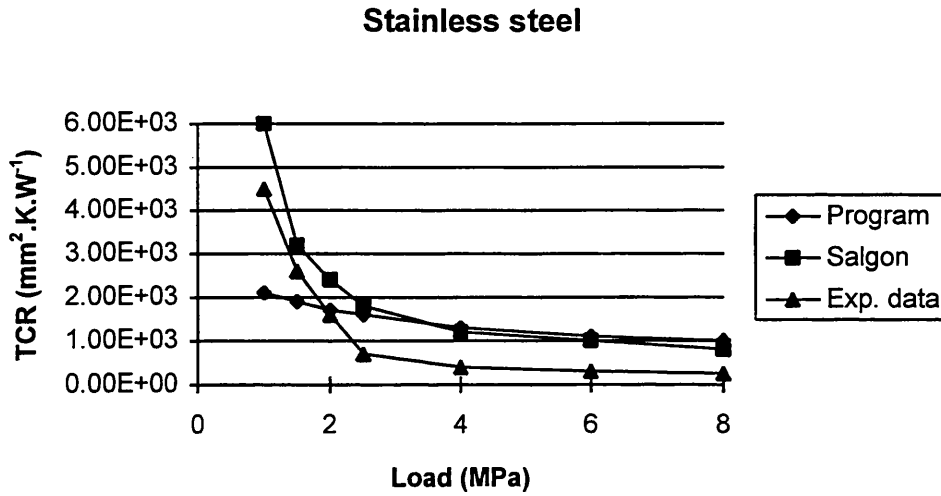
Stainless steel

Figure 7-7 : comparison between the program, Salgon, and MacWaid data, (Stainless steel)

Figure 7-6 and Figure 7-7 illustrate the comparisons. For loads over 2 MPa, there is reasonable correlation, however, for loads lower than 2 MPa, the values diverge. This is principally due to the wide scattering of experimental data reported by Salgon, and to some degree, the limitations of the accuracy of the interpolations of the functions, which may be further modified for low loads.

8. Influence of thermal contact resistance on the CHF equations for a T-fillet joint

8.1 Comparison between radiation, convection and thermal contact resistance

Rosenthal assumed that the losses due to convection and radiation were small enough to be ignored. By analysing the losses due to radiation and convection during the course of the experimentation using various assumptions, it was concluded that whilst losses due to convection and radiation are not zero, it was reasonable for Rosenthal to ignore them because they are very small when compared to the heat losses due to conduction.

The losses due to convection and radiation depend on surface finish, joint geometry and position, size, and fluid (air) flow. Radiation was considered in certain models, and this suggested that it could be important in situations where radiation impinges on an opposite surface due to joint set-up, typically in a 45° fillet or V butt.

- The general equation for the energy, (Watts), loss due to convection is :

$$q_{convection} = hA(T_1 - T_2), \text{Watts}$$

where h is a convection heat transfer coefficient, A is area, T_1 is the temperature of the surface giving $q_{convection}$, and T_2 is the temperature of the surface

receiving $q_{convection}$. Free convection of a vertical plate 0.3m high in a fluid (air) of temperature of 30°C, h = 4.5 J/s/m^2 °C.

- For radiation, the equation for energy loss, (Watts), is :

$$q_{emitted} = \epsilon \sigma A T^4 \text{ , Watts}$$

where (T) is the absolute temperature (in Kelvin) of the body and (σ) is the proportionality constant, called the Stefan-Boltzmann constant, whose value is $5,669.10^{-8}$ W/m^2 K^4. This is the Stefan-Boltzmann law of thermal radiation.

The equation above includes an emmissivity coefficient, (ϵ), which varies with surface finish, since without it, the equation is only valid for black bodies. Such an equation depends also on the angle relationship of the receiving surface.

In considering the effect of thermal contact resistance, (TCR), in a T-fillet joint, the transfer/conduction of heat in the homogenous parent metal must be considered. The calculation and analytical solution in the case of a transient (unsteady) state situation is somewhat complicated and cumbersome, as shown in the next section.

In the transient condition, a point on the surface of the material will experience a thermal history resulting from the direct heat of the arc or conducted heat resulting from the arc/energy source, plus or minus the conducted heat due to the relative difference of heat (ΔT) between the two plates through a thermal contact resistance.

Such conduction and phenomena have already been expressed as continuous functions, (CHF equations), in Chapter 6.

To examine this further, the thermal history at a point, P, on the surface, 2mm from the weld centre line, illustrated in Figure 8-1, with the following parameters was considered.

- ♦ Current (I) :   300 Amps
- ♦ Voltage (V) :   22 Volts
- ♦ Transfer efficiency :   0.9
- ♦ Speed of travel :   4.5 mm/s
- ♦ Material thickness :   25mm
- ♦ Original plate temperature :   20°C
- ♦ Joint set-up :   90° 'T' fillet
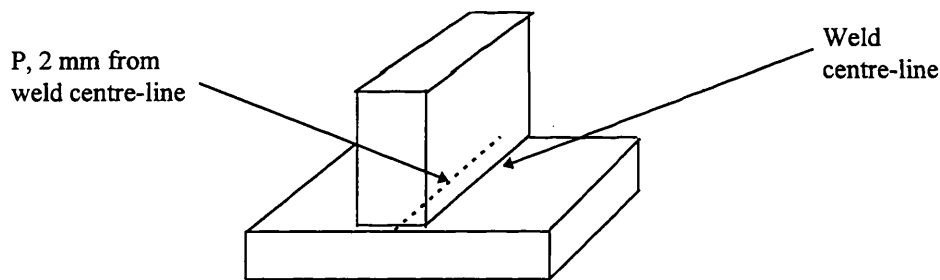
Figure 8-1 : examination of thermal history at point P

Table 8-1, below, summarises the results of the investigation, where radiation, convection and thermal contact resistance are neglected : (t [time] =0 is the instant when the contact source hits the point, P). Note that the peak temperatures shown above are at precise time points and may not represent the maximum temperature for this location.

If the peak temperature achieved at the location is considered as a steady state for even the briefest of interval, the equations for radiation, convection and thermal

contact resistance may be considered as accurate enough to provide an indication of the maximum losses likely to occur.

Time (s)	T in upper plate (°C)	T in lower plate (°C)	Temperature difference (°C)
-10	20	20	0
-9	20	20	0
-8	20	20	0
-7	20	20	0
-6	20	20	0
-5	20	20	0
-4	21	20	1
-3	24	22	2
-2	50	35	15
-1	250	135	115
0	1576	798	778
1	1372	696	676
2	1049	534	515
3	878	449	429
4	770	395	375
5	694	357	337
6	638	329	309
7	593	307	286
8	557	289	268
9	527	274	253
10	502	261	241
11	480	250	230
12	461	240	221
13	443	232	211
14	428	224	204
15	415	217	198

Table 8-1 : summary of peak temperatures in a T-fillet joint

Thus, for an area of 1 mm^2 where T_0 = 20°C and taking emmisivity as 0.15 (milled surfaces) :

Calculating an equivalent loss (q $_{conduction}$), (Watts) due to conduction only, using

$$q_{conduction} = -kA\frac{(T_2 - T_1)}{\Delta x}, \text{ Watts}$$

with,

- ◆ k = thermal conductivity (k=0.037 W/mm.°C)

- ◆ A = area of resistance to the heat flow

- ◆ T$_2$ = surface temperature (surface 2)

- ◆ T$_1$ = surface temperature (surface 1)

- ◆ Δx = thickness between T$_2$ and T$_1$ (Δx=1mm)

then, (abridged),

Time (s)	Upper plate(C)	Equivalent loss (W)	Convection, q (W)	Radiation, q (W)	Contact, q (W)
1	1372.07	11.95	0.006039315	0.0301	0.09658
2	1048.81	19.21	0.004584645	0.0103	0.07349
3	877.70	10.02	0.00381465	0.00505	0.0613
15	414.61	0.08007	0.0018	0.00025	0.028

Table 8-2 : Analysis of losses in the upper plate

Thus, in a steady state, although the loss due to contact, (Table 8-2 above), is almost a thousandth of the conduction loss (Δx=1mm), it is almost 100 times greater than convection and at least 3 times greater than radiation. Therefore, if the level of TCR is more than zero, it may be necessary to take account of its influence. The calculation shows that radiation and convection, can, in general, be ignored.

8.2 Modelling heat flow across the fillet weld interface

8.2.1 Semi-infinite plate and additional heat flow:

It is necessary to determine the temperature distribution in a semi-infinite plate, heated by a source, (Q), travelling along an edge, but additionally subject to a heat flow, (Qtcr), through one of its faces, namely the interface between the two plates in the fillet weld joint, as illustrated in Figure 8-2.
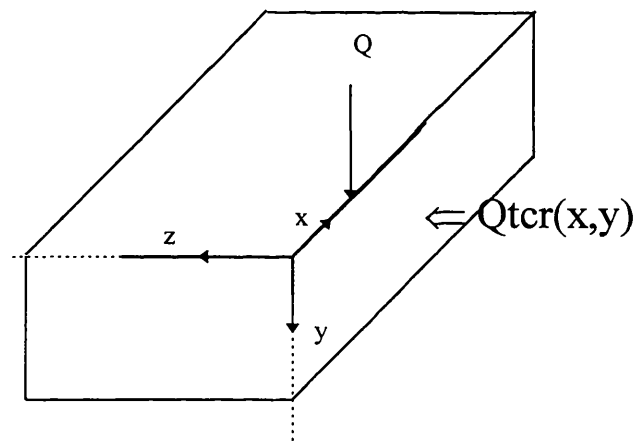
Figure 8-2 : heat sources in the upper plate

Note: Figure 8-2, illustrates an upper plate with the contact surface clearly visible, for clarity.

Having regard to the Rosenthal expansion, detailed in Appendix C, and initiating with the common Laplace differential equation for the upper plate,

$$\frac{\partial^2 T}{\partial x^2} + \frac{\partial^2 T}{\partial y^2} + \frac{\partial^2 T}{\partial z^2} = 2\lambda \frac{\partial T}{\partial t}$$

Equation 8.1

subject to the following boundary conditions,

$$\frac{\partial T}{\partial x} \to 0 \text{ as } x \to \pm\infty$$

$$\frac{\partial T}{\partial y} \to 0 \text{ as } y \to +\infty$$

$$\frac{\partial T}{\partial z} \to 0 \text{ as } z \to +\infty$$

$$-\frac{\partial T}{\partial r} \pi r^2 k \to Q \text{ as } r \to 0$$

However, the presence of a thermal resistance layer at the interface requires a new boundary condition, namely,

$$-\frac{\partial T}{\partial z} k = Q_{tcr}(x,y) \quad , \text{ on the plane } z=0$$

where (Qtcr) is the heat flow due to the second plate through a contact resistance, (R_{tc}), and expressed per unit area of the boundary surface (W/mm^2), and also assuming a quasi-stationary state. Therefore the temperature, T(x,y,z), in the upper plate may be considered as the **sum** of the temperature change due to **conduction** of heat in the upper plate, and the **additional temperature change** due to heat conducted through a **thermal contact resistance** from the adjacent plate.

No suitable analytical solution was found for this problem. To avoid using a finite-difference method to solve it, the problem was simplified by considering a plate of finite dimensions, as illustrated below in Figure 8.3.
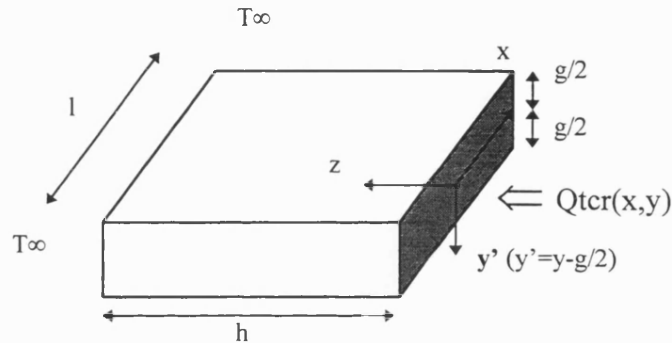
Figure 8-3 : simplified problem; plate of finite dimensions

- **Note : y'=y-g/2**

Under the assumption that (g), (h) and (l) are "large", it may be considered that the first three boundary conditions above are therefore equivalent to :

$$T(\pm l/2, y', z) = T_\infty$$

$$T(x, g/2, z) = T_\infty$$

$$T(x, y', h) = T_\infty$$

$$-\frac{\partial T}{\partial z} k = Q_{tcr}(x,y'), \ \forall (x,y') \in [-l/2, l/2] \times [-g/2, g/2] \text{ and } z = 0$$

This type of problem may be solved by separating the variables, and further, an analogy in 3D space may be used to transpose the function f(x,y,z), into a convergent trigonometric series by decomposition into its harmonic components.

Application in this manner, (See Appendix D), leads to,

$$T(x, y, z) = \sum_{m=0}^{\infty} \sum_{n=0}^{\infty} a_{mn} \cdot \cos(\omega_n x) \cdot \cos(\delta_m y) \cdot \cosh(\chi_{mn} z) \cdot [\tanh(\chi_{mn} z) - \tanh(\chi_{mn} h)]$$

Equation 8.2

Applying the equation to both upper and lower plates, (See Appendix D), leads to a solvable linear system, but one which comprises an infinity of equations. In this regard the computing time was extensive and it must be concluded that other approaches, such as through the use of numerical methods such as partial differential equations or finite element analysis may prove of value given the accuracy of the assumptions in the originating CHF equation of fixed thermal conductivity and specific heat capacity of the material under investigation.

8.2.2 Numerical analysis

In concluding that numerical methods may be more applicable to rapid soving of the problem, and given that the analytical approach had been computerised, a study into the possible derivation of a simplified approach was undertaken. To this extent, the program provided first order results and these were examined with regard to the potential for matching an appropriate transendental function.

The program relied on the assumption that

$$Qtcr(x, y, t) \approx \frac{T_{rB}(x, y, 0, t) - T_{rA}(x, y, 0, t)}{R_{tc}}$$

and was examined for various values of (R_{tc}). Table 8-3 details the parameters used, and Table 8-4 details the output.

p	0.007833 g/mm^3
C	0.67 J/g.°C
k	0.037 J/s.mm.°C
λ	0.5*p*C/k= 0.070920 s/mm^2
v	4 mm/s
g	20 mm
Q	5800 J/s
l	250 mm
w	150 mm
h	100 mm
x	0 mm
T$_0$	20 °C

Table 8-3 : Parameters used in numerical approximation

Rtc (mm^2.W^{-1}.K)	Upper plate limit (no TCR)	Upper plate limit (TCR)	Lower plate limit (no TCR)	Lower plate limit (TCR)
7000	7.4 (t=4s)	7.3 (t=3.9s)	3.5 (t=1s)	3.48 (t=0.99s)
3500	``	7.2 (t=3.9s)	``	3.47 (t=0.99s)
1000	``	6.9 (t=3.5s)	``	3.6 (t=1.0s)
500	``	6.5 (t=3.1s)	``	3.7 (t=1.1s)
200	``	5.4 (t=2.2s)	``	4.2 (t=1.5s)
150	``	4.9 (t=1.8s)	``	4.5 (t=1.8s)
0*	``	4.8 (t=1.8s)	``	4.8(t=1.8s)

Table 8-4 : Numerical approximation output - HAZ limits at z=0.

- Notes :

1) "no TCR" means that the assessment was carried out using the original CHF equations, with no heat transfer due to the TCR.

2) Rtc=0* : The corresponding HAZ limit was assessed in the same way as "no TCR", but with plate A, receiving the power Q/3 instead of Q/2 and plate B, receiving 2Q/3 instead of Q/2, since the two plates at this resistance are a homogeneous block, (detailed in full, later, in Chapter 9).

Figure 8-4, below, illustrates a graph of the output.
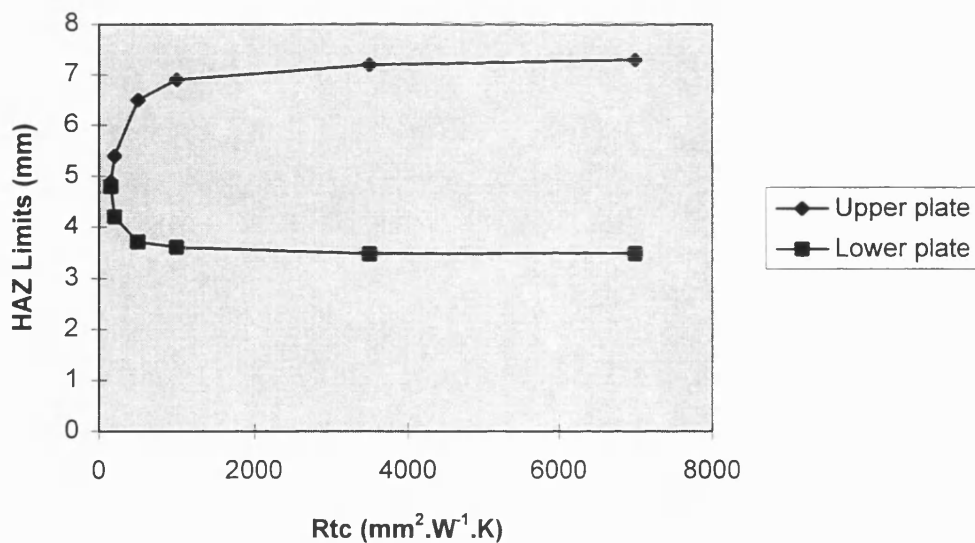
Figure 8-4 : graph of the HAZ limits.

The graph shows the evolution of the limits of the two HAZ when (Rtc) is decreasing from 7000 $mm^2.W^{-1}.K$ to 150 $mm^2.W^{-1}.K$, though the lowest values of

(Rtc) may be out of the range of validity of the simplifications, as previously discussed.

The two curves highlight that the HAZ limits tends towards a common value, as expected. The last row of the table underlines that this value seems to be the limit reached with the plates receiving Q/3 and 2Q/3 instead of Q/2 and Q/4 in the CHF equations. This new distribution of the input heat flow can be justified analytically, and is explained in the next chapter. The curves suggest that an exponential variation of the HAZ limits along with Rtc would be the simplest approximation of the computed results, and this is illustrated in Figure 8-5.
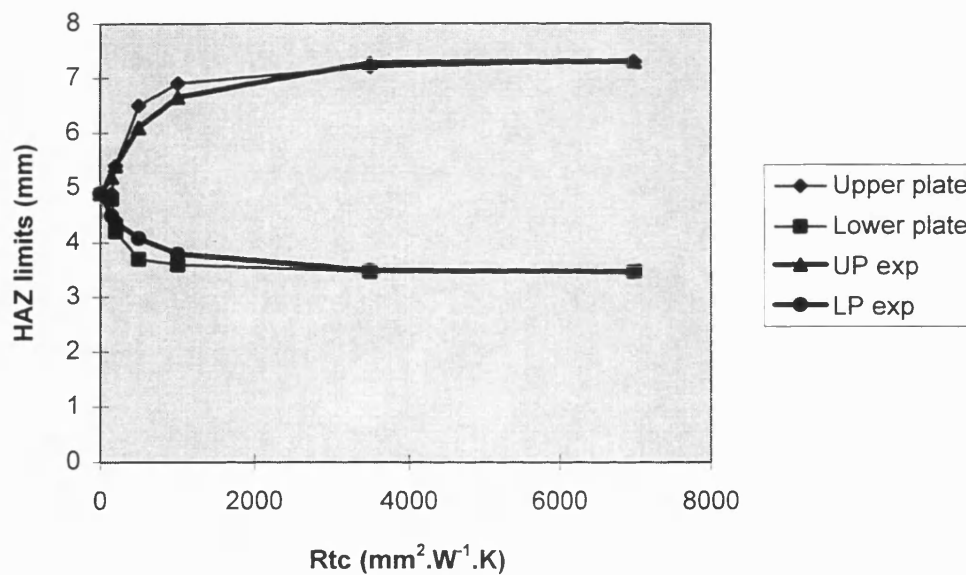
Figure 8-5 : exponential approximations

with $y_{LA}(Rtc) \approx 7.3.(1-\exp(-0.0012857.Rtc))$ (Upper Plate = UP exp)
and $y_{LB}(Rtc) \approx 3.5.(1+\exp(-0.0012857.Rtc))$ (Lower Plate = LP exp)

The highest value Rtc=7000 $mm^2.W^{-1}.K$ was chosen because it was the measured value on the samples. However, where continuity of the heat affected zone was observed in the experimental plates (i.e. heat transfer occurring between the

plates), the assessed values of the HAZ dimensions are almost the same as in the "no TCR" case (i.e. when no heat transfer occurs between the two plates). Thus, continuity was achieved for a lower value of (Rtc).

This may be explained by two reasons.

Firstly, in the program, only the first term of the cosine series was assessed. This implies that the real "transfer" of temperature should be marginally greater than that obtained for low values of (Rtc).

Secondly, the pressure applied over the contact surface between two plates during the welding sequence may well be different from atmospheric pressure alone, (plus the upper plate weight), initially expected, and used to assess the Rtc values of the samples, since following tack welding of the two plates, there is a contraction of the welded metal which to some degree increases the load over the interface, and decreases the initial Rtc values in the same proportion. Moreover, additional contractions are likely to occur during welding, and the temperature may also influence the value of (Rtc).

9. Simplified analytical approach to TCR

9.1 Introduction

The previous chapter concluded that an exponential expression could adequately model the heat flow across the interfaces of a fillet joint through a thermal contact resistance. It is further suggested that such a conclusion may provide the basis for a simplified analytical approach to such phenomena, and this chapter examines the derivation of a multiplicative coefficient to replace the previous complex model, to enable it to be applied to the CHF equation.

Such conclusions at this time are limited to 90° T-fillet joints only, pending further research.

9.2 Boundary conditions

The transition between the two extreme cases of contact quality is modelled in two cases,

1) a gap between the plates, to model infinite resistance,
2) a perfect contact, in order that the two plates behave as a single homogeneous domain, to model zero resistance.

An illustration of the two cases is shown in Figure 9-1, below.
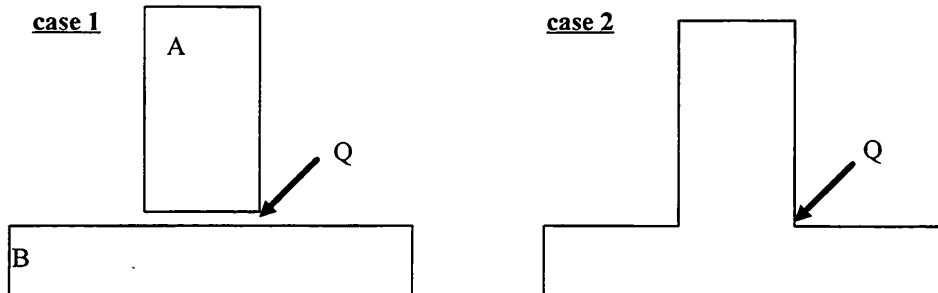
Figure 9-1 : two extreme cases, case 1 - 100% resistance, case 2 - 0% resistance

- **Case 1 : Thermal discontinuity** :

The revised general form of the CHF equation is :

$$T - T_0 = \left(\frac{C\pi}{\pi}\right) \cdot \frac{C_Q \cdot Q}{k(10\log_{10} g)} \cdot \left(\frac{\pi}{2\lambda v}\right)^{1/2} \cdot \left[\frac{e^{-\lambda \, v[(v^2 t^2 + y^2 + z^2)^{1/2} - vt]}}{(v^2 t^2 + y^2 + z^2)^{1/4}}\right]$$

where (C_Q) and (C_π) are coefficient applied to the (Q) and (π) terms in the equation.

In Case 1, given the symmetry of the problem, each plate receives $C_Q.Q=Q/2$, with $C_\pi/\pi=1/\pi$ for the upper plate (A), since the heat dissipates radially from the point source and meets the plate through a quarter of a sphere, (inverse of $4\pi/4$). For plate (B), the lower plate, $C_\pi/\pi=1/2\pi$, as the heat dissipates radially from the point source through half a sphere, (inverse of $4\pi/2$):

Thus, $\left(\dfrac{C\pi}{\pi} \bullet C_Q \cdot Q\right)_A = \dfrac{Q}{2\pi}$ and $\left(\dfrac{C\pi}{\pi} \bullet C_Q \cdot Q\right)_B = \dfrac{Q}{4\pi}$

Equation 9.1

• **Case 2 : homogeneous material** :

In this case, the distribution of heat between the upper and lower plate is no longer applicable, (since the two plates are a homogeneous block). It is assumed that this may be expressed by adjustment to the shape factor based on the proportionality of the shape, (to a sphere), and thus yielding 4π * $3/4$, (since the homogeneous block in this case represents $3/4$ of a sphere). This may be further justified by a symmetrical decomposition of the theoretical domain into three virtual sub-domains, as illustrated in Figure 9-2.
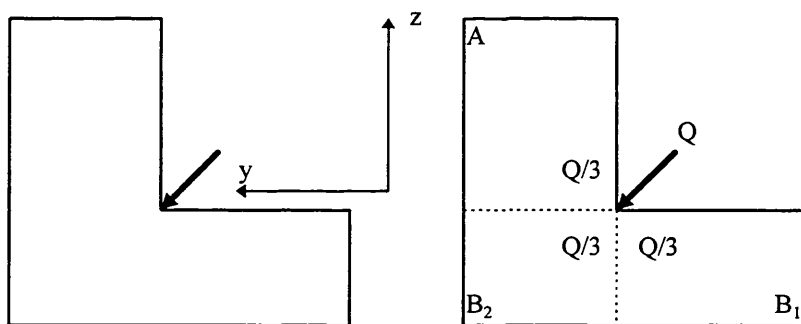
Figure 9-2 : decomposition into 3 virtual sub-domains

This decomposition gives the solution for plate (A) directly,

where $C_Q.Q=Q/3$ and $C_\pi/\pi=1/\pi$.

Concerning sub-domain B,

$B = B_1 \cup B_2$, $C_Q.Q = 2Q/3$ and $C_\pi/\pi = 1/2\pi$.

Therefore, $\left(\dfrac{C\pi}{\pi} \bullet C_Q \cdot Q \right)_A = \dfrac{Q}{3\pi}$ and. $\left(\dfrac{C\pi}{\pi} \bullet C_Q \cdot Q \right)_B = \dfrac{Q}{3\pi}$

This implies that (T_A) and (T_B) have the same values at the junction of the two sub-domains (z=0), as expected. Therefore, for the homogeneous (or TCR=0), 90° plates, the CHF equation is:

$$(T - T0)_A = (T - T0)_B = \frac{Q/3}{\pi \; k(10\log_{10} g)} \bullet \left(\frac{\pi}{2\lambda \, v} \right)^{1/2} \bullet \left[e^{-\lambda \; v[(v^2 t^2 + y^2 + z^2)^{1/2} - vt \;]} \frac{}{(v^2 t^2 + y^2 + z^2)^{1/4}} \right]$$

Equation 9.2

giving an all encompassing simplified cooling rate for both cases, where y = 0 and z = 0,

$$\frac{\partial T}{\partial t} = -(T - T_o)^3 \bullet \frac{2\pi k\rho C}{2} \bullet \left(\frac{v[10(Log_{10} g)]}{C_\pi \cdot C_Q \cdot Q} \right)^2$$

Equation 9.3

9.2.1 Intermediate thermal contact resistance state

In order to develop a simplified equation to express the consequence of thermal

contact resistance in relation to intermediate, (non-boundary, where the plates are

neither wholly independent nor homogeneous), states, (even if they exist in only a

small proportion of cases), it is necessary to evaluate a coefficient $\{\Gamma(Rtc)\}$

modelling cases 1 and 2, for each plate.

Thus,

$$\left(\frac{C\pi}{\pi} \bullet C_Q \cdot Q\right)_A (Rtc = \infty) = \frac{Q}{2\pi} \xrightarrow{\Gamma_A(Rtc)} \left(\frac{C\pi}{\pi} \bullet C_Q \cdot Q\right)_A (Rtc = 0) = \frac{Q}{3\pi}$$

<div align="right">Equation 9.4</div>

and

$$\left(\frac{C\pi}{\pi} \bullet C_Q \cdot Q\right)_B (Rtc = \infty) = \frac{Q}{4\pi} \xrightarrow{\Gamma_B(Rtc)} \left(\frac{C\pi}{\pi} \bullet C_Q \cdot Q\right)_B (Rtc = 0) = \frac{Q}{3\pi}$$

<div align="right">Equation 9.5</div>

Therefore $\Gamma_A(Rtc=\infty)=1/2$ and $\Gamma_A(Rtc=0)=1/3$

and $\Gamma_B(Rtc=\infty)=1/4$ and $\Gamma_B(Rtc=0)=1/3$

A function giving the transition between $Rtc=0$ and $Rtc=\infty$ is necessary, and in

order to determine the type of such a function, a number of experimental results

were considered. Following an analysis of the experimental output, reports of which have been made later, in Chapter 11, it is considered that further work would be required before conclusive determination of the required function may be made. However, the numerical results obtained from the simplified algorithm explained in the previous section, gives, for the experiments carried out, an acceptable level of accuracy for limited industrial use.

9.2.2 Exponential approach

The previous graph of the HAZ limits implies that $\Gamma(Rtc)$ remains close to 1/2 or 1/4 unless (Rtc) has a relatively "low value. Since Rtc can only be measured when the plates are still separated ($P\approx1MPa$), it is considered that a "low value" is close to 7000 $mm^2.W^{-1}.K.$, as revealed by the experiments. This means that $\Gamma(Rtc)$ is given as a function of Rtc measured without load, which is a readily measurable parameter.

Following the conclusions of the previous chapter, it is considered likely that $\Gamma(Rtc)$ tends exponentially toward 1/3, as (Rtc) tends towards zero, (Figure 10.3). Thus, it is considered, that by reference to the approximated variation of the HAZ limits, the coefficient would be of the type:

$$\Gamma_A(Rtc) = \frac{1}{2}\left(1 - \frac{\exp(-w\,Rtc)}{3}\right)$$

and

$$\Gamma_B(Rtc) = \frac{1}{4}\left(1 + \frac{\exp(-w\,Rtc)}{3}\right)$$

where $w = 7.14e\text{-}5\ mm^{-2}.W.K^{-1}$
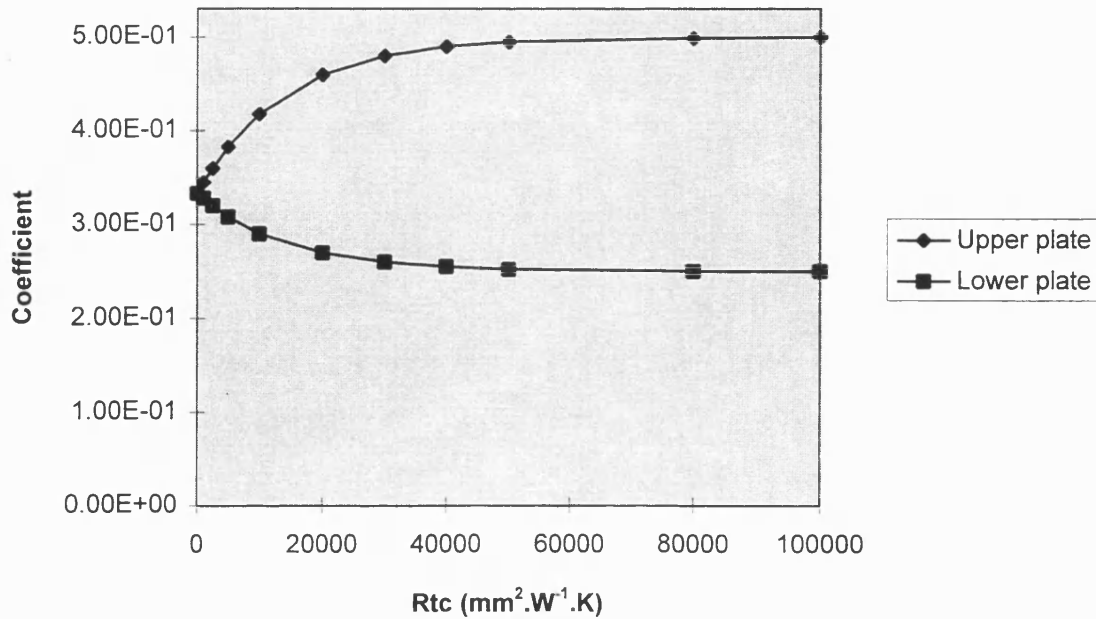
Figure 9-3 : Γ_A(Rtc) and Γ_B(Rtc).

(w) has been chosen here to make (Γ_A) and (Γ_B) equate to 1/3 for Rtc=7000 mm^2.W^{-1}.K. as observed in the experiments. With this value of (w), Γ_A(Rtc=7000)=0.39, Γ_B(Rtc=7000)=0.30.

It is concluded, therefore that simplified equations may be developed empirically from the result of future experimental research and that this may lead to tables of (w) which may be used to evaluate the effect of thermal contact resistance in the welding of a number of joint setups.

10. Experimental validation and testing - I
Set-up and welding operations

10.1 Overview

In order to validate the equations and models derived in previous chapters, experiments were conducted to provide physical evidence of the effect of heat flow in welded joints over a range of thicknesses, and to show the effect of changes to surface quality on the thermal contact resistance between contact surfaces of the fillet welded joint. This chapter reviews the preparation of plates and welding operations to enable this to be accomplished.

10.2 Preparation of plates and assessment of surface quality

It is necessary to determine whether the quality of the contact surface affects the heat flow between the upper and lower plates and under what circumstances there is a significant thermal conduction between the two plates.

Direct temperature measurement was investigated but was found difficult to carry out in the HAZ, due to the rapidity of the weld thermal cycle and the extremely high temperatures involved in fusion of material. However it is possible to compare the dimensions of the extent of the HAZ and its average hardness, (since, the hardness depends on the microstructure resulting from the cooling rates), and this method was used to analyse several T-fillet joints, whose contact surface qualities were made to be different.

10.3 Materials

The material used was a high strength low alloy steel of specification EN 10025 S355. Plates of various thickness, (10 mm, 15 mm, 20 mm, 25 mm, and 30 mm), and contact surfaces were welded, using a robot to ensure that speed and electrode extension, (12 mm.), were constant.

The welding equipment was a 500A DC pulsed arc power source, with a consumable flux-cored wire, (SAF SAFDUAL 100), with a shielding gas, (BOC ARGOSHIELD 20). Specifications are detailed below.

- ARGOSHIELD : reported composition :

20% CO_2, 2% O_2, balance Ar

- SAFDUAL 100 : reported average chemical analysis :

%C	%Mn	%Si	%S	%P
0.05	1.4	0.5	0.014	0.012

- EN 10025 S355 : average reported composition :

%C	%Mn	%Si	%S	%P	%Al	%N	%Nb
0.16	0.5	1.6	0.025	0.030	0.02	0.009	0.1

10.4 Preparation of test pieces

In order to validate the theoretical concept, the surface quality of the plates in contact were assessed by considering the roughness after machining.

The presence of microscopic cavities create an air layer which may be wide enough to insulate the two plates thermally. Therefore the experiment was designed to achieve a wide range of roughnesses to replicate various joint setups and heat flows. Figure 10-1, below, illustrates this concept.

Perfectly smooth contact : 100% of the surface is efficient for heat conduction

Rough surface contact : x% of the surface is efficient for heat conduction

No contact : 0% of the surface is efficient for heat conduction
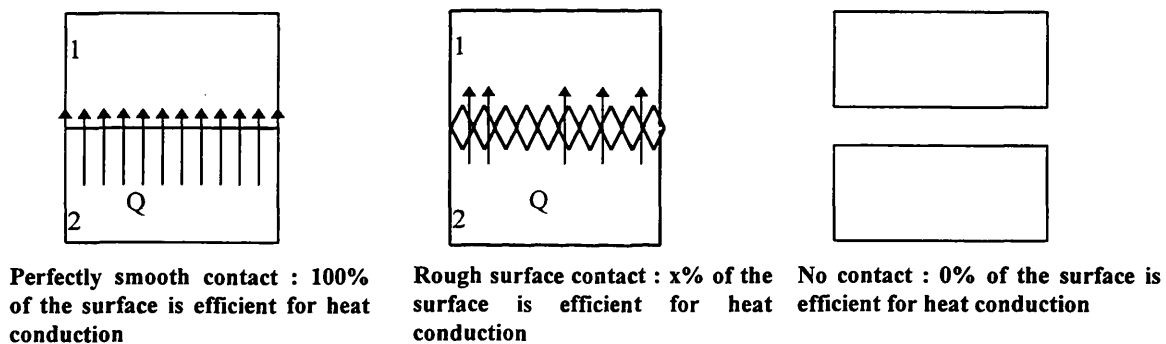
Figure 10-1 : efficient surface for heat flow through the contact zone

Examination of different machining methods reveals that there is a close link between the surface quality and the equipment used to produce the surface. This is illustrated in Figure 10-2.
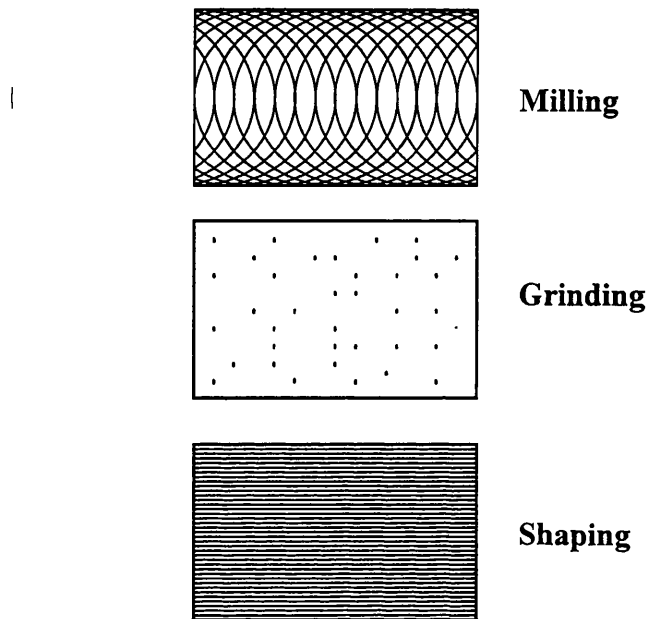
Figure 10-2 : three different machined surfaces

Though the features on the surfaces are different, the measured values of roughness, (Ra), may be similar.

10.5 Surface quality of the samples

Four surface qualities were chosen, allowing the corresponding TCR to be different enough to assess the influence of this parameter over a wide range of values. The analytical approach has highlighted that the TCR value was linked to the apparent, (nominal), area of contact, (An), the mean peaks square height of the equivalent surface, (m_0), and the mean square curvature of the equivalent surface, (m_2). The values of these three parameters are linked to the procedure used to produce the surface.

There are two ways to obtain a wide scope of TCR values: keeping (An) constant and modifying the topographic parameters (m_0) and (m_2); or keeping the topographic parameters (m_0) and (m_2) constant and modifying (An).

10.5.1 Keeping (An) constant and modifying the topographic parameters (m_0) and (m_2)

In this case, such surfaces could be generated with a milling machine since it is relatively easy to alter the surface quality. To maintain equivalence, four roughnesses were chosen for the upper plate edge, with the base plate corresponding to the smoothest quality.

As a result of the characteristic geometric lay left by the tool on the surface, the roughness is not isentropic, and therefore two perpendicular measures with the profilemeter would be required on each surface in order to estimate the TCR, as illustrated in Figure 10-3.
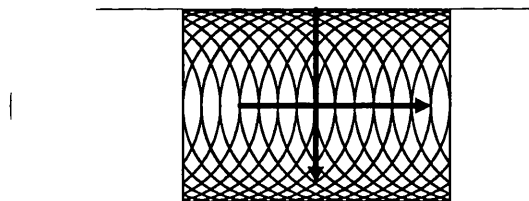
Figure 10-3 : characteristic geometric lay on an end milled surface and directions of measurement

Such an assessment would become difficult if the tool quality deteriorated, since any defects are macroscopic and the surface is heterogeneous. In view of this, since such a solution requires frequent machine parameter adjustment, the second solution reported below, was considered.

10.5.2 Keeping the topographic parameters (m_0) and (m_2) constant and modifying (An)

Very smooth surface (m_0,m_2). TCR of value Rn

Very smooth surface (m_0,m_2), but shaped with grooves. TCR=Rp
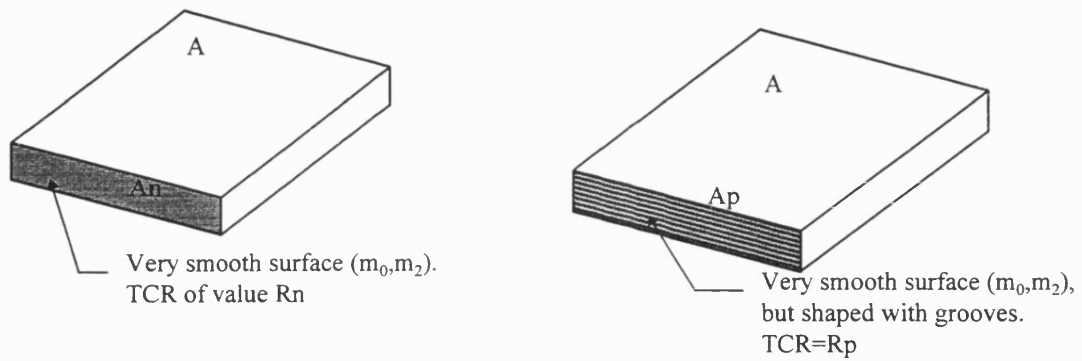
Figure 10-4 : reducing the apparent contact surface (An) with grooves

a) Joint contact set-up

b) Groove detail

pitch p

A

grooves

depth d
angle α

B

α

d
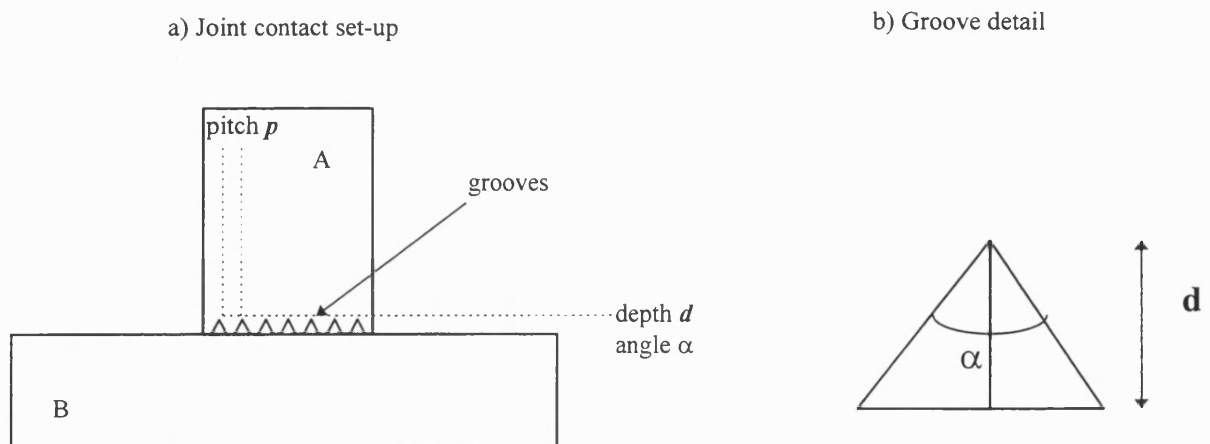
Figure 10-5 : design of the grooves

Subsequent to these considerations it was decided that the samples would be machined with a shaper in order to generate the required grooves, (See Figure 10-4 and Figure 10-5). This permitted ease of assessment of the value of the prepared surface, (Ap), in order to calculate the thermal transfer through the contact zone (Ap<An). Thus, with the geometry of the machined grooves known, it was possible to deduce (Ap), and various surface qualities were obtained by changing the pitch, notwithstanding that the gap between the two consecutive contact strips needed to be macroscopic in order that the surfaces could be considered as independent thermal contact resistances. The analytical value of the ratio

$$\Psi = \frac{Ap}{An} = \frac{remaining\ surface}{initial\ surface}$$ was therefore assessed from the shape of the tool, the pitch, the depth and the numbers of runs.

As the thermal contact resistance (Rtc) of the joint is inversely proportional to (Ap), it is determined that:

$$\Psi = \frac{Ap}{An} = \frac{Rn}{Rp}.$$

Thus, one set of profile analysis is required for assessing (Rn), and four values of (Ψ) could be tested, as illustrated in Figure 10-6, (though noting that 100% cannot be achieved in practice).
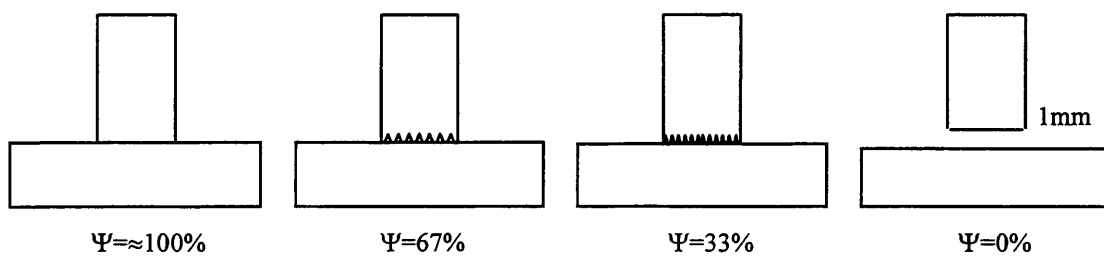
Figure 10-6 : the four values of (Ψ) to be tested

10.5.3 Evaluation of the topographic parameters

As explained previously, the first step in the prediction of the TCR across a given contact is the evaluation of the topographic parameters of the contacting surfaces. A surface profilemeter was used to determine the surface characteristics.

Each of the contacting surfaces was assessed using a Taylor Hobson Talysurf 50 profilemeter to obtain the surface data.

A sampling interval of $2.5\mu m$ was used. The scan length of each trace was 5 mm, thus each profile trace was comprised of 2000 data points. The radius of the diamond stylus was $3\mu m$.
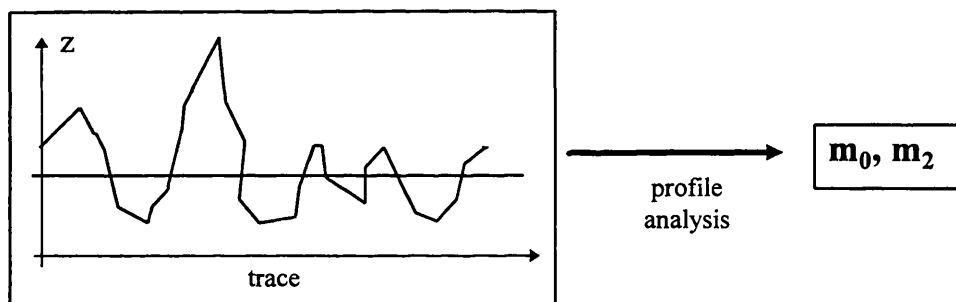
Figure 10-7 : profile trace to be analysed in order to assess (m_0) and (m_2)

The milled surfaces were assessed by four traces of the profilemeter. Two traces were taken parallel to the surface lay, and two traces were taken perpendicular to the surface lay, thus, (m_0) and (m_2) were evaluated from each profile. The average of the two sets of values obtained from the profile were used to determine the surface topography.

A least squares line was applied to each set of data, thus constituting the mean profile height. No long-wavelength filtering was used (i.e. "roughness filter") since the long wavelength irregularities (asperities) could play a critical role in determining a TCR. Therefore, each profile was subject to a short-wavelength filter (i.e. a "waviness filter"). As the minimum resolvable frequency of the sampling process equaled twice the sampling interval, each profile was subject to a short-wavelength cut-off of 8μm.

(This procedure has been designed to be as close as possible to the description given by MacWaid, 1992 to enable comparisons to be made).

10.5.4 Quality achieved

The plates were profiled to a size in concord with EN 288 to permit adequate mass effect, and the plates were machined, as illustrated in Figure 10-8 and Figure 10-9 below, with a table of measurements detailed in Table 10-1.

For all the surfaces to be milled, an Ra value of 3 μm was specified.
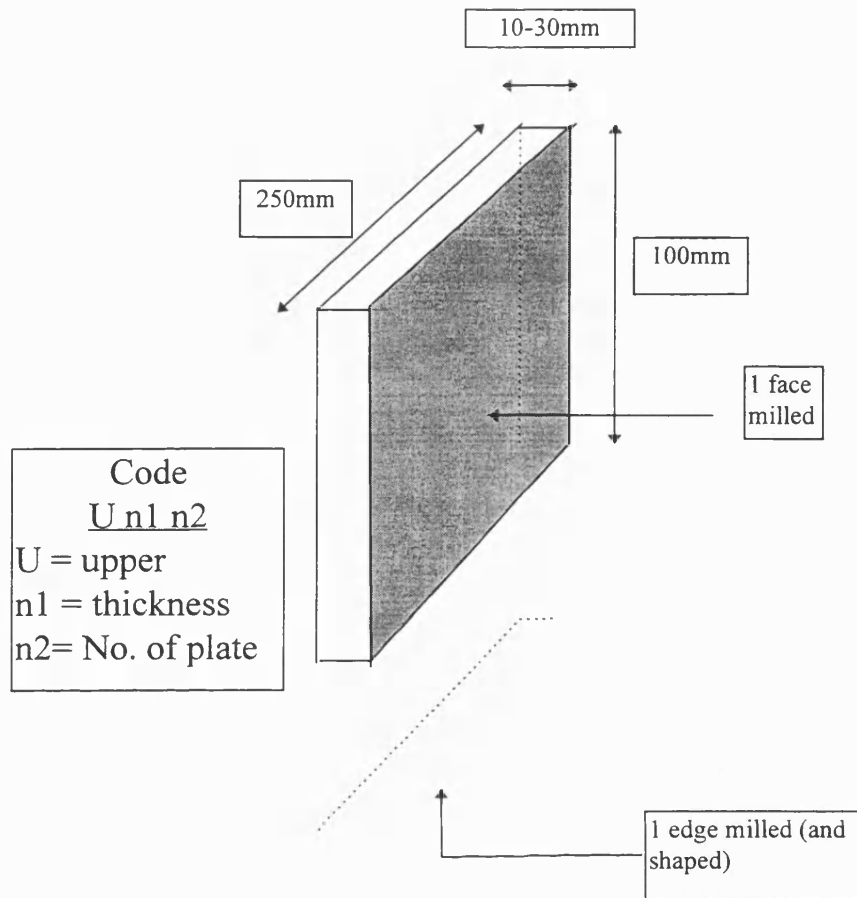
Figure 10-8 : upper plates milling procedure and encoding
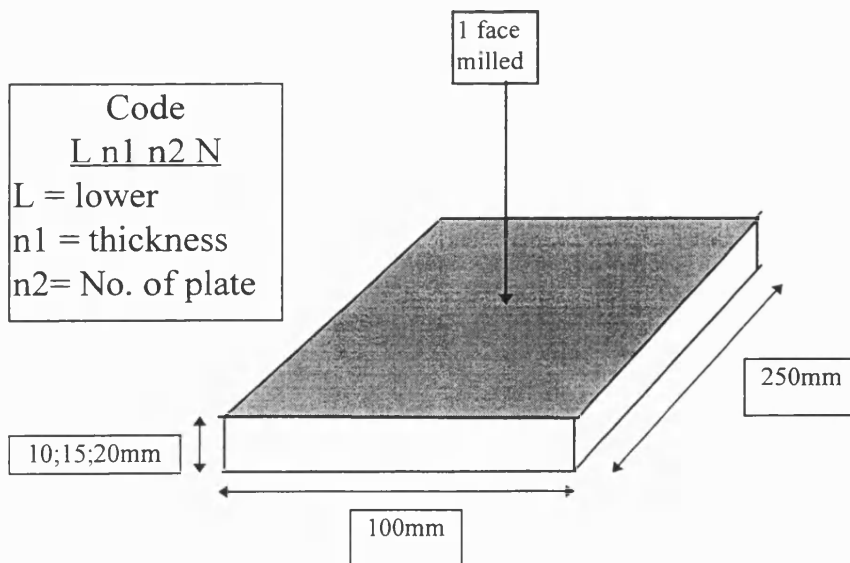
Figure 10-9 : lower plates milling procedure and encoding

CODE	Contact	l*w*h (mm^3)	Thermal contact resistance, (Rtc) (mm^2.W^{-1}.K)
U101N	≈100%	250.2*9.7*99.8	5600
L101N	≈100%	251.1*9.7*151.3	
U102N	≈67%	250.5*9.7*99.2	6400/0.54
L102N	≈67%	251*9.7*151.2	=12000
U103N	≈33%	250*9.7*97.4	6800/0.3
L103N	≈33%	251.1*9.7*151.2	=23000
U104N	0%	251*9.8*99	6900/0
L104N	0%	251.4*9.7*151	=∞
U151N	≈100%	250*14.7*99.3	3900
L151N	≈100%	250.1*14.6*150.1	
U152N	≈67%	252*14.7*98.2	6600/0.60
L152N	≈67%	250*14.2*150.2	=11000
U153N	≈33%	250.3*14.7*99	7500/0.27
L153N	≈33%	250.2*14.4*150.3	=30000
U154N	0%	250.5*14.7*99.5	5800/0
L154N	0%	249.8*14.6*150.3	=∞
U201N	≈100%	250*19.8*99.5	7000
L201N	≈100%	249.5*19.8*150.6	
U202N	≈67%	250*19.6*97.5	7100/0.60
L202N	≈67%	250.1*19.8*150.6	=12000
U203N	≈33%	249.5*19.8*96.8	8500/0.25
L203N	≈33%	250.2*19.8*250	=34000
U204N	0%	250*19.9*99	9100/0
L204N	0%	249.5*19.9*150.5	=∞

Table 10-1 : plate features after milling/shaping operations

The Ra values deteriorated slightly during the milling operations due to tool wear. However the mean value of Rtc, (before shaping), was calculated to be $7000 \ mm^2.W^{-1}.K$.

The six plates marked in Table 10.1, were shaped and measured, as shown in Figure 10-10, Figure 10-11, Figure 10-12 and Figure 10-13 below.
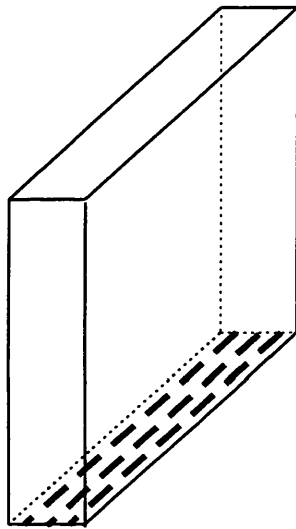
Figure 10-10 : grooves on one edge
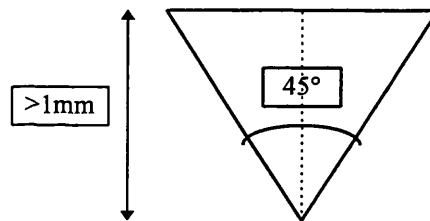
Figure 10-11 : tool tip definition
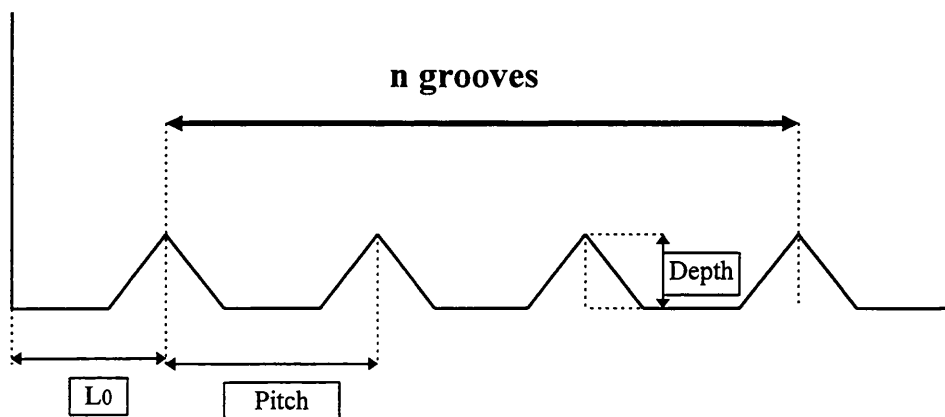
Figure 10-12 : grooves definition

CODE	SHAPING (mm)		L₀	n	Ψ	Ψ
	Depth	Pitch	(mm)		expected	obtained
U102N	1	2	2	4	0.66	0.55
U103N	1.1	1.3	1.1	7	0.33	0.30
U152N	1	2	2.5	6	0.66	0.60
U153N	1.1	1.3	1	11	0.33	0.27
U202N	1	2.3	2	8	0.66	0.60
U203N	1.1	1.3	0.9	15	0.33	0.25

Figure 10-13 : instructions for shaping and results on (Ψ)

10.6 Experimental equipment

A flexible welding cell was used, coupled with a computerised data recording system in order to monitor the current and voltage during the welding operations. The key elements were :

- a pulsed-arc power source, (no pulse used),
- the robot and the off-line control system,
- the wire feeder, connected to the power source,
- an extractor,
- the fixture,
- a PC to record the welding current and voltage.

10.6.1 Experimental cell

1	welding table
2	wire feeder
3	welding power source
4	robot
5	control unit
6	off-line PC
7	recorder (PC)

- - - -►	wire
——►	current
——►	orders
·········►	voltage
○·········►	current
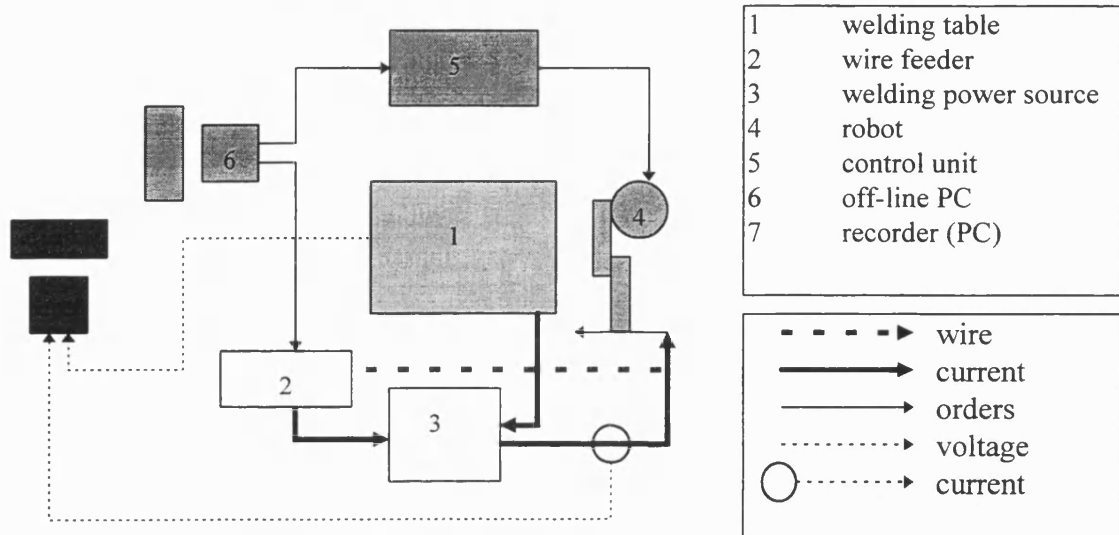
Figure 10-14 : organisation of the experimental cell

An illustration of the structure of the cell is shown above in Figure 10-14.

10.6.2 Welding equipment

For the experiment, a 500A, pulsed, arc power source was used, with a wire feed which supplied the flux-cored wire at constant speed. The trigger of the wire feeder was switched on and off from the control system of the robot in order that the whole welding sequence was under the control of one program.

Kirk, C.S., 1997, Experimental validation and testing - I /155

10.6.3 Fixture

A fixture was designed and manufactured to ensure replicability. The plates were tack welded together with an alpha angle of 90°, then welded in the flat position, in order to reduce the likelihood of unequal leg lengths or undercut through gravitational pull, as illustrated in Figure 10-15.
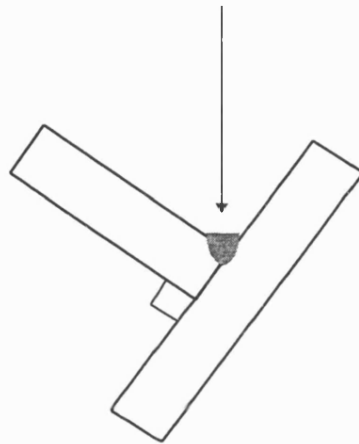
Figure 10-15 : welding in the flat, position, $\theta = 90°$.

10.6.4 The robot and the off-line control system

The robot was a Rediffusion Reflex 6-axis robot (1986), of the anthropomorphic type. The trajectories were taught off-line by editing a program on the robot control computer. The programs were written in AR-BASIC, with specific commands for the movements of the robot.

The program incorporated five principal subroutines, to enable,

1. **Teaching the tool axis**, in order to define the torch orientation and the position of the wire tip. This calibration was automatic since the corresponding co-ordinates were assessed from the geometry of the torch and its position in respect to the robot arm.

2. **Teaching the fixture frame** : the location of the fixture must be known with respect to the absolute frame of the cell.

3. **Teaching the reference joint** : the reference joint was defined by moving the robot arm to two successive points. These reference points defined the joint extremities. This could be carried out without specific torch orientation

4. **Setting the welding parameters** : running the program requires the definition of three parameters,

   - *the thickness of the plates* (mm) : the reference joint is translated to the correct z-co-ordinate,

   - *the speed of travel* (mm/s),

   - *the torch angle with respect to the vertical position* (°). The torch orientation was known in the fixture frame, thus enabling adjustment of the welding angle.

5. **Welding** : four welding points were generated. The second and the third defined the welding trajectory, and they were deduced from both the reference joint and the thickness of the plates. The first and the last points have the same x and y co-ordinates as the two previous points, with a higher z co-ordinate, thus optimising user adjustment.

An illustration of the weld points is shown below in Figure 10-16.
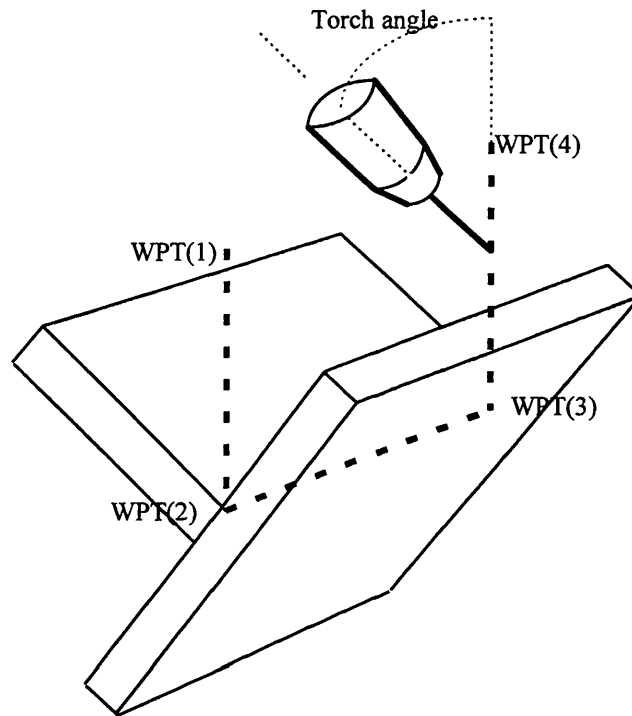
Figure 10-16 : programming the welding cycle

A listing of the program is detailed in Appendix E.

10.7 Welding

The plates were tack welded together, and stored at room temperature ($\approx 20°$) for four hours prior to commencement of welding operations. (The room temperature was recorded using a calibrated thermometer prior to the commencement of each weld). A table of final parameters appears in Table 10-2 below.

CODE	T₀ (°C)	l*w*h (mm³)	Rtc (1MPa) (m².W⁻¹.K)	U (V)	I (A)
U101N	22	250.2*9.5*99.8	5.6E-3	22.6	295.8
L101N		251.1*9.5*151.3			
U102N	22	250.5*9.7*99.2	6.4E-3/0.54 =1.2E-2	23.3	260.8
L102N		251*9.6*151.2			
U103N	22	250*9.7*97.4	6.8E-3/0.3 =2.3E-2	23.4	296.8
L103N		251.1*9.8*151.2			
U104N	22	251*9.6*99	6.9E-3/0 =∞	23	296
L104N		251.4*9.7*151			
U101K	22.5	251*9.6*99	6.0E-3	23.1	265.0
L252K		250.6*24.1*150.6			
U151N	22	250*14.7*99.3	3.9E-3	23.0	270.4
L151N		250.1*14.6*150.1			
U152N	22	252*14.6*98.2	6.6E-3/0.60 =1.1E-2	23.1	267.5
L152N		250*14.4*150.2			
U153N	22	250.3*14.6*99	7.5E-3/0.27 =3E-2	23.0	278.8
L153N		250.2*14.6*150.3			
U154N	22	250.5*14.5*99.5	5.8E-3/0 =∞	22.3	301.7
L154N		249.8*14.7*150.3			
U201N	22	250*19.6*99.5	7.0E-3	23.0	269.8
L201N		249.5*19.6*150.6			
U202N	22	250*19.4*97.5	7.1E-3/0.60 =1.2E-2	23.04	272.5
L202N		250.1*19.7*150.6			
U203N	22	249.5*19.7*96.8	8.5E-3/0.25 =3.4E-3	22.8	278
L203N		250.2*19.7*250			
U204N	22	250*19.7*99	9.1E-3/0 =∞	22.9	277.4
L204N		249.5*19.8*150.5			
U201K	22.5	250*19.6*99.1	9.0E-3	23.9	268.0
L251K		250.5*24.0*150.6			
U251K	22.5	251*24.3*99.4	7.1E-3	22.5	298.0
L101K		250.8*9.5*151.2			
U252K	22.5	250.5*24.2*100	6.5E-3	23.2	260
L201K		249.6*19.8*150.6			
U253K	22.5	251*24.0*100	6.3E-3	23.1	269.4
L253K		250.5*23.1*151			
U301K	22.5	250.5*29.2*98.6	7.5E-3	23.3	261
L301K		250*29.3*150.1			

Table 10-2 : Welding parameters and material specifications

Note: The torch angle was constant at 20° drag to the vertical, and speed of travel of the arc constant at 4 mm per second.

The plates were allowed to cool slowly to room temperature prior to sectioning and preparation for microscopic examination and evaluation.

11. Experimental validation and testing - II

Destructive testing, results and analysis

11.1 Preparation of coupons

All joints were sectioned with a band-saw and 8 mm thick coupons cut with an *Exotom* machine (see Figure 11-1 below). The cut-off wheel was an 84Exo type (350mm dia.x 12.5mm), recommended for medium hard and soft ferrous metal (HV<500). The specimens were drench cooled whilst being sectioned.
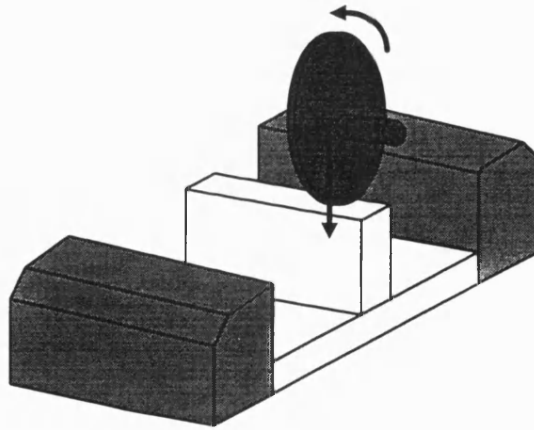
Figure 11-1 : Exotom cut-off machine

The surfaces to be examined were ground using polishing wheels of increasing qualities to ensure that the surface state met the standard for microscopic

observation. The final quality was achieved after four operations, carried out over a three day period, on a *Buehler* spinning grinding machine (see Figure 11-2), using the following strict grinding procedure :

1) **Planar grinding stage** : a self adhesive carbon grinding paper, (120 grit) quality, was used on the base wheel in order to remove the macroscopic surface defects. The specimens were ground for 2 mins, at 150 rev/min, with a water flush. (Specimens and grinding wheels rotated complementary to each other to preclude damage to the spheroidal structures).

2) **Sample integrity stage-*step 1*** : a smoother quality was achieved by polishing the samples with a self adhesive polishing cloth placed on the base wheel. This *Ultra Pad* cloth (from *Buehler*) was coated with a 15μm water based diamond suspension. The speed was 240 rev/min for 6 mins, with lubricant.

3) **Sample integrity stage-*step 2*** : using a nylon cloth with a 3μm water based diamond suspension sprayed over the cloth by an automatic fluid dispenser at a regular frequency (1 spray / 60s, 0.1s / spray), alternatively with lubricant, a smoother finish was obtained. The speed was again 240 rev/min for 6 mins.

4) **Polishing stage** : for the last operation a *Mastertex* cloth was used in association with the *Masterpolish* polishing suspension. *Masterpolish* is a mixture of silica and alumina (SiO_2 and Al_2O_3) with a crystal size of 0.05μm. The speed was 100 rev/min for 4 mins.
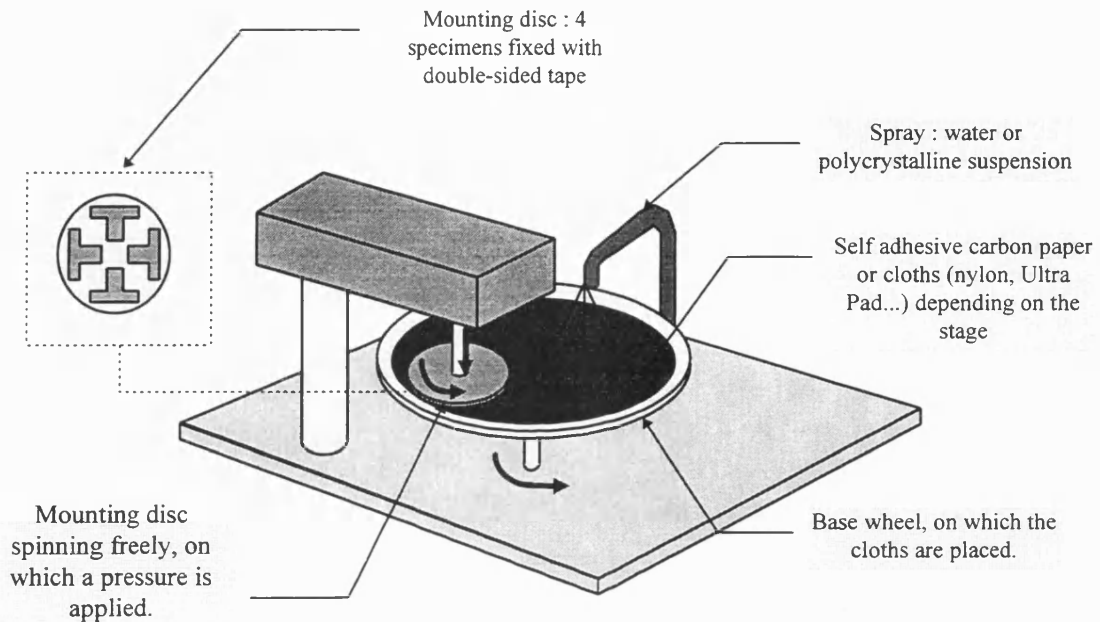
Figure 11-2 : *Buehler* grinding machine

Etching stage : Before examining the specimens under the microscope, the samples were etched for 15 seconds with 2% Nital, (nitric acid in alcohol). Nital is used to change the light reflection coefficient of pearlite which then appears black, whereas the other phases (ferrite, martensite...) remain bright. Coupons were cleaned with alcohol and dried with hot air.

11.2 Examination

Microscopic examination of the samples sought to determine the accuracy of the CHF equations and the influence of the thermal contact resistance.

Therefore, four operations were undertaken.

1) **Photographing a general view of each specimen** in order to record the shape of both the weld and its HAZ. These photographs were shot using a *Wild M3Z* microscope, with a magnification of 8.

2) **Photographing a closer view of the interface** between the upper and the lower plates, in order to analyse the heat flow through the contact zone. These photographs were shot using a *Wild M3Z* optical microscope, with a magnification of 13.

3) **Measuring the dimensions of the heat affected zone** and the width of the successive layers included into it, and photographing them. Each layer contains a specific type of microstructure (martensite, ferrite, pearlite...) depending on the distance from the welded zone. The limit of the HAZ is defined as the last layer where grains from the base metal have been transformed.

For this study, a *ZEISS ICM 402* optical microscope was used, with the following range of magnification : 40 for measuring the distances (with the vernier of the microscope), and 800 for identifying and photographing the phases, crystal structure, and grains.

Measuring the Vickers hardness in the heat affected zone, in order to assess its mean value, and comparing this value with the prediction given by the CHF and associated equations and formula. These measures were carried out on a *LECO M400* hardness tester. The size of the diamond probe was small enough to measure the hardness at three points within the heat affected zone. The test parameters for hardness testing were :

♦ Load : 300g

♦ Time of loading : 20s

11.3 Analysis of results

Analysis of the destructive testing and evaluation resulted in a large data sample which is summarised below.

1) **The HAZ discontinuities** : on the contact surface. Qualitative analysis.

2) **Measuring** :

- *the dimensions of the HAZ*, in order to compare the experimental values with theoretical results.

- *the hardness value*, to compare it with the predicted values.

3) **Metallurgy** : observing and identifying the different transformed products in the HAZ.

11.3.1 The HAZ discontinuities

The photographs referred to in this section are presented in Appendix F in the order in which they are referred to in the text.

The observations are discussed in the following order:

The two boundary cases first :

1) 100% contact (no grooves),

2) 0% contact (1mm gap).

Followed by a qualitative analysis carried out on the intermediate cases :

3) contact between two altered surfaces.

- ## **Full surface to surface (near 100%) contact** :

Figure F1, is a typical example of a number of coupons which suggest that the material interfaces prior to welding were sufficiently smooth, (and that they were in sufficiently close contact at the point of sectioning of the weld), to achieve a high level of thermal continuity. The HAZ appears continuous, extending smoothly from the upper to the lower plate, with Figure F2 illustrating the microstructure across the interface of a similar coupon.

- ## **0% contact** :

Figure F3 suggests that the pre-set 1mm root-gap created artificially between the two plates during tack welding prevented any heat from flowing through the interface of the joint, (by conduction).

- ## **Contact between two altered surfaces** :

Figure F4 illustrates a typical coupon in which the upper plate had been shaped to simulate changes due to TCR. Although the HAZ appears continuous, the two grain structures are not exactly the same, (Figure F5), as the pearlite appears more

agglomerated in the lower plate than in the upper plate. This suggests that the lower part has been slightly less heated than the upper one: a difference of temperature exists, even if it is small. It is considered that this is the real effect of the thermal contact resistance.

Most coupons exhibited welds of good quality. However, Figure F6 illustrates the effect of a slag inclusion and poor contact at the interface of two 25 mm. thick plates. The interface is wide enough to prevent any conduction from the upper to the lower plate. The temperature difference is undoubtedly very important, as the micro-crystalline structure of the upper plate, (Figure F7), appears to consist of acicular ferrite, whilst in the lower plate, the base metal does not appear to have been altered, (peak temperature below 723°C). Hence, for a slight variation of the initial surface quality, the HAZ behaviour appears to shift between continuity and discontinuity, which suggests that the HAZ is highly sensitive to Rtc values below a "threshold". This could be due to separation during tack welding or due to surface waviness rather than roughness.

11.3.2 Conclusion - The effect of thermal contact resistance

A critical value for Rtc seems to exist, and both the continuous and discontinuous HAZ behaviors depend on that "threshold". Under the circumstances explained, the experiments suggest that the surface quality achieved for 3μm rough milled surfaces could be close to that threshold. This quality is much higher than the usual standards in general fabrication where the elements to be welded are seldom

machined, or where they are aligned after being flame cut, (flame cutting quality being very coarse respecting to 3µm).

Thus, the hypothesis that a thermal discontinuity exists in the majority of fillet welded assemblies appears to be upheld.

11.3.3 Heat affected zone dimensions and hardness measurements

Measures of the hardness of the HAZ, (at 1 mm intervals intervals), and the ultimate dimension of the HAZ were compared with assessments from the CHF equation. Following the physical analysis of the specimens, the following results were found, (hardness values are for the position in the HAZ closest to the weld).

Specimen Number	Predicted HAZ(mm) 723°C	Exp. HAZ(mm) 723°C	% Variance of HAZ	Predicted Hardness HV	Exp. Hardness HV	% Variance of HV
104 C*	4.11	3.5	17.4	290	237	22.4
154 C*	3.34	3.3	1.2	315	309	1.9
204 C	3.30	3.2	3.1	330	299	10.4
253 C	3.04	2.9	4.8	358	343	4.4
301 C	2.72	2.8	-2.9	387	381	1.6
104 2d*	4.11	3.5	17.4	290	237	22.4
154 2d	3.05	3.3	-7.6	341	309	10.4
204 2d	1.98	3.2	-38.1	n/a	299	n/a
253 2d	1.58	2.9	-45.5	n/a	343	n/a
301 2d	1.11	2.8	-60.4	n/a	381	n/a
104 3d*	6.02	3.5	72.0	327	237	38.0
154 3d*	6.01	3.3	82.1	332	309	7.4
204 3d*	5.80	3.2	81.3	334	299	11.7
253 3d*	5.73	2.9	97.6	352	343	2.6
301 3d*	5.66	2.8	102.1	370	381	-2.9

Table 11-1: table of results.

Notes to Table 11-1:

a) Specimens numbered with a C, indicate that the CHF equation was used, whilst 2d = Rosenthal thin plate, and 3d = Rosenthal thick plate.

b) The first two numbers in the numbering system indicate plate thickness. For example, plate 104 C is 10 mm thick, whilst plate 301 C is 30 mm thick.

c) The thin plate equations were not valid above 15 mm plate thickness for this experiment.

d) Micro-hardness sensitivity +/- 15 HV.

e) (*) denotes that the constant values for thermal conductivity, specific heat and density were adjusted, (see section 11.3.4, below).
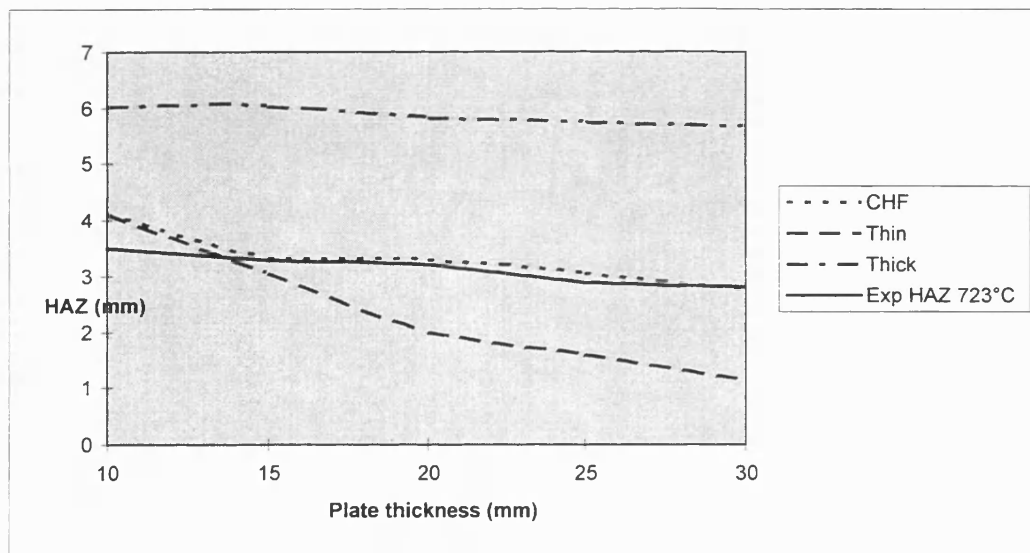
Figure 11-3 : graph of HAZ distances.
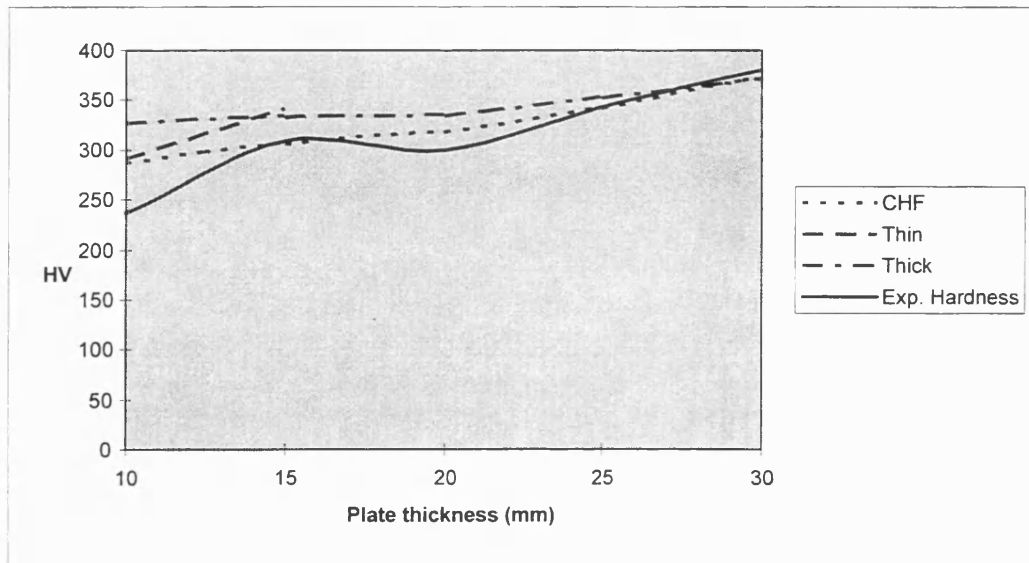
Figure 11-4 : graph of Hardness Values.

11.3.4 Comments - HAZ dimensions and hardness values

◊ HAZ dimensions :

Assessments undertaken with values for thermal conductivity and specific heat fixed at 773 K resulted in a high variance for the HAZ dimensions in plates 104K and 154K. It is suggested that this was caused by prolonged time at elevated temperatures thus invalidating the use of the fixed values for thermal conductivity and specific heat (773 K). Therefore, the thermal conductivity value, for these plates was adjusted to closer approximate that given by the literature at higher temperatures, as detailed in the table below.

	Original	Revised
C specific heat (J/kg.K)	0.67	0.821
k thermal conductivity (W/K.m)	0.037	0.0264
p specific gravity (g/mm^3)	0.7833 * from Kaye+Laby 773 K	0.785 * from Smithells 1073 K

After Kaye, GWC, and Laby T H, Table of Physical and Chemical Constants, Longman London (16th edn 1995)

In the context and validity of the experimental results, it is suggested that where steel remains at a temperature above the selected constant temperature (values) by more than 2.5 seconds, the assumption that a constant may be used becomes flawed, though reasonable approximations may still be achieved with a fixed constant.

In such cases, the precise distance at which the heat affected zone occurs may be best approximated by systems such as finite element methods. However, in order to provide a reasonable basis on which to proceed in daily calculations, a study of the data reveals that it would be reasonable to use the constants from the next higher temperature banding, which, in this case have been determined at 1073 K. Accordingly the relevant CHF and Rosenthal equations were adjusted.

The HAZ graph, Figure 11-3, which plots predictions based on the experimental current and voltages recorded, shows, as expected, that for thin plates, the CHF equation is similar to the thin plate Rosenthal equation. However, as the thickness increases, the CHF equation closer approximates actual values. It is submitted that the predictions given by this equation, subject to the minor limitations noted above), represent a closer more realistic result than the existing thin and thick plate equations over a range of thicknesses.

◊ Hardness values :

In respect of the hardness values, Figure 11-4, though the comparison between the variances of the three equations is in favour of the CHF equation, there is high variance in the 10 mm plate.

It is considered that the most likely reason is the lack of precision of the measured hardness value. Indeed, the reading of the dimensions of the indentation left by

the probe implies a large amount of subjective appreciation, which may change from one operator to another. Systematic errors in this type of analysis are in the order of +/- 15 HV, with additional errors possibly arising with siting of the probe.

11.3.5 Metallurgy

The photographs referred to in this section are presented in Appendix G.

The steel used in the experiment was a Niobium microalloyed steel, with a fine grained ferrite-pearlite structure, Figure G1, though this may be described as a 'dispersion strengthened ferrite alloy' due to the additions of Niobium which restrict grain growth.

In examination of the heat affected zone surrounding a welded joint, the heating cycle is at least as important as the holding and cooling cycles, since this affects the rate of recrystallisation, the degree of superheating in the various phases, particularly the alpha gamma phase, the rate of coarsening of the carbides and nitrides and the solubility and the rate and extent of grain growth.

In its 'normal' form at room temperature, (20°C), the steel has a body-centred cubic structure (alpha) in which 0.006% carbon may be dissolved, increasing to not more than 0.02% carbon at 723°C. Excesses of carbon above 0.02% which may have been absorbed into solid solution in the face centred form are precipitated on slow cooling whilst fast cooling prevents such precipitation. Solid solutions of face centred cubic iron (γ, gamma) is named Austenite. The body centred cubic solid solution (α, alpha) is named Ferrite. If rapid cooling does not occur, any carbon precipitated is in the form of hard iron carbide, Fe_3C, sometimes named Cementite.

In the steel examined, the chemical analysis data supplied by the mill suggested that it contained 0.16% carbon. This suggests that some carbon, up to 0.006% is dissolved in a solid solution of ferrite, whilst excess carbon additionally exists precipitated in the form of cementite, (iron carbide) layered with ferrite forming a laminated structure known as pearlite.

As the lower critical temperature, (723°C), is reached on heating, each patch of pearlite begins to transform to many small austenite crystals. Cooling at this stage causes immediate reprecipitation of the ferrite, Figure G2.

Such manifestations are not common as it is difficult to cause a steel to rise just to *A1*, (723°C), and then fall away immediately thus preserving the crystalline structure. In this case however, the heating cycle due to the welding process has caused the steel at the furthest edge from the weld to momentarily achieve such a temperature before the combination of the receeding heat source and the mass cooling effect of the base material caused rapid partial reprecipitation.

As heating continues through the *A1* temperature through to the *A3* temperature, the body-centred cubic structure becomes unstable, the polymorphic transformation to face-centred cubic structure commences, and the austenite fraction grows to the deficit of ferrite. This partial transformation stage is now known as the intercritical region.

As the temperature rises through *A3*, any remaining ferrite transforms to austenite and the whole of the material is a solid solution of austenite, (γ phase), (face-centered). Thus, in the steel examined, the austenite now contains 0.16% carbon dissolved interstitially in face centred iron.

As the material is progressively heated, (rapidly), the structure goes through a peritectic interaction through a loss of the dendrite structure of crystals, (δ), body-

centered cubic structure, at approximately 1400°C, (*44*), intermixing with austenite (γ), transforming to δ + liquid, and then wholly liquid.

As the liquid cools, the first solid nuclei formed are δ crystals, (dendritic crystals), with an extremely low carbon content, (<0.05%), gradually absorbing carbon to 0.07% at a temperature of approximately 1490°C. The liquid contains approximately 0.55% carbon and between 1490°C and 1450°C is in the two-phase state (δ + γ), and as it solidifies causes a reduction in δ-ferrite and a peritectic transformation to austenite. The final structure is shown in Figure G3.

Depending on the rapidity of cooling, the solid solution of carbon interstitially dissolved in the face centered structure will be modified. Figure G4 shows how rapid cooling presents a mertensitic structure.

As the steel further away from the weld cools marginally less quickly, the austenite forms into upper and lower bainite except that this product is distinguishable from martensite due to its associated diffusion of carbon atoms. Upper bainite exhibits an acicular structure of large needles of supersaturated ferrite with carbon collecting around the needle boundaries enriching the austenite.

In lower bainite the supersaturated needles form in a short time with carbides forming on the close packed planes. These needles grow slowly and to a limited extent.

Both upper and lower bainite are now called, ferrite with martensite/austenite/carbides (M-A-C), with aligned carbides, being designated (AC), and non-aligned, (FN). Most of the carbides in this region will be aligned, but of smaller size lathes than martensite or massive martensite. Aligned carbides are darker than martensite and are easily seen in Figure G5.

Further away in the region, where the material has only partially transformed to austenite and thus where there is little or no austenitic grain growth, the grain sizes of the ferrite and austenite are similar in size, and thus on cooling, a fine structure results, and is called the grain refined region. This is illustrated in Figure G6. Even here the cooling rate may be sufficient to cause some hardening.

The investigation into materials of different thicknesses gave rise to a range of structures due to the effect of differering cooling rates. The photographic material obtained in the course of this research is therefore extensive and has been archived in Department of Mechanical Engineering Report Number 36/97.

12. Conclusions and further work

12.1 Conclusions

This research has shown that attention to, and control of, process variables markedly affects weld quality. Examination of the effect of changes to electrode extension in semi-automatic welding in particular indicated that this variable plays a major part in altering penetration and extent of the heat affected zone by changing current drawn.

Developments in steel production have brought about reductions in the thickness of steel used to fabricate a number of applications. An examination of the principal equations used to model the weld thermal cycle revealed that subjective decisions are clearly being taken to control weld parameters because models based on equations developed a number of years ago are not able to definitively account for different material thicknesses.

A new single equation, (CHF), has been derived, which is a modified Rosenthal equation, which incorporates a coefficient to adapt the influence of material thickness. This new equation has been partially differentiated and transposed to model the cooling rates in the weld heat affected zone, and further transposed to model important influencing factors such as preheat and speed of travel. The series of equations thus derived have been incorporated into a computer program, which, when combined with other existing equations, can predict the microstructure and hardness in the weld heat affected zone. This is a major contribution to prediction of the consequences of weld parameter and material selection and will improve quality of product.

The CHF equations accurately predict temperature change and cooling rates when welding beads on plates. However, when considering industrial applications it was considered advantageous to develop the equations to account for welding different joint configurations, and in this regard the equations were developed to account for the effect of welding complex joints such as fillet joints of any angle.

The effect of a thermal discontinuity between the two plates in the fillet joint was investigated successfully by assuming a split heat source and by modelling the two plates independently both with, and without, a root gap. The equations thus derived enable accurate prediction of heat affected zone dimensions, microstructure and hardness in all the major joint set-ups. The authors hypothesis that a thermal discontinuity exists in almost all fillet welded joints in general fabrication was upheld, and therefore it has been concluded that those models which do not take thermal discontinuities into account are not complete. This is the first time that complex heat flows in fillet welds have been modelled analytically without recourse to numerical methods.

The equations were developed for use in the research context and have been simplified to enable their use as rapid indicators of thermal events. This will enable their use in everyday circumstances and lead to reduction in set-up costs and lead time by reducing pre-fabrication testing, and contribute to increasing safety and longevity of welded joints. The successful validation of the equations by experiment leads to the conclusion that they enable improvements in quality through weld thermal cycle modelling.

The equations are flexible enough to enable their use over a range of materials, welding processes, and welding speeds. However the full equations to predict microstructure and hardness are limited to hypo-eutectoid steels.

12.2 Recommended further work

12.2.1 Improving and justifying the expression of the corrective coefficient:

The results of the theoretical approach has shown that it may be beneficial to consider using numerical methods such as partial differential equations or finite element methods. This may lead to a more accurate definition of the corrective coefficient used to model the thermal contact resistance in simplified equations.

12.2.2 Numerical analysis

The approach adopted to analytically model the transfer of of heat across a thermal contact resistance led to an infinite number of equations. It is considered that benefits may be obtained through the application of partial differential equations to solve this problem.

12.2.3 Further experimental work

This research has considered the effect on fillet welded joints of varying thickness. It is considered that further benefits may be achieved if similar experiments and research were undertaken to consider fillet joints of varying angles and butt welded joints. It is further considered that the presence of hard microstructures in an otherwise ductile heat affected zone, as modelled, may cause premature failure, typically due to fatigue, and complementary research into this area is recommended.

13. Bibliography of published works

Kirk, C.S., Mileham , A.R., (1994), *Gas Shielded Metal Arc Welding, Improving Quality by Minimisation of Defects*, Advances in Manufacturing Technology VIII, Proceedings of Tenth National Conference on Manufacturing Research, Loughborough University, 5-7 September 1994, (Case, K., and Newman, S. T., eds.), pp. 617 - 621. London: Taylor and Francis.
ISBN 0-7484-0254-3.

Kirk, C.S., Mileham, A.R., and Yeo, R.B.G., (1995), *The role of wire resistivity in semiautomatic welding quality; Part I*, Advances in Manufacturing Technology IX, Proceedings of the Eleventh National Conference on Manufacturing Research, De Montfort University, Leicester, 12-14 September 1995, (Stockton, D., and Wainwright, C., eds.), pp. 47-51. London: Taylor and Francis. ISBN 0-7484-0400-7.

Kirk, C.S., Mileham, A.R., and Yeo, R.B.G., (1995), *The role of wire resistivity in semiautomatic welding quality; Part II*, Proceedings of the Third International Conference on Sheet Metal, University of Central England, 26-28 June 1995, (Shirvani, B., Singh, U.P., and Kals, H.J.J., eds.), pp. 240-247. Birmingham: University of Central England. ISBN 0-952-7664-OX.

Kirk, C.S., and Mileham, A.R., (1996), *An evaluation of flux-cored wire metal-arc welding and it's effect on cost of production*, Proceedings of the Second International Conference on Manufacturing Processes, Systems and Operations Management, in Less Industrialised Regions, National University of Science and Technology, Bulawayo, 22-24 April 1996, (Kanhukamwe, Q.C., ed.), pp. 16-26. Bulawayo, Zimbabwe: National University of Science and Technology. ISBN Not Quoted.

Kirk, C.S., and Mileham, A.R., (1996), *The significance of electrode extension on critical cooling rates and the heat affected zone*, Proceedings of the Second International Conference on Manufacturing Processes, Systems and Operations Management, in Less Industrialised Regions, National University of Science and Technology, Bulawayo, 22-24 April 1996, (Kanhukamwe, Q.C., ed.), pp. 27-34. Bulawayo, Zimbabwe: National University of Science and Technology. ISBN Not Quoted.

Kirk, C.S., and Mileham, A.R., (1996), *Predicting the weld thermal cycle and microstructure, in hypoeutectoid steels*, Advances in Manufacturing Technology X, Proceedings of the Twelfth National Conference on Manufacturing Research, University of Bath, 9-11 September 1996, (Owen, G., Mileham, A.R., and Bramley, A.N., eds.), pp. 16-20. Bath: University of Bath. ISBN 1-85790-031-6.

Kirk, C.S., Shirvani, H., Rees, D.A.S., and Mileham, A.R., (1996), *Mathematical prediction of the weld thermal cycle and HAZ microstructure*, Proceedings of the Second International Conference on Coasts, Ports, and Marine Structures, National University of Science, Tehran, Iran, 1-4 December 1996, pp. 159-173. Tehran, Iran: National University of Science. ISBN Not Quoted.

Journals

Kirk, C.S., and Mileham, A.R., (1996), The influence of electrode extension on cored wire welding quality, *Construction Monthly*, May 1996, **Vol 2 Issue 5,** pp. 65-68 Birmingham, USA: Franklin Publishing. ISSN Not Quoted.

Kirk, C.S., Shirvani, H., Rees, D.A.S., and Mileham, A.R., (1998), Modelling the weld thermal cycle and microstructure, *Welding Journal*, **Vol** (), Submitted for publication, AWS, Miami, USA.

Kirk, C.S., Debrie, N.P.E., Rees, D.A.S., and Mileham, A.R., (1998), Modelling the weld thermal cycle - fillet welds, *Welding Journal*, **Vol** (), Submitted for publication, AWS, Miami, USA.

Posters

Kirk, C.S., and Mileham, A.R., 1996, Poster Presentation - *The role of wire resistivity in semi-automatic welding quality*, Poster Session of the Professional Program, 77th Annual AWS Convention and International Welding and Fabrication Exposition, Chicago, Illinois, United States of America. 21-25 April 1996.

14. References

Adam, G. and Siewert, T.A., (1990), Sensing of GMAW Droplet Transfer Modes Using an ER100S1 Electrode, *Welding Journal*, **Vol. 69 (3)**, Research Supplement, 103s - 108s.

Adams, Jr., C.M., (1958), Cooling rates and peak temperatures in fusion welding, *Welding Journal*, **Vol. 37 (5)**, Research Supplement, 210-s to 215-s.

Bailey, N., (1970a), Determination of welding procedures for four low alloy steels, *Metal Construction and British Welding Journal*, **2, 7**, 279 - 284.

Bailey, N., (1970b), Welding carbon-manganese steels, *Metal Construction and British Welding Journal*, **2, 10**, 442 - 446.

Baker, R.G., Haddrill, D.M., and Roberts, J.E., (1971), *Assessment of Material weldability*, Proceedings of the International Symposium on cracking and fracture in welds, **C.5. 1-9 PII**, 1971

Blondeau, Maynier, and Dollet, (1973), Prevision de la durete et de la resistance des aciers au carbone et faiblement allies d'apres leur structure et leur composition, *Memoires Scientifiques Revue de Metallurgie*, **70**, 883 - 892

Blondeau, Dollet, and Bastien, (1978), *Prediction of microstructure via empirical formulae based on CCT diagrams*, Hardenability concepts with applications to steel, Conf. Proceedings, Warrendale, PA, USA: American Institute of Mining, Metallurgical and Petroleum Engineers,163-176.

Boo, K.S., and Cho, H.S., (1990), *Transient temperature distribution in arc welding of finite thickness plates*. Proceedings of the Institution of Mechanical Engineers, Part B., 204 (B3), 175-183.

Christenson, N., Davies, V. de L., and Gjermundsen, K., (1965), Distribution of temperatures in arc welding, *British Welding Journal*, Feb. 1965, **Vol. 12**, 54 - 75,

Cottrell, C.L.M., and Bradstreet, B.J., (1954), Cooling rates in typical arc-welded joints, *British Welding Journal*, **1, 7,** 322 - 326.

Cottrell, C.L.M., and Bradstreet, B.J.(1955), A method for calculating the effect of preheat on weldability, *British Welding Journal*, **2, 7,** 305 - 309.

Easterling, K.E., (1983), *Introduction to the physical metallurgy of welding*, London: Butterworths & Co.

Essers, W.G., and Walter, R., (1979), *Some aspects of the penetration mechanisms in MIG*, Proc. of the International Conference on Arc Physics and Weld Pool Behaviour, Cambridge: The Welding Institute.

Gage, 1953, through Welding Handbook, 1991.

Gerdien and Lotz, 1922, through Welding Handbook, 1991.

Graville, B.A., 1968, Effect of fit-up on heat affected zone cold cracking, *British Welding Journal*, April 1968, 183-190.

Grosh, R.J., Trabant, E.A., and Hawkins, G.A., (1955), Temperature distribution in solids of variable thermal properties heated by moving heat sources. *Quarterly Journal of Applied Mathematics*, **13 (2)** 161 - 167.

Hess, W.F., Merrill, L.L., Nippes, Jr., E.F., and Bunk, A.P., (1943), The measurement of cooling rates associated with arc welding and their application to the selection of optimum welding conditions, *Welding Journal*, **Vol. 22 (9)**, Research Supplement, 377-s to 422-s.

Jeong, S.K., and Cho, H.S., (1997), An analytical solution to predict the transient temperature distribution in fillet arc welds, *Welding Journal*, **Vol. 76 (6)**, Research Supplement, 223-s to 232-s.

Jhaveri, P., Moffatt, W.G., and Adams, C.M. Jr., (1962), The effect of plate thickness and radiation on heat flow in welding and cutting, *Welding Journal*, 41(), 12s -16s

Kielland, Alexander, L., (1981), Norwegian Public Reports, NOU 1981, 11, The <Alexander L. Kielland> - accident, English translation: Oslo, University Press.

Kirk, C.S., and Mileham, A.R., (1994), *Gas Shielded Metal Arc Welding, Improving Quality by Minimisation of Defects*, Advances in Manufacturing Technology VIII, Proceedings of Tenth National Conference on Manufacturing Research, Loughborough University, 5-7 September 1994, (Case, K., and Newman, S. T., eds.), pp. 617 - 621. London: Taylor and Francis.

Kirk, C.S., Mileham, A.R., and Yeo, R.B.G., (1995a), *The role of wire resistivity in semiautomatic welding quality; Part I*, Advances in Manufacturing Technology IX, Proceedings of the Eleventh National Conference on Manufacturing Research, De Montfort University, Leicester, 12-14 September 1995, (Stockton, D., and Wainwright, C., eds.), pp. 47-51. London: Taylor and Francis.

Kirk, C.S., Mileham, A.R., and Yeo, R.B.G., (1995b), *The role of wire resistivity in semiautomatic welding quality; Part II*, Proceedings of the Third International Conference on Sheet Metal, University of Central England, 26-28 June 1995, (Shirvani, B., Singh, U.P., and Kals, H.J.J., eds.), pp. 240-247. Birmingham: University of Central England.

Kirk, C.S., Shirvani, H., Rees, D.A.S., and Mileham, A.R., (1996), *Mathematical prediction of the weld thermal cycle and HAZ microstructure*, Proceedings of the Second International Conference on Coasts, Ports, and Marine Structures, National University of Science, Tehran, Iran, 1-4 December 1996, pp. 159-173. Tehran, Iran: National University of Science. ISBN Not Quoted.

Kunitake, T., and Ohtani, H., (1967), *Tetsu-to-Hagane 53*, 1280.

Lancaster, J.F., (1984), The Physics of Welding, 2nd edition, International Institute of Welding, Study Group 212, Oxford: Pergamon Press.

Lancaster, J.F., (1987), Metallurgy of Welding, 4th Edition, London: Allen and Unwin.

Lancaster, J.F., (1992), Handbook of Structural Welding, 1st edition. Cambridge: Abington Publishing.

MacWaid, T., and Marschall, E., (1992), Thermal contact resistance across pressed metal contacts in a vacuum environment, *Int. J. Heat Mass Transfer*, 35, 2911-2920.

Maynier, Ph., Jungmann, B., and Dollet, J., (1978), *Creusot-Loire system for the prediction of the mechanical properties of low alloy steel products*, Hardenability concepts with applications to steel, eds Doane, D.V., and Kirkaldy, J.S., Conference Proceedings, Warrendale, PA, USA: American Institute of Mining, Metallurgical and Petroleum Engineers, 518 - 544.

Nippes, E.F., Merrill, L.L., and Savage, W.F., (1949), Cooling rates in arc welds in 1/2 inch plate, *Welding Journal,* **28(11),** 556s-564s

Okada, T., Yamamoto, H., and Harada, S., (1979), *Observations of the shielding gas flow pattern during arcing by the use of a laser light source*, Proc. of the International Conference on Arc Physics and Weld Pool Behaviour, Cambridge: The Welding Institute.

Raja, A., Rohira, K.L., Srinivasmurthy, K.S., Ramura, K.S., (1989), Some aspects of the penetration mechanisms in Flux Cored Arc Welding, Tiruchirapalli, India: *Welding Research Institute*.

Rhee, S., and Kannatey-Asibu, Jr., E., (1991), *Observation of Metal Transfer During Gas Metal Arc Welding,* Proc. of the Winter Annual Meeting of the ASME, New York: ASME.

Rosenthal, D., (1935), *Etude theorique du regime thermique pendant la soudure a l'arc.* 2-me Congres National de Sciences, Brussels, 1277-1292

Rosenthal, D., (1941), Mathematical Theory of Heat Distribution During Cutting & Welding, *Welding Journal,* **Vol. 20 (5)** Research Supp.,220-s - 234-s

Rykalin, N.N., (1957), *Berechnung der Warmevorgange beim Schweissen,* Verlag Technik: Berlin.

Salgon, J.J., Robbe-Valloire, F., Blouet, J., and Bransier, J., 1997, A mechanical and geometrical approach to thermal contact resistance, *Int. J. Heat and Mass Transfer,* **Vol. 40 (5),** 1121-1129.

Steven, W.S., and Haynes, A.G., (1956), *J Iron Steel Institute:*London 183,349.

The Physics of Welding, (1984), 1st edition, International Institute of Welding, Study Group 212, (Lancaster, J.F., ed.), Oxford: Pergamon Press.

Welding Handbook, (1987), Volume 1, 8th edition., (Connor, L.P., ed.), Miami: American Welding Society.

Welding Handbook, (1991), Volume 2, 8th edition, (O'Brien, R.L., ed.), Miami: American Welding Society.

Yeo, R.B.G., (1989), Cored Wires for lower cost welds, *Joining and Materials*, **Vol 2**, 68-73

Yeo, R.B.G., (1993), Electrode Extension Often Neglected When Using Self-shielded Cored Wires, *Welding Journal*, **Vol. 72 (1)**, 51-53.

Appendix A

Partial differentiation of the Continuous Heat Flow equation

$$T - T_o = \frac{Q}{2\pi k \left[10(Log_{10}g)\right]\left(v^2 t^2 + y^2 + z^2\right)^{\frac{1}{4}}} \bullet \left(\frac{\pi}{2\lambda v}\right)^{\frac{1}{2}} \bullet \left[e^{-\lambda v\left[\left(v^2 t^2 + y^2 + z^2\right)^{\frac{1}{2}} - vt\right]} \right]$$

the expressions

$$\frac{Q}{2\pi k \left[10(Log_{10}g)\right]} \bullet \left(\frac{\pi}{2\lambda v}\right)^{\frac{1}{2}}$$

are assigned to a coefficient C_A thus requiring only a partial differentiation with respect to time (t), of

$$\frac{e^{-\lambda v\left[\left(v^2 t^2 + y^2 + z^2\right)^{\frac{1}{2}} - vt\right]}}{\left(v^2 t^2 + y^2 + z^2\right)^{\frac{1}{4}}}$$

which, using

$$\frac{d}{dt}\left(\frac{f(t)}{g(t)}\right) = \frac{gf' - fg'}{g^2}$$

expands to

$$\frac{d}{dt} \rightarrow \frac{\left(v^2 t^2 + y^2 + z^2\right)^{\frac{1}{4}} \cdot \frac{d}{dt}\left[e^{-\lambda v\left[\left(v^2 t^2 + y^2 + z^2\right)^{\frac{1}{2}} - vt\right]} \right] - e^{-\lambda v\left[\left(v^2 t^2 + y^2 + z^2\right)^{\frac{1}{2}} - vt\right]} \cdot \frac{d}{dt}\left[\left(v^2 t^2 + y^2 + z^2\right)^{\frac{1}{4}}\right]}{\left(v^2 t^2 + y^2 + z^2\right)^{\frac{1}{2}}}$$

thus g' becomes

$$\frac{d}{dt}\left(v^2t^2 + y^2 + z^2\right)^{\frac{1}{4}} = \frac{1}{4}\left(v^2t^2 + y^2 + z^2\right)^{-\frac{3}{4}} 2v^2t = \frac{v^2t}{2\left(v^2t^2 + y^2 + z^2\right)^{\frac{3}{4}}}$$

and f'

$$\frac{d}{dt}\left[e^{-\lambda v\left[\left(v^2t^2 + y^2 + z^2\right)^{\frac{1}{4}} - vt\right]}\right] \qquad \text{using } \frac{d}{dt}\left[e^{f(t)}\right] = e^{f(t)} f\left(\frac{1}{t}\right)$$

becomes

$$\left[e^{-\lambda v\left[\left(v^2t^2 + y^2 + z^2\right)^{\frac{1}{4}} - vt\right]}\right] \bullet [-\lambda v] \bullet \left[\frac{v^2t}{\left(v^2t^2 + y^2 + z^2\right)^{\frac{1}{2}}} - v\right]$$

therefore

$$\frac{\partial T}{\partial t} = C_A \bullet \frac{e^{-\lambda v\left[\left(v^2t^2 + y^2 + z^2\right)^{\frac{1}{4}} - vt\right]} \cdot \left[-\lambda v\left[\frac{v^2t}{\left(v^2t^2 + y^2 + z^2\right)^{\frac{1}{2}}} - v\right]\left(v^2t^2 + y^2 + z^2\right)^{\frac{1}{4}} - \frac{v^2t}{2\left(v^2t^2 + y^2 + z^2\right)^{\frac{3}{4}}}\right]}{\left(v^2t^2 + y^2 + z^2\right)^{\frac{1}{2}}}$$

simplifying, becomes

$$\frac{\partial T}{\partial t} = C_A \bullet e^{-\lambda v \left[\left(v^2 t^2 + y^2 + z^2\right)^{\frac{1}{2}} - vt\right]} \bullet \left[\frac{\lambda v^2}{\left(v^2 t^2 + y^2 + z^2\right)^{\frac{1}{4}}} - \frac{\lambda v^3 t}{\left(v^2 t^2 + y^2 + z^2\right)^{\frac{3}{4}}} - \frac{v^2 t}{2\left(v^2 t^2 + y^2 + z^2\right)^{\frac{5}{4}}}\right]$$

In certain cases it is required to consider the cooling rate as a function of temperature change, as in the usage of preheat calculations. Thus, partial differentiation leaving the T-T$_0$ term as the coefficient is as follows, using

$$T - T_o = C_A \bullet \left[\frac{e^{-\lambda v \left[\left(v^2 t^2 + y^2 + z^2\right)^{\frac{1}{2}} - vt\right]}}{\left(v^2 t^2 + y^2 + z^2\right)^{\frac{1}{4}}}\right]$$

transposing to,

$$C_A = \frac{\left(T - T_o\right)}{e^{-\lambda v \left[\left(v^2 t^2 + y^2 + z^2\right)^{\frac{1}{2}} - vt\right]}} \bullet \left[\frac{\left(v^2 t^2 + y^2 + z^2\right)^{\frac{1}{4}}}{1}\right]$$

therefore as before

$$\frac{\partial T}{\partial t} = C_A \bullet e^{-\lambda v \left[\left(v^2 t^2 + y^2 + z^2\right)^{\frac{1}{2}} - vt\right]} \bullet \left[\frac{\lambda v^2}{\left(v^2 t^2 + y^2 + z^2\right)^{\frac{1}{4}}} - \frac{\lambda v^3 t}{\left(v^2 t^2 + y^2 + z^2\right)^{\frac{3}{4}}} - \frac{v^2 t}{2\left(v^2 t^2 + y^2 + z^2\right)^{\frac{5}{4}}}\right]$$

integrating to

$$\frac{\partial T}{\partial t} = \frac{\left(T - T_o\right)}{e^{-\lambda v \left[\left(v^2 t^2 + y^2 + z^2\right)^{\frac{1}{2}} - vt\right]}} \bullet \left[\frac{\left(v^2 t^2 + y^2 + z^2\right)^{\frac{1}{4}}}{1}\right] \bullet \frac{e^{-\lambda v \left[\left(v^2 t^2 + y^2 + z^2\right)^{\frac{1}{2}} - vt\right]}}{1} \bullet$$

$$\left[\frac{\lambda v^2}{\left(v^2 t^2 + y^2 + z^2\right)^{\frac{1}{4}}} - \frac{\lambda v^3 t}{\left(v^2 t^2 + y^2 + z^2\right)^{\frac{3}{4}}} - \frac{v^2 t}{2\left(v^2 t^2 + y^2 + z^2\right)^{\frac{5}{4}}}\right]$$

and simplifying to

$$\frac{\partial T}{\partial t} = (T - T_o) \bullet \left(v^2 t^2 + y^2 + z^2\right)^{\frac{1}{4}} \bullet$$

$$\left[\frac{\lambda v^2}{\left(v^2 t^2 + y^2 + z^2\right)^{\frac{1}{4}}} - \frac{\lambda v^3 t}{\left(v^2 t^2 + y^2 + z^2\right)^{\frac{3}{4}}} - \frac{v^2 t}{2\left(v^2 t^2 + y^2 + z^2\right)^{\frac{5}{4}}}\right]$$

expanding to

$$\frac{\partial T}{\partial t} = (T - T_o) \bullet \left[\frac{\lambda v^2}{1} - \frac{\lambda v^3 t}{\left(v^2 t^2 + y^2 + z^2\right)^{\frac{1}{2}}} - \frac{v^2 t}{2\left(v^2 t^2 + y^2 + z^2\right)}\right]$$

simplifying and re-arranging to become finally,

$$\frac{\partial T}{\partial t} = (T - T_o) \bullet \left[\frac{-v^2 t}{2\left(v^2 t^2 + y^2 + z^2\right)} + \lambda v^2 \left(1 - \frac{vt}{\left(v^2 t^2 + y^2 + z^2\right)^{\frac{1}{2}}}\right)\right]$$

Appendix B

Deriving the short form of the CHF equation

$$T - T_o = \frac{Q}{2\pi k [10(Log_{10}g)]} \bullet \left(\frac{\pi}{2\lambda v}\right)^{\frac{1}{2}} \bullet \left[\frac{e^{\left[-\lambda v\left[\left(v^2 t^2 + y^2 + z^2\right)^{\frac{1}{2}} - vt\right]\right]}}{\left(v^2 t^2 + y^2 + z^2\right)^{\frac{1}{4}}}\right] \tag{B1}$$

If y = 0 and z = 0, then the exponential expression = 1, leaving

$$T - T_o = \frac{Q}{2\pi k [10(Log_{10}g)]} \bullet \left(\frac{\pi}{2\lambda v}\right)^{\frac{1}{2}} \bullet \left[\frac{1}{\left(v^2 t^2\right)^{\frac{1}{4}}}\right] \tag{B2}$$

Simplifying, by assigning a coefficient, C_A, where,

$$C_A = \frac{Q}{2\pi k [10(Log_{10}g)]} \bullet \left(\frac{\pi}{2\lambda v}\right)^{\frac{1}{2}}$$

then,

$$T - T_o = C_A \bullet \frac{1}{\left(v^2 t^2\right)^{\frac{1}{4}}} = \frac{C_A}{\left(v^2 t^2\right)^{\frac{1}{4}}} \tag{B3}$$

differentiating with respect to time (t), using the power rule,

$$\frac{d}{dt} = nct^{n-1}$$

$$T = \frac{C_A}{\left(v^2t^2\right)^{.25}} = C_A \bullet \left(v^2t^2\right)^{-.25} = C_A \bullet -.25 \cdot \left(v^2t^2\right)^{-.25-1} \bullet 2 \cdot v^2t$$

rearranging,

$$\frac{\partial T}{\partial t} = C_A \bullet -\frac{1}{4} \bullet \frac{1}{\left(v^2t^2\right)^{\frac{5}{4}}} \bullet 2 \bullet v^2t$$

and simplifying,

$$\frac{\partial T}{\partial t} = C_A \bullet \frac{-v^2t}{2\left(v^2t^2\right)^{\frac{5}{4}}} \qquad (B4)$$

If, by rearranging equation B3 to give,

$$C_A = (T - T_o) \bullet \left(v^2t^2\right)^{\frac{1}{4}} \qquad (B5)$$

then substituting equation B5 for (C_A) in equation B4, equation B4 becomes,

$$\frac{\partial T}{\partial t} = (T - T_o) \bullet \left(v^2t^2\right)^{\frac{1}{4}} \bullet \frac{-v^2t}{2\left(v^2t^2\right)^{\frac{5}{4}}} \qquad (B6)$$

expanding $\left(v^2t^2\right)^{\frac{1}{4}}$, gives

$$\frac{\partial T}{\partial t} = (T - T_o) \bullet \frac{-v^2 t}{2(v^2 t^2)} \tag{B7}$$

$$\frac{\partial T}{\partial t} = (T - T_o) \bullet \frac{-v^2 t}{2(v^2 t^2)} \Rightarrow -(T - T_o) \bullet \frac{v^2 t}{2(v^2 t^2)} \Rightarrow -(T - T_o) \bullet \frac{t}{2t^2} \Rightarrow -(T - T_o) \bullet \frac{1}{2t} \tag{B8}$$

$$\frac{\partial T}{\partial t} = -(T - T_o) \bullet \frac{1}{2t} \Rightarrow -(T - T_o) \bullet \frac{1}{2} \bullet \frac{1}{t} \tag{B9}$$

Considering now also the last term in the original equation B2

$$\frac{1}{(v^2 t^2)^{\frac{1}{4}}} = \frac{1}{(vt)^{\frac{1}{2}}} = \frac{1}{\sqrt{vt}}$$

Giving for equation B2,

$$T - T_o = C_A \bullet \frac{1}{\sqrt{vt}} \Rightarrow C_A \bullet \frac{1}{vt^{\frac{1}{2}}}$$

Rearranging, gives,

$$T - T_o = \frac{C_A}{vt^{\frac{1}{2}}} \tag{B10}$$

Squaring both sides gives,

$$(T - T_o)^2 = \frac{C_A^{\,2}}{vt} \tag{B11}$$

rewriting, gives,

$$\frac{1}{t} = \frac{v}{C_A^2} \bullet (T - T_o)^2 \qquad \qquad \text{(B12)}$$

Noting from equation B9 that,

$$\frac{\partial T}{\partial t} = -(T - T_o) \bullet \frac{1}{2} \bullet \frac{1}{t} \qquad \qquad \text{(B13)}$$

and integrating B12 into B9

$$\frac{\partial T}{\partial t} = -(T - T_o) \bullet \frac{1}{2} \bullet \frac{v}{C_A^2} \bullet (T - T_o)^2 \qquad \qquad \text{(B14)}$$

finally simplifying to,

$$\frac{\partial T}{\partial t} = -(T - T_o)^3 \bullet \frac{v}{2C_A^2} \qquad \qquad \text{(B15)}$$

since,

$$C_A = \frac{Q}{2\pi k \left[10 \left(Log_{10} g \right) \right]} \bullet \left(\frac{\pi}{2\lambda v} \right)^{\frac{1}{2}} \qquad \qquad \text{(B16)}$$

Squaring both sides, gives

$$C_A^2 = \frac{Q^2}{4} \bullet \frac{1}{\pi^2} \bullet \frac{1}{k^2} \bullet \frac{1}{\left[10 \left(Log_{10} g \right) \right]^2} \bullet \frac{\pi}{2\lambda v}$$

and eliminating pi and multiplying the constants gives,

$$C_A{}^2 = \frac{Q^2}{8\pi k^2 \left[10(Log_{10}g)\right]^2 \lambda v} \tag{B17}$$

therefore,

$$\frac{v}{2C_A{}^2} = \frac{v8\pi k^2 \left[10(Log_{10}g)\right]^2 \lambda v}{2Q^2} \tag{B18}$$

simplifying by reducing the constant gives,

$$\frac{v^2 4\pi k^2 \left[10(Log_{10}g)\right]^2 \lambda}{Q^2} \tag{B19}$$

and rearranging,

$$2\lambda \bullet \frac{2}{Q^2} \bullet \pi k^2 \left(10 \log_{10} g\right)^2 v^2 \tag{B20}$$

since $2\lambda = \dfrac{\rho C}{k}$ integration into B20 gives,

$$\frac{v}{2C_A{}^2} = 2\pi k\rho C \bullet \left(\frac{v\left[10(Log_{10}g)\right]}{Q}\right)^2 \tag{B21}$$

finally giving,

$$\frac{\partial T}{\partial t} = -(T-T_o)^3 \bullet 2\pi k\rho C \bullet \left(\frac{v\left[10(Log_{10}g)\right]}{Q}\right)^2 \tag{B22}$$

similarly for the solution including the coefficients C_π and C_q, from equation B16

$$C_A = \frac{C\pi \cdot Cq \cdot Q}{\pi k \left[10\left(Log_{10}g\right)\right]} \bullet \left(\frac{\pi}{2\lambda v}\right)^{\frac{1}{2}} \qquad (B23)$$

Squaring both sides, gives

$$C_A^{\,2} = \frac{Cq^2 \cdot Q^2}{1} \bullet \frac{C\pi^2}{\pi^2} \bullet \frac{1}{k^2} \bullet \frac{1}{\left[10\left(Log_{10}g\right)\right]^2} \bullet \frac{\pi}{2\lambda v}$$

and eliminating pi,

$$C_A^{\,2} = \frac{C\pi^2 \cdot Cq^2 \cdot Q^2}{\pi k^2 \left[10\left(Log_{10}g\right)\right]^2 2\lambda v} \qquad (B24)$$

therefore,

$$\frac{v}{2C_A^{\,2}} = \frac{v\pi k^2 \left[10\left(Log_{10}g\right)\right]^2 2\lambda v}{2 \cdot C\pi^2 \cdot Cq^2 Q^2} \qquad (B25)$$

simplifying by reducing the constant gives,

since $2\lambda = \dfrac{\rho C}{k}$,

$$\frac{v}{2C_A^{\,2}} = \frac{\pi k \rho C}{2} \bullet \left(\frac{v\left[10\left(Log_{10}g\right)\right]}{C\pi \cdot Cq \cdot Q}\right)^2 \qquad (B26)$$

finally giving,

$$\frac{\partial T}{\partial t} = -(T-T_o)^3 \bullet \frac{\pi k \rho C}{2} \bullet \left(\frac{v[10(Log_{10}g)]}{C\pi \cdot Cq \cdot Q} \right)^2 \qquad (B27)$$

where for example,

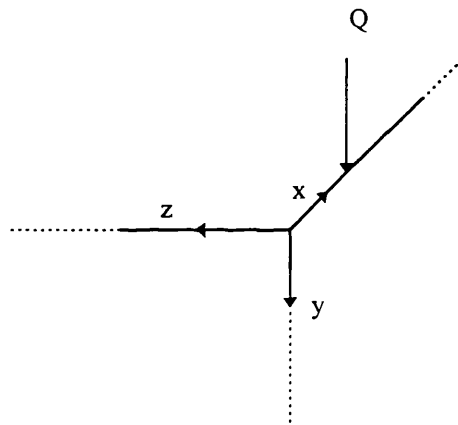|		
Lower plate	$C\pi$=0.5	Cq=0.5
Upper plate	$C\pi$=1.0	Cq=0.5

Appendix C

The 3d Rosenthal equation and its development

Three dimensional flow of heat, semi-infinite plate :

Figure : semi-infinite plate

The initial equation developed by Rosenthal for a moving point source over an semi-infinite plate from the Laplace equation,

$$\frac{\partial^2 T}{\partial x^2} + \frac{\partial^2 T}{\partial y^2} + \frac{\partial^2 T}{\partial z^2} = 2\lambda \frac{\partial T}{\partial t}$$ [e1]

or if x is replaced by $\xi = x - vt$,

$$\frac{\partial^2 T}{\partial \xi^2} + \frac{\partial^2 T}{\partial y^2} + \frac{\partial^2 T}{\partial z^2} = -2\lambda \, v \frac{\partial T}{\partial \xi}$$ [e1']

[e1'] written in spherical co-ordinates gives:

$$\frac{\partial^2 \varphi}{\partial r^2} + \frac{1}{r} \frac{\partial \varphi}{\partial r} = (\lambda \, v)^2 \, \varphi$$ [e2]

where (φ) is defined by $T = T_0 + e^{-\lambda \xi} \varphi \, (\xi, y, z)$ and $r = \sqrt{\xi^2 + y^2 + z^2}$,

with the boundary conditions :

$$\frac{\partial T}{\partial \xi} \to 0 \text{ as } \xi \to \pm\infty \text{ (also equivalent to } \frac{\partial T}{\partial x} \to 0 \text{ as } x \to \pm\infty)$$ [c1]

$$\frac{\partial T}{\partial y} \to 0 \text{ as } y \to +\infty$$ [c2]

$$\frac{\partial T}{\partial z} \to 0 \text{ as } z \to +\infty$$ [c3]

and by considering a quarter of a sphere drawn around the heat source:

$$-\frac{\partial T}{\partial r} \pi \, r^2 k \to Q \text{ as } r \to 0$$ [c4]

where Q is the heat source power (Watt) and k the thermal conductivity of metal (W/mm°C).

The solution has already been mentioned:

$$T - T_0 = \frac{Q}{\pi\ k} \cdot \left[\frac{e^{-\lambda\ v[(\xi^2 + y^2 + z^2)^{1/2} + \xi\ ]}}{(\xi^2 + y^2 + z^2)^{1/2}} \right] \qquad [s1]$$

with the assumption of a quasi-stationary state, i.e. $\dfrac{\partial\ T}{\partial\ t} = 0$.

and for intermediate thickness :

$$T - T_0 = \frac{Q}{\pi\ k(10\log_{10}g)} \cdot \left(\frac{\pi}{2\lambda\ v}\right)^{1/2} \cdot \left[\frac{e^{-\lambda\ v[(\xi^2 + y^2 + z^2)^{1/2} + \xi\ ]}}{(\xi^2 + y^2 + z^2)^{1/4}} \right] \qquad [s2]$$

Appendix D

Separating the variables

The problem can be solved by separating the variables:

$T(x,y',z) = T_x(x).T_y(y').T_z(z)$, which leads to

$$\frac{1}{T_x}\frac{d^2 T_x}{d x^2} + \frac{1}{T_y}\frac{d^2 T_y}{d y'^2} + \frac{1}{T_z}\frac{d^2 T_z}{d z^2} = 0 \;,\; \text{therefore transposing to,}$$

$$-\frac{1}{T_x}\frac{d^2 T_x}{d x^2} = \frac{1}{T_y}\frac{d^2 T_y}{d y'^2} + \frac{1}{T_z}\frac{d^2 T_z}{d z^2} = \omega^2 \qquad\qquad [e3]$$

The left hand side of the equation, a function of x alone, can only equal the right hand side, the function of y, plus the function of z, only if both sides have a separation constant value, say $\omega^2 > 0$.

The x-eigenfunctions satisfying the condition [c1'], from Appendix C are :

$$T_{xn}(x) = \cos(\omega_n x), \qquad \omega_n = (2n+1)\pi/l, \qquad \text{for } n=0, 1, 2.....$$

Re-arranging the second equality of equation [e3] :

$$-\frac{1}{T_y}\frac{d^2 T_y}{d y'^2} = \frac{1}{T_z}\frac{d^2 T_z}{d z^2} - \omega^2 = \delta^2 \qquad\qquad [e4]$$

which gives with condition [c2'] :

$$T_{ym}(y') = \cos(\delta_m y'), \qquad \delta_m = (2m+1)\pi/g, \qquad \text{for } m = 0, 1, 2\ldots\ldots$$

Concerning (T_z), we must solve : $\dfrac{1}{T_z}\dfrac{d^2 T_z}{d z^2} = \omega^2 + \delta^2 = \chi^2$

The general form of (T_z) is : $C_1.\cosh(\chi z) + C_2.\sinh(\chi z)$

when $z = h$, and $T_z(h) = 0$, because of condition [c3'], $= C1 = - C_2.\tanh(hz)$

condition [c3'] therefore implies $C_1 = -C_2 \tanh(\chi h)$.

giving $T_z(z) = -C_2 \tanh(\chi h).\cosh(\chi z) + C_2 \sinh(\chi z)$

$$T_z(z) = C2 \cdot \cosh(\chi z) \cdot \left[-\tanh(\chi h) + \frac{\sinh(\chi z)}{\cosh(\chi z)} \right]$$

Thus,

$$T_z(z) = C_2 \cosh(\chi z).[\tanh(\chi z) - \tanh(\chi h)]$$

and the general solution is :

$T_{zmn}(z) = \cosh(\chi_{mn}z).[\tanh(\chi_{mn}\ z) - \tanh(\chi_{mn}\ h)]$, with $\chi_{mn}^2 = \omega_n^2 + \delta_m^2$ for $m = 0,1\ldots$
$n = 0,1\ldots$

Thus, by superposition :

$$T(x, y', z) = \sum_{m=0}^{\infty}\sum_{n=0}^{\infty} a_{mn}.\cos(\omega_n x).\cos(\delta_m y').\cosh(\chi_{mn}z).[\tanh(\chi_{mn}z) - \tanh(\chi_{mn}h)]$$

Boundary condition [c5'] requires :

$$Q_{tcr}(x,y') = -k\frac{\partial T}{\partial z}(x,y',0) = -k\sum_{m=0}^{\infty}\sum_{n=0}^{\infty}a_{mn}\cdot\chi_{mn}\cdot\cos(\omega_n x)\cdot\cos(\delta_m y')$$

This expression is the double Fourier cosine-series expansion of Qtrc(x,y') over the section x-y' of the plate.

Applying orthogonality, let, *P*, be a point on the curve of the function, and let, *O*, be the origin, as illustrated in below,
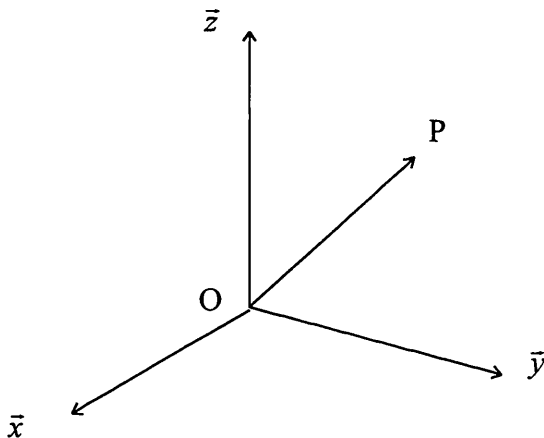
where x, y, z are the scalar components and $\bar{x}$, $\bar{y}$, and $\bar{z}$ are vector components.

For any transient point x,y,z, the vector $\overline{OP}$ is

$$\overline{OP} = x.\ \bar{x} + y.\ \bar{y} + z.\ \bar{z}$$

now considering the vector $\overline{OP}$ in relation to the scalar $\bar{x}$

$$\bar{x}.\overline{OP} = \bar{x}.x.\ \bar{x} + \bar{x}.y.\ \bar{x} + \bar{x}.z.\ \bar{x}$$

in this case, the vector component $\bar{z} = 0$, therefore,

$$x\rightarrow.\overline{OP} = x\rightarrow.x.x\rightarrow + x\rightarrow.y.x\rightarrow$$

and since it is a fixed distance, $\Delta \bar{y} = 0$, therefore,

$$\bar{x}.\overline{OP} = \bar{x}.x.\ \bar{x}, \text{ or, } \bar{x}.\overline{OP} = x.(\ \bar{x})^2$$

transposing to

$$x = \frac{\overline{OP}\cdot\bar{x}}{\bar{x}^2}$$

Such an orthogonal relation permits evaluation of the coefficient a_{mn}, thus,

$$a_{mn} = -\frac{1}{k\,\chi_{mn}}\cdot\frac{\int_{-l/2}^{l/2}\int_{-g/2}^{g/2}Q_{tcr}(x,y').\cos(\omega_n x).\cos(\delta_m y').dy'dx}{\int_{-l/2}^{l/2}\int_{-g/2}^{g/2}\cos(\omega_n x)^2.\cos(\delta_m y')^2.dy'dx}$$

- **Problem (P)=(Pr)+(Ptcr):**

It is necessary to prove that Tr+Ttcr is the solution of (P) :

Both Tr and Ttcr verify $\dfrac{\partial^2 T}{\partial x^2} + \dfrac{\partial^2 T}{\partial y^2} + \dfrac{\partial^2 T}{\partial z^2} = 2\lambda\dfrac{\partial T}{\partial t}$,

Adding the two , the following equation is also true :

$$\frac{\partial^2 (Tr + Ttcr)}{\partial x^2} + \frac{\partial^2 (Tr + Ttcr)}{\partial y^2} + \frac{\partial^2 (Tr + Ttcr)}{\partial z^2} = 2\lambda \frac{\partial (Tr + Ttcr)}{\partial t}, \text{ which is}$$

[e1]

Under the assumptions made above, (Tr) and (Tcr) give :

* $\dfrac{\partial Ttcr}{\partial x} \to 0$ and $\dfrac{\partial Tr}{\partial x} \to 0$ as $x \to \pm\infty$, thus $\dfrac{\partial (Ttcr + Tr)}{\partial x} \to 0$ as $x \to \pm\infty$,

    which is condition [c1].

* For the same reason conditions [c2] and [c3], are also true with Ttcr+Tr.

* $-\dfrac{\partial Tr}{\partial r} \pi r^2 k \to Q$ and $-\dfrac{\partial Ttcr}{\partial r} \pi r^2 k \to 0$ as $r \to 0$, thus

    $-\dfrac{\partial (Tr + Ttcr)}{\partial r} \pi r^2 k \to Q$, which is [c4].

* $-\dfrac{\partial Ttcr}{\partial z} k = Q_{tcr}(x, y)$ and $-\dfrac{\partial Tr}{\partial z} k = 0$ for z=0, therefore

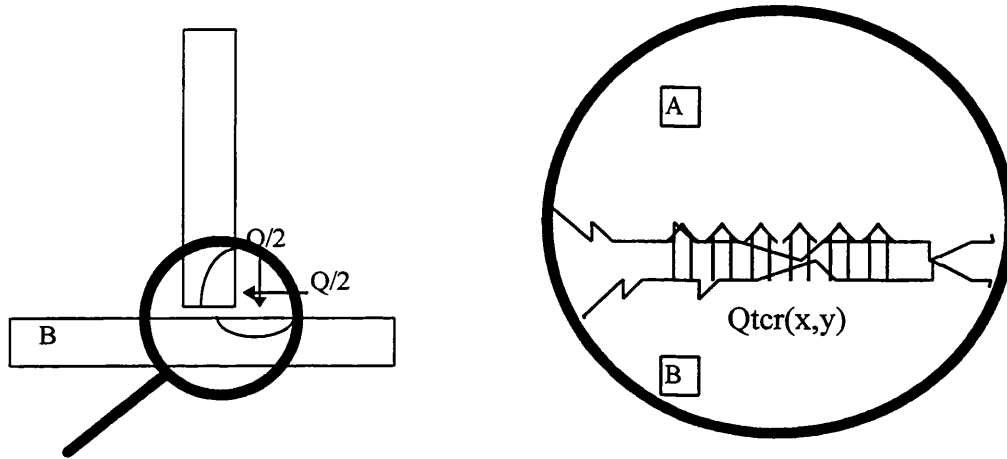 $-\dfrac{\partial (Ttcr + Tr)}{\partial z} k = Q_{tcr}(x, y)$, which is [c5].

Thus, **T=Ttcr+Tr is the solution to (P)**.

• **Note**: (Tr) is now approximated by the new intermediate equation

Application to 90° corner joints

As previously shown, the distribution of the heat flow may be seen as following :

Figure D.1 : Heat flow through contact zone

- **Note**: by convention, (Qtcr) represents the heat flow from (B) to (A). But, in reality, Qtcr<0 since $T_B < T_A$. Thus the real direction of the flow is from (A) to (B).
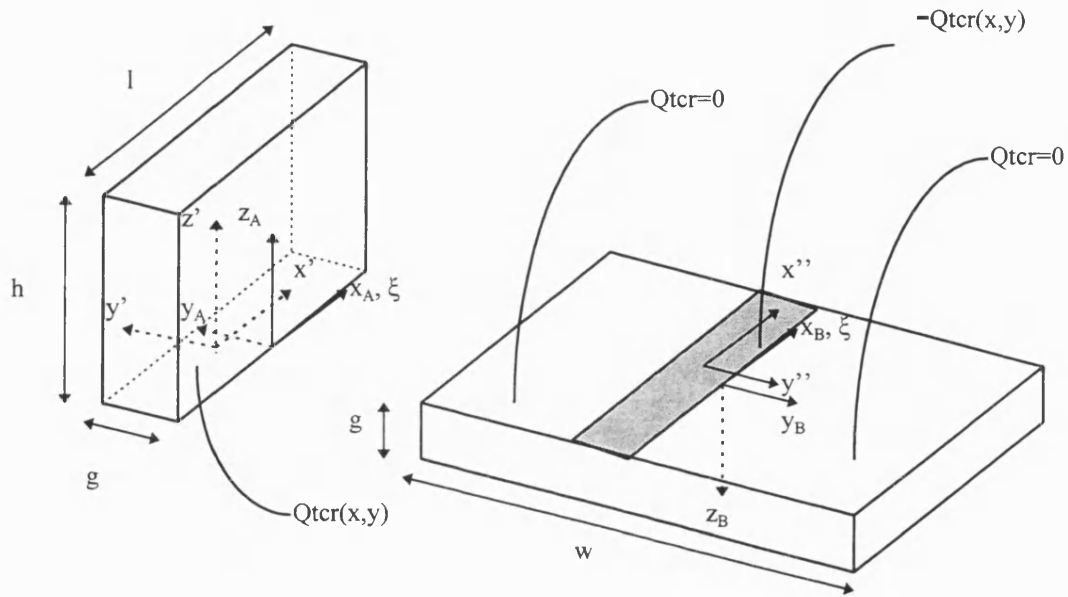
Figure D.2 : nomenclature

- **Notes**:

$x_A = x' = x_B$ and $y_A = y' + g/2 = -y_B$

$x_B = x''$ and $y_B = y'' - g/2$

$T_A(x_A, y_A, 0, t) = T_B(x_A, -y_A, 0, t) = T_B(x_A, y_A, z_A, t)$

With $Qtcr(x_A, y_A, (t)) = (T_B(x_A, y_A, 0, t) - T_A(x_A, y_A, 0, t))/Rtc$ (t [time] is between parenthesis since the solution is known in a steady state).

Therefore, the analytical temperatures of (A) and (B) are :

* $T_A(x_A, y_A, z_A, t) = T_0 + Tr_A(x_A, y_A, z_A, t) + Ttcr_A(x_A, y', z_A, t)$

with

$$Tr_A(x,y,z,t) = \frac{Q/2}{\pi\ k(10\log_{10}g)} \cdot \left(\frac{\pi}{2\lambda\ v}\right)^{1/2} \cdot \left[\frac{e^{-\lambda\ v[(x-vt)^2+y^2+z^2)^{1/2}+(x-vt)]}}{((x-vt)^2+y^2+z^2)^{1/4}}\right]$$

and

$$Ttcr_A(x,y',z,(t)) = \sum_{m=0}^{\infty}\sum_{n=0}^{\infty} a_{mn}(t).\cos(\omega_{na}x).\cos(\delta_{ma}y').\cosh(\chi_{mna}z).[\tanh(\chi_{mna}z)-\tanh(\chi_{mna}h)]$$

and

$$a_{mn}(t) = -\frac{1}{k\,\chi_{mna}} \cdot \frac{\int_{-l/2}^{l/2}\int_{-g/2}^{g/2}\dfrac{T_B(x,y,0,t)-T_A(x,y,0,t)}{Rtc}.\cos(\omega_{na}x).\sin(\delta_{ma}y').dy'dx}{\int_{-l/2}^{l/2}\int_{-g/2}^{g/2}\cos(\omega_{na}x)^2.\cos(\delta_{ma}y')^2.dy'dx},$$

$$\omega_{na}=(2n+1)\pi/l, \qquad \delta_{ma}=(2m+1)\pi/g, \qquad \chi_{mna}{}^2=\omega_{na}{}^2+\delta_{ma}{}^2,$$

and

$$* \quad T_B(x_B,y_B,z_B,t) = T_0+Tr_B(x_B,y_B,z_B,t)+Ttcr_B(x_B,y',z_B,t)$$

with

$$Tr_B(x,y,z,t) = \frac{Q/2}{2\pi\ k(10\log_{10}g)} \cdot \left(\frac{\pi}{2\lambda\ v}\right)^{1/2} \cdot \left[\frac{e^{-\lambda\ v[(x-vt)^2+y^2+z^2)^{1/2}+(x-vt)]}}{((x-vt)^2+y^2+z^2)^{1/4}}\right]$$

and

$$Ttcr_B(x,y',z,(t)) = \sum_{m=0}^{\infty}\sum_{n=0}^{\infty} b_{mn}(t).\cos(\omega_{nb}x).\cos(\delta_{mb}y').\cosh(\chi_{mnb}z).[\tanh(\chi_{mnb}z)-\tanh(\chi_{mnb}g$$

and

$$b_{mn}(t) = -\frac{1}{k\,\chi_{mnb}} \cdot \frac{\int_{-l/2}^{l/2}\int_{-g/2}^{g/2}\dfrac{T_A(x,y,0,t)-T_B(x,y,0,t)}{Rtc}.\cos(\omega_{nb}x).\cos(\delta_{mb}y'').dy''dx}{\int_{-l/2}^{l/2}\int_{-w/2}^{w/2}\cos(\omega_{nb}x)^2.\cos(\delta_{mb}y'')^2.dy''dx}$$

$$\omega_{nb}=(2n+1)\pi/l, \qquad \delta_{mb}=(2m+1)\pi/w, \qquad \chi_{mnb}{}^2=\omega_{nb}{}^2+\delta_{mb}{}^2,$$

Simplifications

As a nomenclature, consider that x= x_A and y= y_A.

The equations above show that an integral equation must be solved to find the coefficients (a_{mn}) and (b_{mn}).

1) **First assumption:**

(a_{mn}) and (b_{mn}) have been computed with the assumption that :

$$Qtcr(x,y,t) = \frac{T_B(x,y,0,t) - T_A(x,y,0,t)}{Rtc}$$

$$= \frac{T_{rB}(x,y,0,t)}{Rtc} \quad \frac{T_{rA}(x,y,0,t)}{Rtc} + \frac{Ttcr_B(x,y'',0,t) - Ttcr_A(x,y',0,t)}{Rtc}$$

$$\approx \frac{T_{rB}(x,y,0,t) - T_{rA}(x,y,0,t)}{Rtc}$$

So that (Qtcr) is no longer unknown.

This assumption is true provided $T_{tcri} \ll T_{ri}$, i.e. for "high" values of (Rtc).

Whilst the full analytical expression can be defined, the computing time on the available equipment is far too long for any valuable use.

2) **Second assumption:**

It is necessary to compute a limited number of coefficients in the Fourier double-cosine series. In order to decrease the computing time, only (a_{00}) and (b_{00}) were computed, which is a coarse approximation.

One test has shown that this term represents the three quarters of the total value.

3) **Third assumption:**

The third assumption concerns the numerical evaluation of $a_{mn}(t)$ and $b_{mn}(t)$. To decrease the computing time, the function $Qtcr(x,y,(t))$ has been interpolated with a polynomial of the third power on its area of definition.

With these simplifications, the computing time is not excessive. Once the coefficients are known, the implemented temperatures distribution is used to assess the new limits of the HAZ before comparing them with the former values.

For that purpose, a program has been written in Qbasic. The y-limit (y_L) of the HAZ in the upper plate or the lower plate, is assessed for each value of z_k =k.dz, k=[0,1,2,...[, with dz to be defined by the user (0.1mm, 0.5mm...). By definition of the HAZ, the grains at the location (y_L) are the last to be transformed due to the increase of temperature.

According to the Fe-C diagram of the steel EN 10025 S355, no metallurgical transformation happens to the grains below Tc≈723°C. Thus, the grains whose peak temperature (maximum temperature reached during the welding heat cycle) is Tc are the last to be transformed.

Finding (y_L) implies also to know the instant (t_L) when such a situation happens. (y_L), which is independent from (x), is therefore solution of the equations:

$$T(0,y_L,z_k,t_L)=Tc, \text{ with } Tc=723°C \qquad [L1]$$

$$T(0,y_L,z_k,t_L)=Max_y(T(0,y, z_k)) \Leftrightarrow \frac{\partial T}{\partial t}(0,y_L, z_k,t_L)=0 \qquad [L2]$$

To solve the system, a double dichotomy is performed on (y) and (t), as the equations [L1] and [L2] are of the kind f(y,t)=0 and g(y,t)=0 with g(y,t) the derivative of f(y,t)=T(0,y,z_k,t)-Tc respecting to time. (T) is the improved distribution of temperature, T=Tr+Ttcr. The coefficients $a_{00}(t_k)$ are read from a file, generated from the computer results. To compute the derivative of Ttcr(0,y,z_k,t), the program relies on a finite difference [Ttcr(0,y,z_k,t+dt)-Ttcr(0,y,z_k,t)]/dt, where dt=0.1s.

Approach of the complete problem

The assumption $Qtcr(x,y,t) \approx \dfrac{Tr_B(x,y,0,t) - Tr_A(x,y,0,t)}{Rtc}$ is no longer valid when Rtc is very "low".

By considering the boundary conditions [c5'] and keeping the initial expression of (Qtcr):

$$-k\frac{\partial\, Ttcr_A}{\partial z}(x,y',0,t) = \frac{Tr_B(x,y,0,t)}{Rtc} \frac{Tr_A(x,y,0,t)}{} + \frac{Ttcr_B(x,y'',0,t) - Ttcr_A(x,y',0,t)}{Rtc}$$

$$-k\frac{\partial\, Ttcr_B}{\partial z}(x,y'',0,t) = \frac{Tr_A(x,y,0,t)}{Rtc} \frac{Tr_B(x,y,0,t)}{} + \frac{Ttcr_A(x,y',0,t) - Ttcr_B(x,y'',0,t)}{Rtc}$$

These two equations lead to the system:

$$\sum_{m=0}^{\infty}\sum_{n=0}^{\infty}\left[a_{mn}(t).c_{na}(x).c_{ma}(y').(-\tanh(\chi_{mna}h) - k.\chi_{mna}.Rtc) + b_{mn}(t).c_{nb}(x).c_{mb}(y'').\tanh(\chi_{mnb}g)\right] =$$
$$Tr_B(x,y,0,t) - Tr_A(x,y,0,t)$$

and

$$\sum_{m=0}^{\infty}\sum_{n=0}^{\infty}\left[b_{mn}(t)\cdot c_{nb}(x)\cdot c_{mb}(y'')\cdot(-\tanh(\chi_{mnb}g)-k\cdot\chi_{mnb}\cdot Rtc)+a_{mn}(t)\cdot c_{na}(x)\cdot c_{ma}(y')\cdot\tanh(\chi_{mna}h)\right]=$$

$$T_{rA}(x,y,0,t)-T_{rB}(x,y,0,t)$$

with $c_{na}(x)=\cos(\omega_{na}\cdot x)$ and $c_{ma}(x)=\cos(\delta_{ma}\cdot x)$

giving, by applying the orthogonality:

$$a_{ij}(t)=-\frac{1}{(\tanh(\chi_{ija}h)+k\cdot\chi_{ija}\cdot Rtc)}\cdot\left(\frac{\int_{-l/2}^{l/2}\int_{-g/2}^{g/2}[T_{rB}(x,y,0,t)-T_{rA}(x,y,0,t)]\cdot c_{ia}(x)\cdot c_{ja}(y')\cdot dy'dx}{\int_{-l/2}^{l/2}\int_{-g/2}^{g/2}c_{ia}(x)^2\cdot c_{ja}(y')^2\cdot dy'dx}\right.$$

$$\left.-\frac{\sum_{m=0}^{\infty}\sum_{n=0}^{\infty}b_{mn}(t)\cdot\int_{-l/2}^{l/2}\int_{-g/2}^{g/2}c_{nb}(x)\cdot c_{mb}(y'')\cdot\tanh(\chi_{mnb}g)\cdot c_{ia}(x)\cdot c_{ja}(y')\cdot dy'dx}{\int_{-l/2}^{l/2}\int_{-g/2}^{g/2}c_{ia}(x)^2\cdot c_{ja}(y')^2\cdot dy'dx}\right)$$

[A1]

and

$$b_{ij}(t)=-\frac{1}{(\tanh(\chi_{ijb}g)+k\cdot\chi_{ijb}\cdot Rtc)}\cdot\left(\frac{\int_{-l/2}^{l/2}\int_{-g/2}^{g/2}[T_{rA}(x,y,0,t)-T_{rB}(x,y,0,t)]\cdot c_{ib}(x)\cdot c_{jb}(y'')\cdot dy''dx}{\int_{-l/2}^{l/2}\int_{-w/2}^{w/2}c_{ib}(x)^2\cdot c_{jb}(y'')^2\cdot dy''dx}\right.$$

$$\left.-\frac{\sum_{m=0}^{\infty}\sum_{n=0}^{\infty}a_{mn}(t)\cdot\int_{-l/2}^{l/2}\int_{-g/2}^{g/2}c_{na}(x)\cdot c_{ma}(y')\cdot\tanh(\chi_{mna}g)\cdot c_{ib}(x)\cdot c_{jb}(y'')\cdot dy''dx}{\int_{-l/2}^{l/2}\int_{-w/2}^{w/2}c_{ib}(x)^2\cdot c_{jb}(y'')^2\cdot dy''dx}\right)$$

[B1]

Replacing (b_{ij}) by [B1] in [A1], or (a_{ij}) by [A1] in [B1], implies that

$$a_{ij} = c_{ij} + f(a_{mn}, m=[0,1,2,...,i,...[, n=[0,1,2,...,j,...[)$$
$$b_{ij} = d_{ij} + f(b_{mn}, m=[0,1,2,...,i,...[, n=[0,1,2,...,j,...[)$$

where (c_{ij}) and (d_{ij}) are constants.

Such a system is linear and thus solvable, but it is made up of an infinite number of equations. Some simplifications can be made by limiting the maximum values of (m) and (n), but is complex.

Appendix E

Program in AR-Basic for the robot

- Listing :

```
!Initial set up
BEGIN :
        MAXSPEED=30
        WSPEED=15
        set_frame to TABLE
        set_speed to MAXSPEED
        set_joystick to STRAIGHT;
        set_motion to STRAIGHT;
        define WELD as d_out(16)
        WELD=0
!-----------------------------------------------
!Main menu
MENU :
        print "1.Teaching the tool axis."
        print "2.Teaching the fixture frame."
        print "3.Teaching the reference joint."
        print "4.Teaching the welding parameters."
        print "5.Welding."
        print "6.Quit."
        input CHOICE
        if CHOICE=1 then gosub TOOLFRAME
        endif
        if CHOICE=2 then gosub JIG
        endif
        if CHOICE=3 then gosub REFJOINT
        endif
        if CHOICE=4 then gosub WELDPARAM
        endif
        if CHOICE=5 then gosub WELDING
        endif
        if CHOICE=6 then gosub GOODBYE
        endif
goto Menu
!-----------------------------------------------
!Tool definition
TOOLFRAME:
```

```
        set_frame to TABLE
        TORCH=def_tool(180,-191,60,-5,0,-54)
        set_tool to TORCH
return
!------------------------------------------------
!Definiton of the fixture frame
JIG:
        set_frame to TABLE
        set_tool to TORCH
        decl_point FIX(3)
        for I=1 to 3
                pause "Move the arm to a new point"
                teach_abs FIX(I)
        next I
        FIXTURE=build_frame(FIX(1), FIX(2), FIX(3))
return
!------------------------------------------------
!Definiton of the reference joint
DEFJOINT:
        set_frame to FIXTURE
        set_tool to TORCH
        print "Thickness of the reference plates ?"
        input REFTHK
        pause "Please, teach the two extrem points defining the joint."
        print "No specific orientation required."
        decl_point REF(2)
        pause "Move the torch to the first point."
        teach_ref REF(1)
        pause "Move the torch to the second point."
        teach_ref REF(2)
return
!------------------------------------------------
!Setting the welding parameters
WELDPARAM:
        print "Thickness of the plates (mm) ?"
        input PTHK
        print "Speed of travel (mm/s) ?"
        input WSPEED
        print "Torch angle respecting to the vertical position (°) ?"
        input ANGLE
        decl_point WPT(4)
        for I=2 to 3
                WPT(I).roll=ANGLE
                WPT(I).pitch=90
                WPT(I).yaw=0
                WPT(I).x=REF(I-1).x-(PTHK-REFTHK)*2^0.5/2
```

```
            WPT(I).y=REF(I-1).y
            WPT(I).z=REF(I-1).z + (PTHK-REFTHK)*2^0.5/2
      next I
      PATH:
      WPT(1)=WPT(2)
      WPT(1).z=WPT(2).z+100
      WPT(4)=WPT(3)
      WPT(4).z=WPT(3).z+100
      WCHECK=WPT(2)
      WCHECK.z=WPT(2).z+5
return
!---------------------------------------------
!Welding
WELDING :
      set_frame to FIXTURE
      set_tool to TORCH
      set_speed to MAXSPEED
      print "Is it a simulation ? (1=YES, 0=NO)"
      input SIM
      pause "Ready?"
      move to WPT(1)
      set_speed to WSPEED
      move to WCHECK
      print "Position correct? (1=YES, 0=NO)"
      input CHOICE
      if CHOICE=1 then START
      gosub ADJUST
      goto WELDING

      START:
      move to WPT(2)
      wait_till stop
      if SIM=0 then WELD=1
      endif
      move to WPT(3)
      wait-till stop
      WELD=0  ·
      delay 1
      set_speed to MAXSPEED
      move to WPT(4)
return
!---------------------------------------------
!Adjust the path
ADJUST:
      pause "Move the torch to the new point."
      teach_ref WPT(2)
```

```
        WPT(3)=WPT(2)
        WPT(3).y=REF(2).y
goto PATH
!----------------------------------------------
!Quit
GOODBYE:
pause "Do not forget to save the points!"
end
```

Appendix F

3 mm
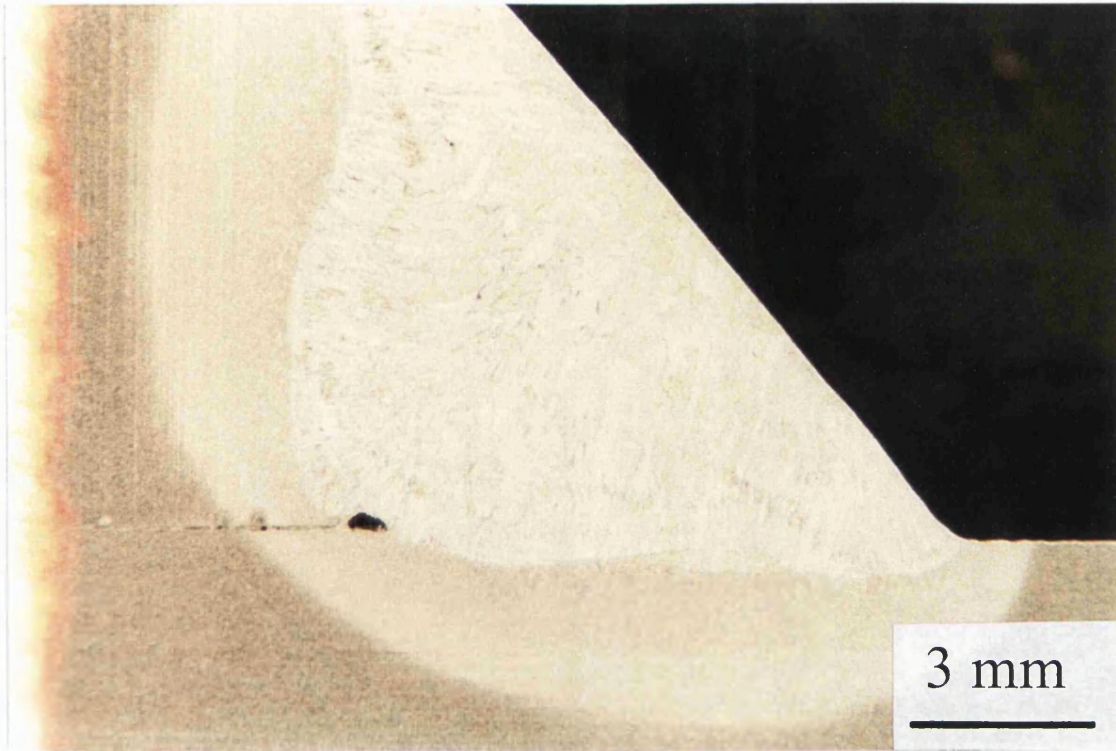
Figure F.1 : 10mm to 10mm fillet, [≈100% contact], (x8, optical), 2% Nital etch

40μm
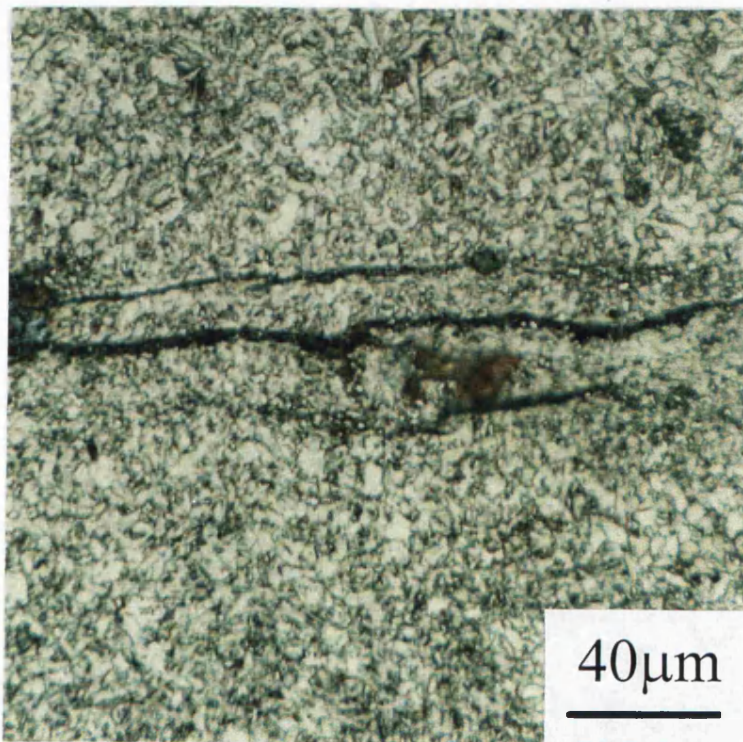
Figure F.2 : 15mm to 15mm fillet, [≈100% contact], (x500, optical), 2% Nital etch

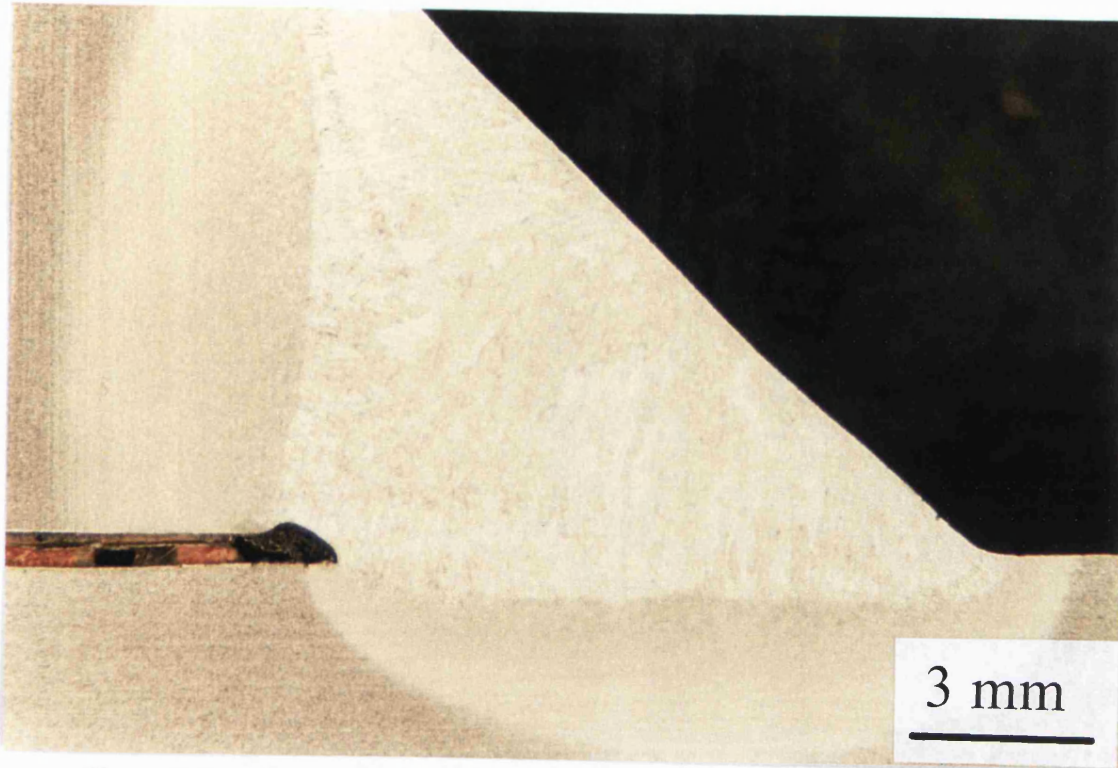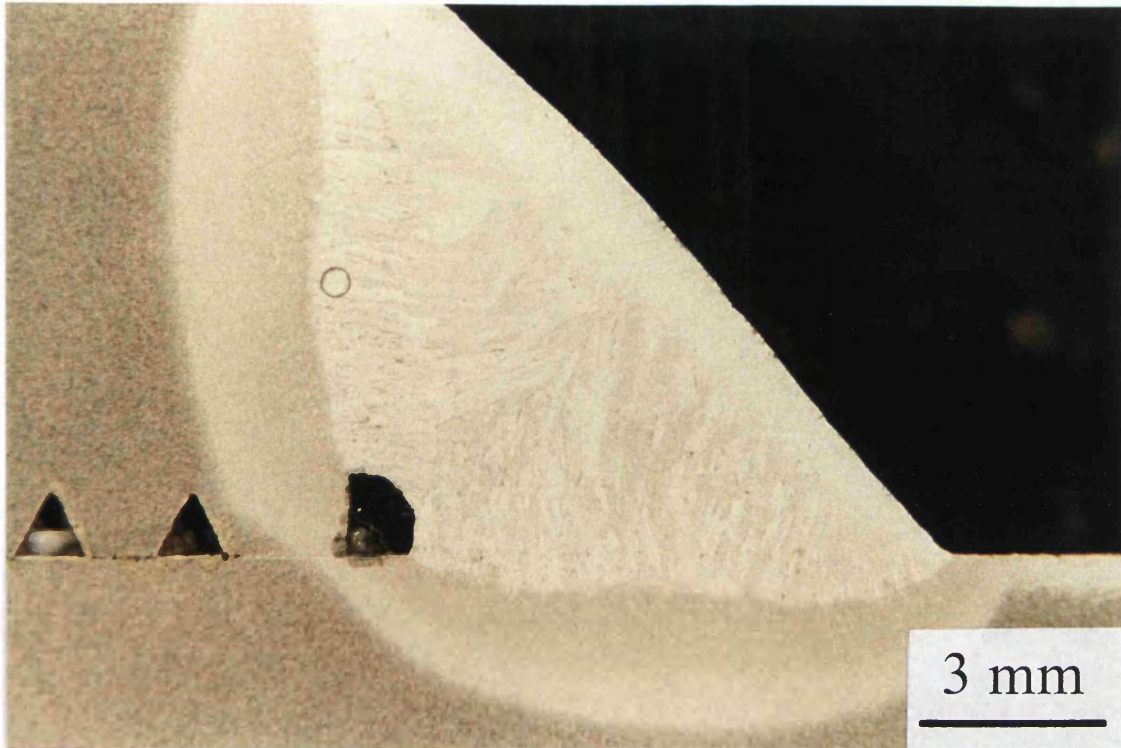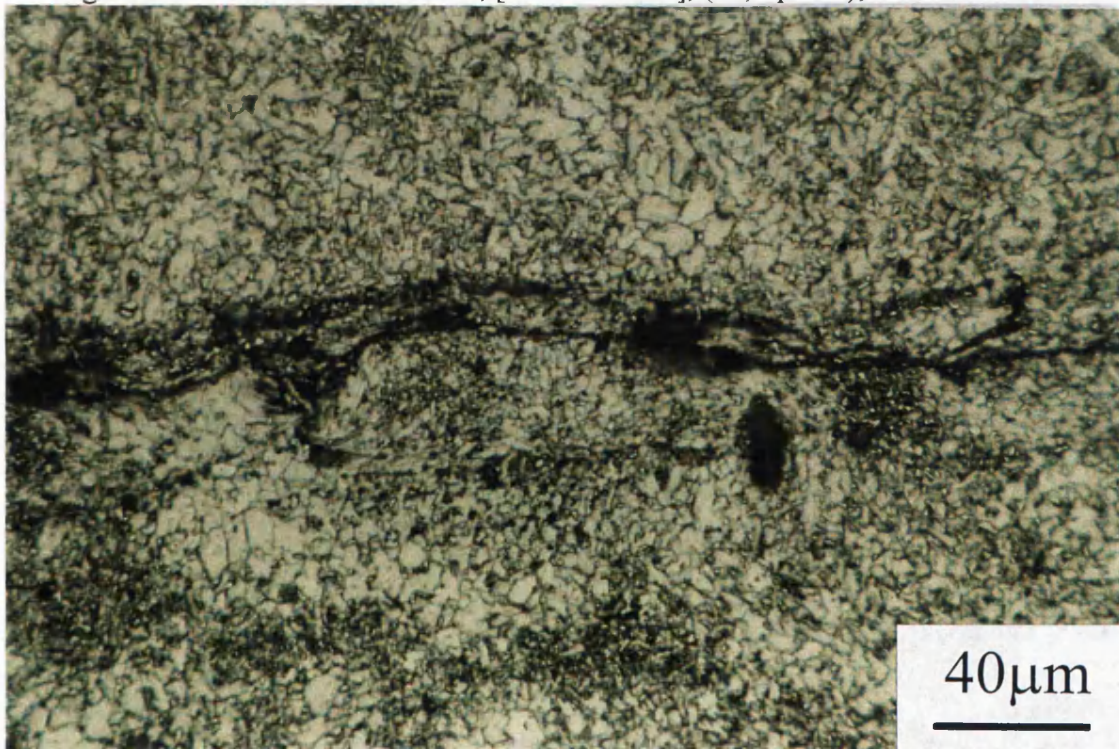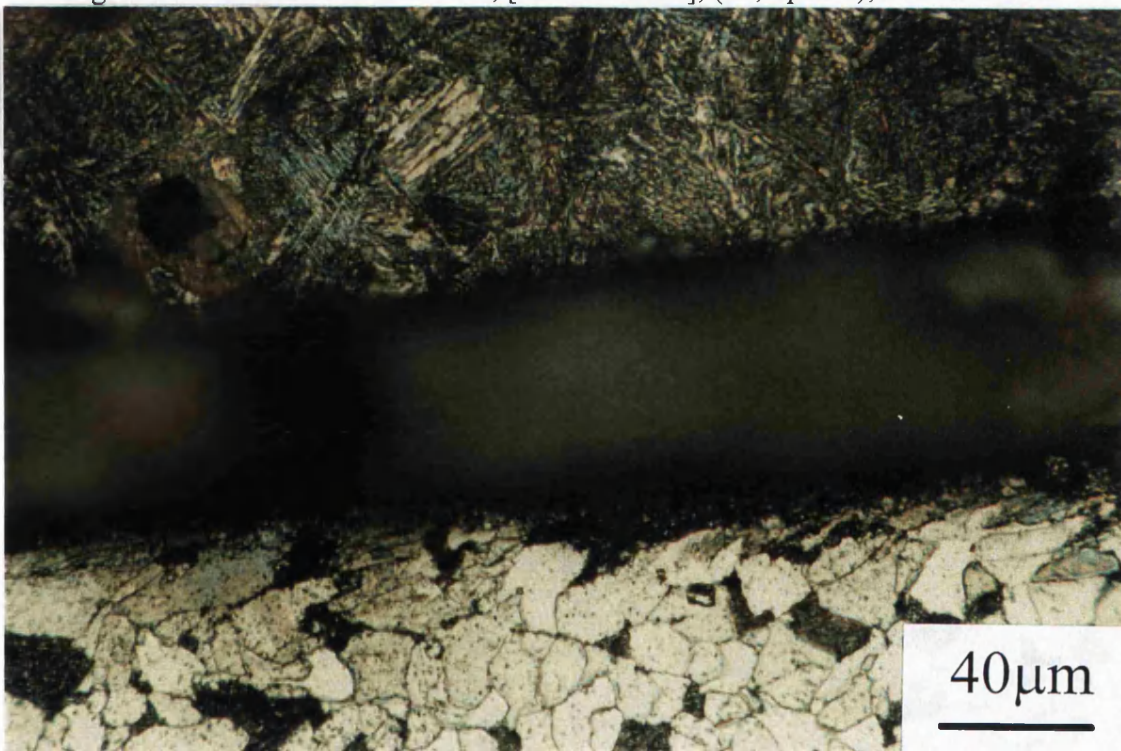Figure F.3 : 10mm to 10mm fillet, [0% contact], (x8, optical), 2% Nital etch

Figure F.4 : 15mm to 15mm fillet, [≈67% contact], (x8, optical), 2% Nital etch

Figure F.5 : 15mm to 15mm fillet, [≈67% contact], (x500, optical), 2% Nital etch
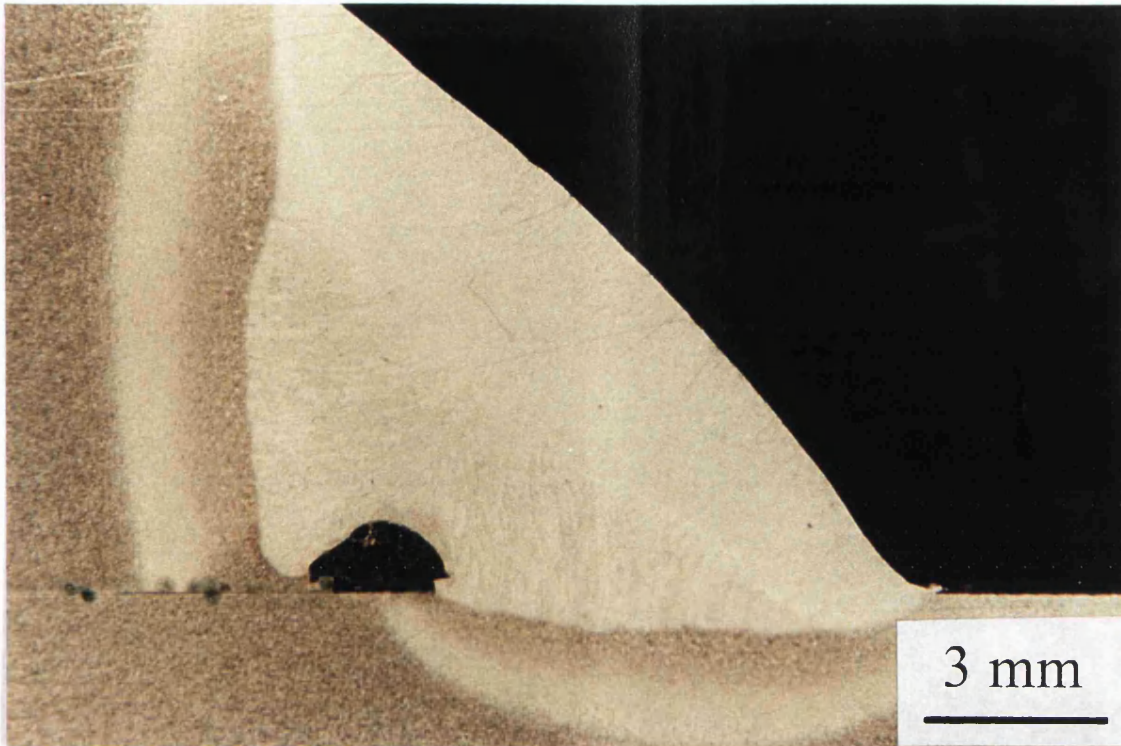
Figure F.6 : 25mm to 25mm fillet, [100% contact], (x8, optical), 2% Nital etch

Figure F.7 : 25mm to 25mm fillet, [upper and lower plates], (x500, optical),
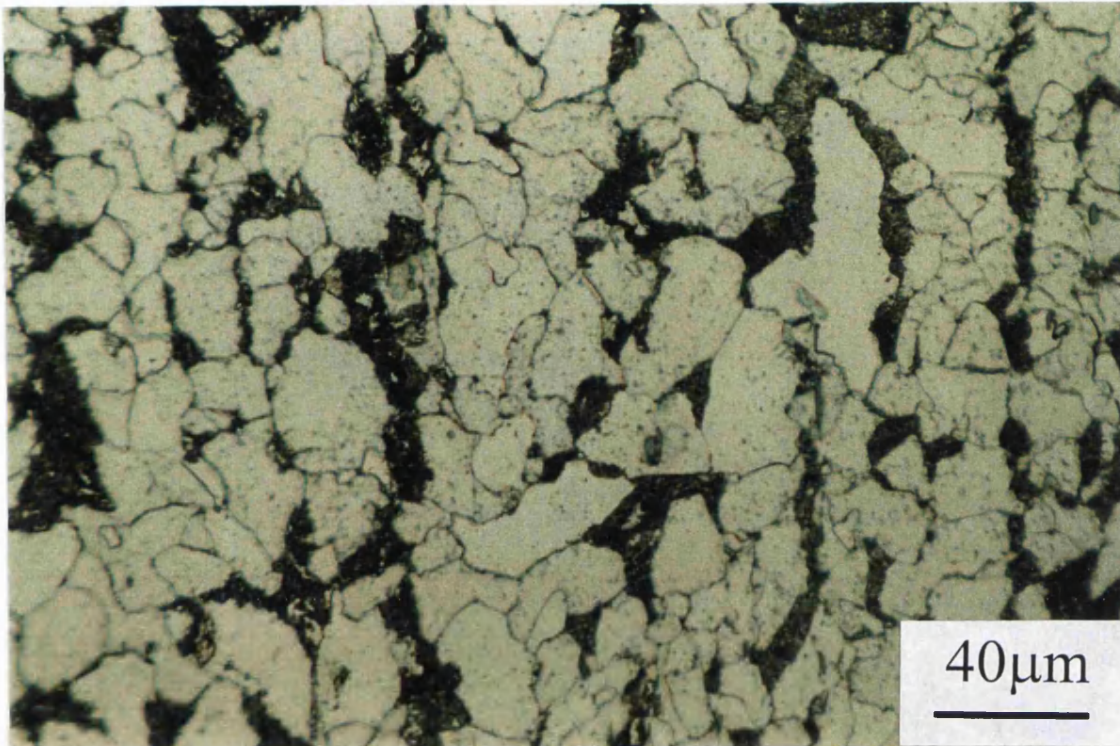2% Nital etch

Appendix G

Figure G.1 : Ferrite-pearlite structure of a Nb micro-alloyed steel, (x500, optical), 2% Nital etch
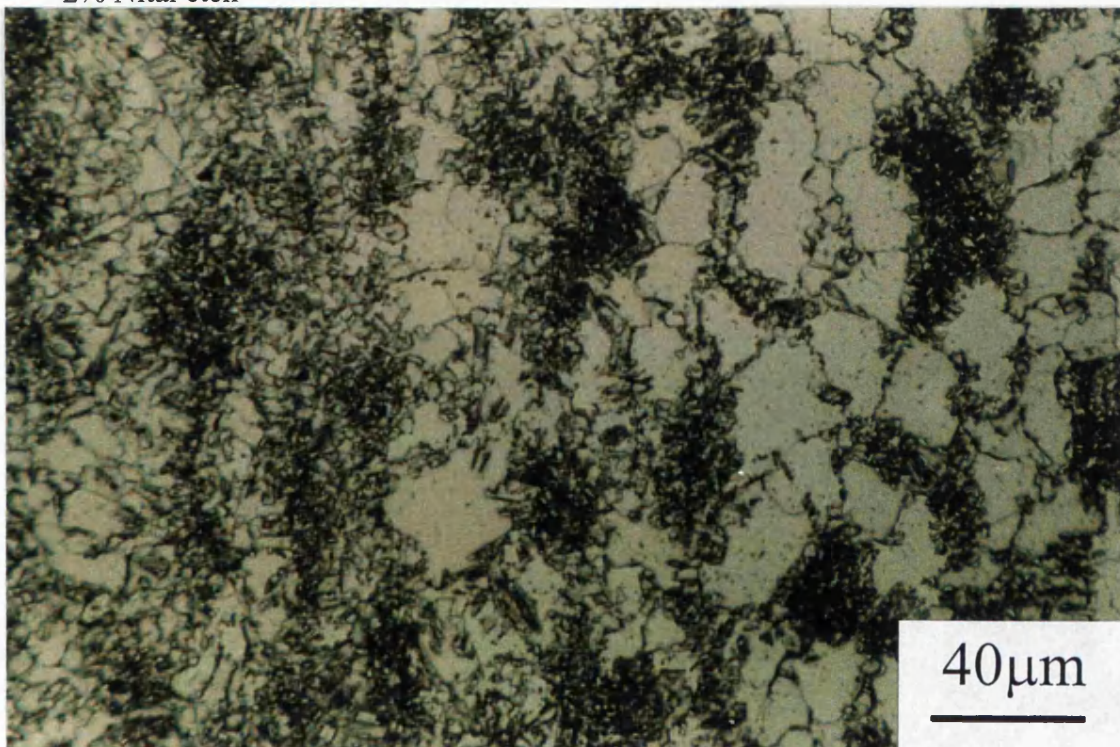

Figure G.2 : Myriad austenite with reprecipitation of ferrite (x500, optical), 2% Nital etch
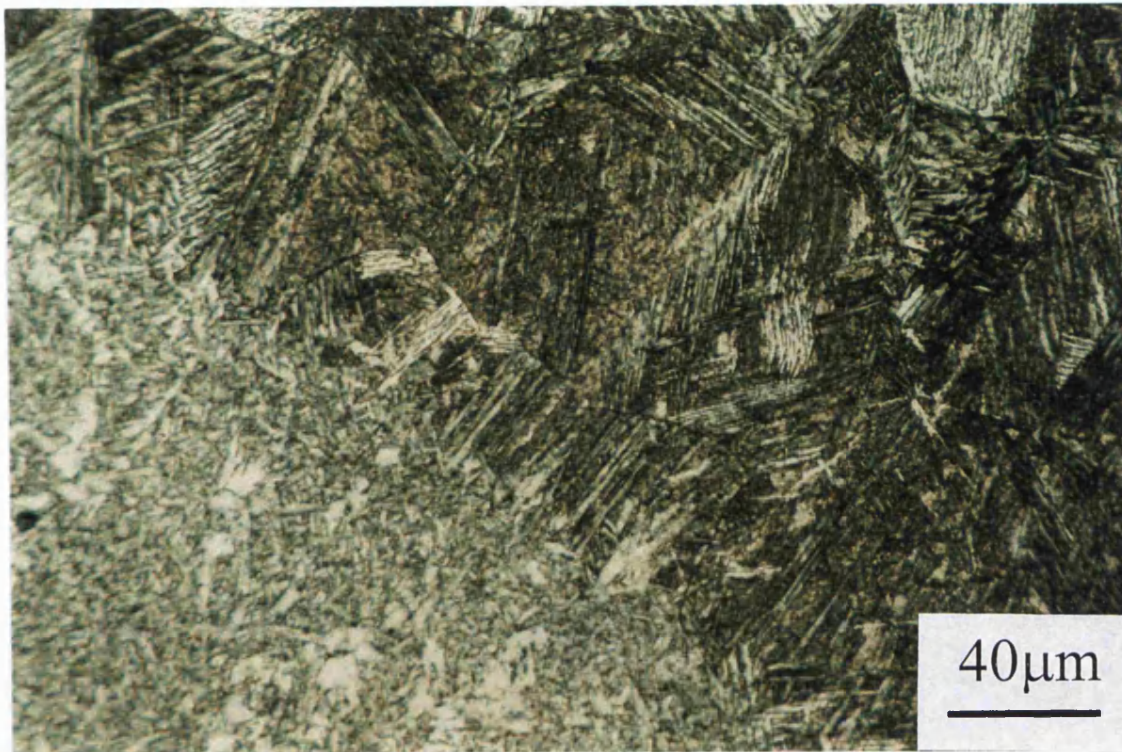
Figure G.3 : Weld metal to heat affected zone transformation region, (x500, optical), 2% Nital etch

Figure G.4 : Typical martensitic structure due to rapid cooling, (x500, optical), 2% Nital etch
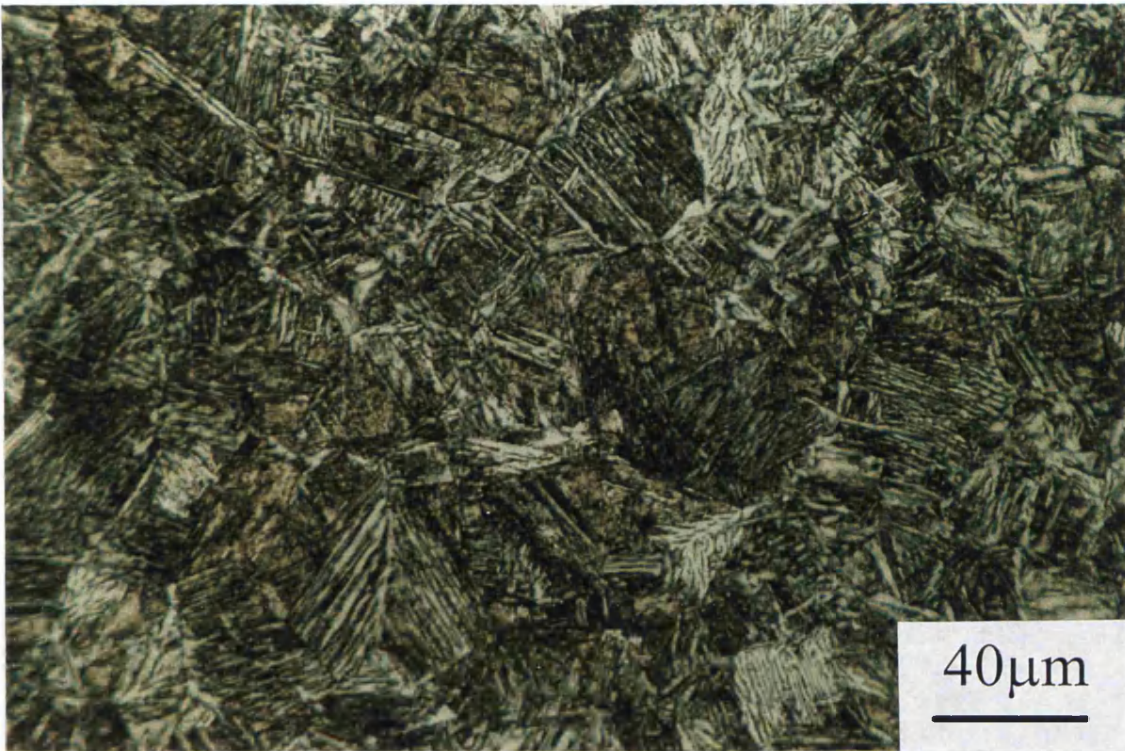
Figure G.5 : Ferrite with aligned MAC, (AC), (x500, optical), 2% Nital etch

Figure G.6 : Fine grains in the grain refined region, (x500, optical), 2% Nital etch